SAHC

Canterbury Cathedral – Structural Analysis of the South Aisle

Georgios Karanikoloudis

Portugal | 2014

ADVANCED MASTERS IN STRUCTURAL ANALYSIS
OF MONUMENTS AND HISTORICAL CONSTRUCTIONS

Master's Thesis

Georgios Karanikoloudis

Canterbury Cathedral – Structural Analysis of the South Aisle

University of Minho

Czech university of Prague

Education and Culture

Erasmus Mundus

ADVANCED MASTERS IN STRUCTURAL ANALYSIS
OF MONUMENTS AND HISTORICAL CONSTRUCTIONS

Master's Thesis

Georgios Karanikoloudis

Canterbury Cathedral – Structural Analysis of the South Aisle

This Masters Course has been funded with support from the European Commission. This publication reflects the views only of the author, and the Commission cannot be held responsible for any use which may be made of the information contained therein.

Portugal | 2014

DECLARATION

Name:	Georgios Karanikoloudis
Email:	Karanikoloudis@hotmail.com

Title of the Msc Dissertation:	Canterbury Cathedral – Structural Analysis of the South Aisle
Supervisor(s):	Paulo B. Lourenco (University of Minho) Claudio Corallo (The Morton Partnership Ltd)
Year:	2013-2014

I hereby declare that all information in this document has been obtained and presented in accordance with academic rules and ethical conduct. I also declare that, as required by these rules and conduct, I have fully cited and referenced all material and results that are not original to this work.

I hereby declare that the MSc Consortium responsible for the Advanced Masters in Structural Analysis of Monuments and Historical Constructions is allowed to store and make available electronically the present MSc Dissertation.

University:	University of Minho
Date:	10/09/2014
Signature:	_____

To my friends and family

ACKNOWLEDGEMENTS

I would like to express my gratitude to the Dean and Chapter of Canterbury Cathedral for financing this Thesis. Special thanks to the Surveyor of the Fabric Jonathan Deeming for the provided information.

This thesis had for me a realistic and practical involvement which wouldn't have been possible without the technical support and assistance provided by the Morton Partnership Ltd, for which I'm grateful and in particular to Claudio Corallo for his valuable guidance.

My deepest acknowledgements to my thesis supervisor, Prof. Paulo B. Lourenco for his commitment, advice and help. His guidance and involvement during my dissertation, in spite his heavy schedule, has given the chance to enrich my technical knowledge and for that I'm grateful.

Throughout this thesis, the PhD Researcher Nuno Mendes has offered an amazing help and assistance in the ambiental vibration tests and the numerical modelling, to whom I would like to express my sincere thanks.

My outmost acknowledgements to the S.A.H.C Consortium, for the scholarship I received that complimented greatly my efforts and studies on the structural analysis of historic constructions.

Lastly, I would like to thank all my friends and colleagues, whom I bothered with queries, during this hard, long effort.

ABSTRACT

The Canterbury Cathedral at Canterbury Kent, in the UK, seat of the Archbishop of Canterbury, head of the Anglican Church, stands as a monument of English Gothic architecture of immense importance, and is part of the UNESCO World Heritage site. Its central nave and lateral aisles, secluded by the twin bell towers of the west front and the west transept, with a 72 m tower at the crossing, is a fine example of the English Gothic style of the early 14th century.

The inspection and damage survey, conducted in the Cathedral's nave, revealed the generally good condition of the skeleton, with the exception of a repetitive crack pattern on the vault's intrados, which intensified in a part of the south aisle, including some outward rotating movement and cracking in the south flying buttresses. Ambient vibration tests were carried out at the nave and south aisle roof level, in order to identify the modal response of the structure.

A Graphic Statics analysis was conducted ,with the aim to compliment the results of the structural analysis, by investigating the load paths in the structural elements and how the geometrical configuration of the Cathedral's nave section advocated its structural performance.

Through the geometrical survey, a 3D CAD model of a typical transversal section of the nave was elaborated and, accordingly, a FE model was built in Midas FX+ for DIANA software, in order to investigate various hypothesis of structural damage, by reproducing the existing crack pattern and obtaining certain levels of structural safety. The results from the ambient vibrations tests were used for the calibration of the FE model. Different nonlinear static analyses under dead loading were performed, by considering model variables, such as the infill volume, the presence of lateral thrust from the nave's roof and differential settlements. A validated FE model, having a sufficient correlation with the existing damage was used to determine to safety factor of the structure in both lateral and vertical loading.

RESUMO

A Catedral de Canterbury localizada no condado de Canterbury, Reino Unido, sede do arcebispo de Canterbury, chefe da Igreja Anglicana, é um monumento de enorme importância para a arquitetura gótica inglesa, sendo parte do Património Mundial da UNESCO. A sua nave central e corredores laterais, abrigados pelas torres da fachada oeste e do transepto oeste, é um belo exemplo do estilo gótico Inglês do início do século 14.

A inspeção e pesquisa de danos, realizadas na nave da Catedral, revelaram um bom estado geral do esqueleto, exceto um padrão de fendilhação que se repete no intradós da abóbada, intensificando-se no corredor sul, incluindo movimento de rotação no sentido exterior e fendas nos arcos dos contrafortes localizados a sul. Foram realizados ensaios de vibração ambiental na nave e no corredor sul ao nível da cobertura, a fim de identificar a resposta modal da estrutura.

Uma análise gráfica estática, complementa os resultados da análise estrutural, investigando a distribuição de carga nos elementos estruturais e em que forma a configuração geométrica da seção da nave da Catedral afeta o desempenho estrutural da mesma.

Através do levantamento geométrico, um modelo 3D CAD de uma seção transversal típica da nave foi elaborado um modelo de elementos finitos, construído em Midas FX + para o software DIANA, a fim de investigar várias hipóteses de danos estruturais, reproduzindo o padrão de fendilhação existente e obtendo os níveis de segurança estrutural. Os resultados dos ensaios de vibração ambiental foram utilizadas para a calibração do modelo de elementos finitos. Foram realizadas analises estáticas não-lineares com cargas permanentes, considerando-se as variáveis do modelo, tais como o volume de enchimento, a presença do impulso lateral da cobertura da nave e assentamentos diferenciais. Um modelo de elementos finitos validado, tendo uma correlação suficiente com os danos existentes, foi utilizado para determinar o fator de segurança da estrutura para carregamentos laterais e verticais.

ΠΕΡΙΛΗΨΗ

Ο Καθεδρικός ναός του Canterbury, στην πόλη του Canterbury της επαρχίας Kent, της Μεγάλης Βρετανίας, αποτελεί την έδρα του Αρχιεπισκόπου του Canterbury, κεφαλή της Αγγλικανικής Εκκλησίας. Δεσπόζει ως μνημείο Αγγλικής Γοτθικής αρχιτεκτονικής εξαιρετικής σπουδαιότητας και ανήκει στον κατάλογο των Μνημείων Παγκόσμιας Κληρονομιάς της UNESCO. Το κεντρικό και τα δύο πλευρικά του κλίτη περιέχονται μεταξύ των δύο δίδυμων πύργων της δυτικής πρόσοψης και του δυτικού εγκάρσιου κλίτους, με τον κεντρικό πύργο ύψους 72 μέτρων, και αποτελούν ένα χαρακτηριστικό παράδειγμα του Αγγλικού Γοτθικού στυλ των αρχών του 14ου αιώνα.

Η επί τόπου έρευνα και μελέτη της παθολογίας, που επικεντρώθηκε στο κεντρικό και πλευρικά κλίτη του ναού, αποφάνθηκε την γενικά καλή κατάσταση του στατικού συστήματος, πέραν μιας αλληλουχίας ρωγμών στο εσωράχιο των θόλων, που εντείνεται σε τμήμα του νότιου πλευρικού κλίτους, περιλαμβανομένης και μιας έξω περιστροφικής κίνησης, με συνεπάγοντες ρωγμές στις νότιες τοξωτές αντηρίδες. Η επιτόπια εκτέλεση ambient vibration tests, στο επίπεδο της στέγης του κεντρικού και του νότιου κλίτους, προσδιόρισαν την ιδιομορφική απόκριση της κατασκευής.

Η γραφική στατική ανάλυση της κατασκευής πραγματοποιήθηκε ώστε να απότελέσει ένα ακόμη κριτήριο σύγκρισης με τα αποτελέσματα της στατικής ανάλυσης, μέσω της διερεύνησης των διαδρομών των φορτίων στα στατικά μέλη και του βαθμού επιρροής της γεωμετρικής διάρθρωσης του ναού στη στατική συμπεριφορά του.

Μέσω της αρχιτεκτονικής αποτύπωσης, παράχθηκε μια τρισδιάστατη γεωμετρική απεικόνιση μιας τυπικής κάθετης τομής του κεντρικού και πλευρικών κλιτών και μέσω αυτής ένα αριθμητικό προσομοίωμα, μέσω του προγράμματος πεπερασμένων στοιχείων Midas FX+ for DIANA, προκειμένου να διερευνηθούν πιθανές αιτίες δομικής βλάβης. Βασικό κριτήριο αποτέλεσε η αναπαραγωγή του υπάρχοντος μοτίβου ρωγμών και ο καθορισμός επιπέδων δομικής ασφάλειας. Μη γραμμικές στατικές αναλύσεις πραγματοποιήθηκαν, υπό την επιρροή μόνιμων φορτίων και μεταβλητών συσχέτισης, όπως ο όγκος πλήρωσης των θόλων, η παρουσία πλευρικής ώσης μέσω της στέγης και η ύπαρξη διαφορικών καθιζήσεων. Το τελικό παραγόμενο αριθμητικό προσομοίωμα της τυπικής τομής του ναού, έχοντας επαρκή συσχέτιση με την υφιστάμενη βλάβη, χρησιμοποιήθηκε για να προσδιοριστεί ο συντελεστής δομικής ασφαλείας τόσο σε πλευρική και κατακόρυφη ώθηση.

TABLE OF CONTENTS

1. INTRODUCTION 1
2. HISTORIC SURVEY 3
2.1 The Gothic Cathedrals: Design and Form – The English Gothic 3
2.1.1 Introduction 3
2.1.2 Gothic Cathedral – Plan arrangement 3
2.1.3 Decisive features of Gothic architecture 4
2.1.4 Other architectural – decorative features 12
2.1.5 The English Gothic 12
2.1.5.1 Distinctive characteristics 12
2.1.5.2 Pointed ribbed cross vault variables 13
2.1.6 Use of materials 16
2.1.7 Gothic Revival of 19th – 20th century 16
2.2 Damage in Gothic Cathedrals 17
2.2.1 Introduction 17
2.2.2 Large deformations 17
2.2.3 Cracks under tensile failure 17
2.2.4 Cracks under compressive failure 18
2.2.5 Material deterioration 18
2.2.6 Other parameters related to damage in Gothic Cathedrals 19
2.2.6.1 Construction process 19
2.2.6.2 Additions – alterations 20
2.2.6.3 Accidental loading 21
2.2.7 Specified damage in structural elements 22
2.2.7.1 Cracks in Gothic cross-vaults 22
2.2.7.1.1 Compatibility cracks 22
2.2.7.1.2 Cracks from lateral instability 22
2.2.7.2 Collapse mechanisms of macroelements 23
2.3 History of Canterbury Cathedral 24
2.3.1 Introduction 24
2.3.2 The Anglo – Saxon period (597 – 1070) 25

2.3.3 The Church of Archbishop Lanfranc 26
2.3.4 The new Choir of Archbishop Anselm (1096-1130) 27
2.3.5 The New Cathedral (1175 -1184) 28
2.3.6 14th – 19th Centuries 29
2.3.7 20th century's intervention & conservation works 30
2.3.7.1 1946 - 1968 30
2.3.7.2 1968 - 1991 31
2.3.7.3 1991 - 2013 31
2.3.7.4 2013 - present 33
3. GEOMETRICAL SURVEY 34
3.1 Introduction 34
3.2 Nave configuration 36
3.3 Lateral aisles configuration 37
3.4 Vertical abutments 39
3.5 Roof trusses in nave and lateral aisles 39
3.6 System of ties 41
3.7 Infill 42
3.8 Flying buttresses 43
4. INSPECTION AND INVESTIGATION SURVEY 44
4.1 Visual inspection plan 44
4.2 Damage survey in nave and aisles vaults 45
4.2.1 Crack pattern 47
4.2.2 Deterioration of plaster 49
4.3 Damage survey in flying buttresses of south aisle 50
4.3.1 Joint failure 53
4.3.2 Crust formation 53
4.3.3 Biological growth 54
4.4 Outward tilting of the vertical elements 55
4.5 Material properties 56
4.5.1 Caen limestone masonry 58
4.5.2 Infill material properties 60
4.5.3 Wrought iron ties and pattress plates 61

4.5.4 Softening behavior and fracture energy 61
4.5.3 Implemented material properties 63
5. DYNAMIC IDENTIFICATION TESTS 64
5.1 Introduction 64
5.2 Test preparation and setup 64
5.3 Experimental results 67
6. GRAPHIC STATICS – LINE OF THRUST 71
6.1 Stability of Gothic arches 71
6.2 Stability of flying buttresses 72
6.3 Stability of Gothic quadripartite cross vaults 73
6.4 Pseudo 3D thrust analysis with the sliding technique 73
6.5 Line of thrust in a typical bay section 75
6.6 Level of stresses 77
7. FE ANALYSIS 78
7.1 FE model generation 78
7.2 Inelastic behavior 80
7.3 FE model update 81
7.4 Simulations 84
7.5 Conclusions 104
8. CONCLUSIONS OF THE THESIS 107
9. REFERENCES 109

List of Figures

Figure 2-1. Gothic Cathedral's schematic plan (left) and cross section (right) ("Gothic Architecture" 2014b). 4

Figure 2-2. Transverse 3D representation based on Exeter Cathedral. Main architectural parts ("Nevertopia" 2014). 5

Figure 2-3. Different kinds of pointed arches in Gothic architecture ("Gothic Arches" 2014)... 6

Figure 2-4. (Left) York Minster Cathedral, England, York (1338-1408). Equilateral arches at the east front ("York Minster" 2014). (Right) Gloucester Cathedral, England (1089–1499). Depressed arches at the east front ("Gloucester Cathedral" 2014). 6

Figure 2-5. Representation of the construction process of a pointed ribbed cross-vault, by means of centering (Climent 2014). 7

Figure 2-6. (Left) In the appearing typical section of a Gothic Cathedral, the upper flying buttress receives the lateral thrust from the weight of the roof, the wind and the weight of the clerestory wall, whereas the lower one counteracts the lateral outward forces from the weight of the nave vaults. Many possible thrust lines are shown (Luca et al. 2014). (Middle) Villard de Honnecourt's drawing of the flying buttresses system at Reims Cathedral ("Reims Cathedral" 2014). (Right) Exterior view of the east front of Reims Cathedral at Reims, France (1211-1275). System of flying buttresses ("Reims Cathedral" 2014). 7

Figure 2-7. Inside view of La Sainte-Chappelle in Paris, France. 1239-1248. Stained glass windows of enormous size cover all the facades, reducing the stone framework to the minimum ("Sainte-Chappelle" 2014). 8

Figure 2-8. Salisbury Cathedral (1220-1258). The spire in the tower of the crossing is the tallest in United Kingdom (123 m in height) ("Salisbury Cathedral" 2014)..... 9

Figure 2-9. Milan Cathedral. Advanced use of pinnacles and spires in the vertical arrangement of piers, buttresses and roof gables ("Milan Cathedral" 2014). 9

Figure 2-10. (Left) Notre Dame Cathedral, Reims, France (1211). (Right) York Minster Cathedral, York, United Kingdom (1250). Typical arrangement of a Gothic Cathedral's Majesty in France and England ("Gothic Architecture" 2014a). 9

Figure 2-11. Configuration of two main timber roof trusses; King post (Left) and Queen post (Right) and their structural components ("Timber Roof Truss" 2014). 10

Figure 2-12. Connection of the timber trusses to form the structural roof system ("Timber Roof Truss" 2014). 11

Figure 2-13. Nave section, Cathedral of Notre-Dame de Reims, Reims, France (1211-1417). Timber roof truss configuration ("Cathedral of Notre-Dame" 2014)..... 11

Figure 2-14. Complex timber roof structure of Soissons Cathedral in Soissons, France (1180-1479). Photo from reconstruction during the 18th century ("Gothic Cathedral and Church Construction" 2014). 11

Figure 2-15. (Left) View of the central nave of the Canterbury Cathedral (1070-1834) in the UK. The pier molds are incorporated with the arch molds, resulting in a vertical continuity, thus creating a series of tree-like patterns ("Canterbury Cathedral" 2007). (Right) Pier section in the nave (center section), additional portion of the pier next to tower (left section) and arch mold (right section) (Willis 1845). 12

Figure 2-16. (Left) East end in York Minster Cathedral, showing the typical square configuration ("York Minster" 2014). (Right) East end of Canterbury Cathedral, having a semi-circular plan with three chapels ("Canterbury Cathedral" 2014). 13

Figure 2-17. (Left) Quadripartite pointed crossed-ribbed vault with transverse, diagonal and wall ribs, with no ridge ribs ("Medieval Construction" 2014). (Right) Durham Cathedral, England (1093-1133), Romanesque Style ("Durham Cathedral" 2014). 13

Figure 2-18. (Left, middle) Quadripartite pointed crossed-ribbed vault with ridge ribs ("Medieval Construction" 2014). (Right) St. Albans Cathedral, England (1077-1893), Romanesque/Gothic Style ("St. Albans Cathedral" 2014). 14

Figure 2-19. (Left, middle) Tierceron vault. Consists of additional secondary diagonal ribs, called tiercerons, extended from the springers to the transverse ridge ribs ("Medieval Construction" 2014). (Right) Exeter Cathedral, England (1112-1400), Norman/Gothic Style ("Exeter Cathedral" 2014). 14

Figure 2-20. (Left, middle) Lierne vault. The main and secondary diagonal ribs intersect in nodes around the boss perimeter and additional tertiary ribs span between those nodes and the boss. In more complicated connections between liernes Stellar vaults are produced ("Medieval Construction" 2014). (Right) Ely Cathedral, England (1083-1375), Romanesque /Gothic Style ("Ely Cathedral" 2014). 15

Figure 2-21. (Left, middle) Fan vault. Many ribs, having the same curvature, extend from the springers, thus forming fan-conical shaped vaults. Flat central spandrels fill the voids. Depending on the type of bay (square or rectangular) the shape of the central spandrel changes. In a more complex design, these vaults were combined with lierne ribs ("Medieval Construction" 2014). (Right) Canterbury Cathedral, England (1070-1834), Romanesque /Gothic Style. Fan square vault at the tower in the crossing ("Canterbury Cathedral" 2014). 15

Figure 2-22. (Right) Notre Dame in Paris (1163-1345). From 1845-1870 the monument undertook a controversial restoration, resulting in many additions and reconstructions, such as the chimeras that were extracted from other Gothic buildings (Left) ("Notre Dame de Paris" 2014). 16

Figure 2-23. Deformation patterns in a transverse section of Mallorca Cathedral. Chromatic scale distribution of normal stresses. The white color represents cracking. (Left) Deformation under dead load. (Right) Deformation under seismic loads (Roca et al. 2005). 17

Figure 2-24. Pier of Tarazona Cathedral. Under excessive compressive stresses stone crushing and detachment occurred (Roca et al. 2005) 18

Figure 2-25. In 1984 a great fire, believed to have been caused by a lighting strike, destroyed the timber roof of the south transept of York Minster. Additional damage was caused by the

vast quantities of water used to put out the fire. ("An Introduction to the History of York" 2014) 19

Figure 2-26. (Left) Typical cross-section of a Gothic Cathedral at an intermediate construction stage, prior to the construction of the nave's vault. Arrows showing the counteracting lateral forces. (Right-up) Construction phase involving the erection of piers and buttresses and the centering of flying buttresses. (Right-down) Sketch showing the system of timber trusses. The nave's vault is not yet constructed ("Index of /URBS110/Gothic" 2014). 20

Figure 2-27. (Left) Chronological construction phases hypothesis and additions in elevation of the central crossing tower in Wells Cathedral in UK (1176-1490). Settlements and foundation failure have occurred. (Right) FEM model of the tower showing westward leaning (D'Ayala et al. 2003) 21

Figure 2-28. Reims Cathedral, Reims, France. (Left) Picture at the time of struck from German shellfire in September 1914. (Right) Inside view. Holes in the vault system from the bombarding (Theodossopoulos et al. 2008). 21

Figure 2-29. Typical crack patterns for masonry vaults. (a) Cracks running parallel with the side walls (Sabouret's cracks). (b) Typical pathologies for some common vaults (Roca 2014). 22

Figure 2-30. Crack pattern in Gothic vaults under outward movement of the supports. (Left) Outward movement of all supports. (Right) Relative movement of middle abutments. Hinges form in the area of springing and in the proximity of the crown. Higher compressive stresses concentrate near the supports (Theodossopoulos 2008) 23

Figure 2-31. (Left) Kinematic failure mechanisms applied on the facade of Santa Maria del Mar, Barcelona, Spain (1329-1383) (Roca et al. 2010). (Right) Photo revealing fragmentation cracks due to uneven settlements and the tower's rotation (Roca 2014). 23

Figure 2-32. (Left) Aerial view of Canterbury Cathedral from southeast ("Canterbury Cathedral Aerial" 2013). (Right) Northwest view of Canterbury Cathedral ("Britain's Greatest Cathedrals" 2012). 24

Figure 2-33. (Above left) Photo taken from the nave's ceiling, showing the western apse foundation of the Saxon Cathedral ("Canterbury Cathedral" 2008). (Above right) Imaginary representation of the Anglo-Saxon Cathedral, as believed during the final phase IV (1025), comprised by the Cathedral and many additional buildings ("AD 1000 - Canterbury Cathedral" 2007). (Below) Plan of the Anglo-Saxon Cathedral showing parts from the four different phases, as identified from the archaeological excavation in 1993 ("Canterbury Cathedral" 2008). 26

Figure 2-34. (Left) Ground plan of Lanfranc's Canterbury Cathedral (1070-1077). The exact form of the apses is uncertain, as only remains of their foundations were uncovered. The plan and proportions were based on Lanfranc's abbey in Normandy (Dudley 2010). (Right) Imaginary representation of Canterbury's Norman Cathedral under Archbishop Lanfranc (1077), comprised by the Cathedral and many additional buildings ("Canterbury Cathedral" 2007). 27

Figure 2-35. Plan of Canterbury Cathedral in 1174. The lighter shading pattern in the crossing of the new Choir is the intersecting termination of Lanfranc's Cathedral on the eastern front (Willis 1845). 27

Figure 2-36. (Left) Ground plans of Canterbury Cathedral as it evolved over time, from 1070 to 1175. (a) The Cathedral of Lanfranc, (b) the Cathedral of Anselm, (c) the Cathedral of William of Sens ("Canterbury Cathedral" 2007).(Right) Transverse section of the choir. In the left cross section the new Gothic Choir after the reconstruction is presented. In the right part of the cross section Archbishop Anselm's Choir before the fire is depicted. (Willis 1845)..... 28

Figure 2-37.(Above) Geometrical representation of Canterbury Cathedral's west front in different time phases (Dudley 2010): (a) The geometry of Lanfranc's west front 1070-1077, (b) Prior's Thomas Chillenden west front completed in 1401, (c) Completion of southwest tower in 1459, (d) First construction phase of central tower (1470-1490) after demolition in 1430. Architects: R. Beck & J. Wastell, (e) Second construction phase of central tower completed in 1504 by J. Wastell, (f) Aspect of the west front as it exists in present time. (Below left) The west front aspect of Canterbury Cathedral in 1821 before the completion of the north-west tower ("Canterbury Cathedral" 2014). (Below right) West front configuration of Canterbury Cathedral at present time ("Canterbury Cathedral" 2005). 30

Figure 2-38.View of the interior nave roof void, depicting the concrete infill layer and the drilled hole for drainage. 32

Figure 2-39. (Left) The Great South Window of the South West Transept behind scaffolding. (Right above) Inside view of the Great South Window tracery of the South West Transept. The glass panels have been removed and stone parts are been taken off piece by piece. (Right below) Process of removal of damaged stone masonry in the Great South Window tracery of the South West Transept which will later be replaced by replicas. View of the tracery at top level. ("The Great South Window" 2014). 33

Figure 3-1. (Left) Top plan of Canterbury Cathedral depicting the nave and lateral aisles area, as well as the case study area of the critical cross sections. (Right) Transverse cross section of the nave and lateral aisles of Canterbury Cathedral looking west (Morton Partnership Ltd). 34

Figure 3-2. Longitudinal cross section and top plan of the nave, transepts and choir of Canterbury Cathedral (Willis 1845). 34

Figure 3-3. Top plan of the vertical abutments and vault configuration of the critical area of the nave, depicting dimensions (meters) based on the historic survey, the in situ inspection and the geometrical survey provided by Morton Partnership Ltd. 35

Figure 3-4. Generated geometrical model of the critical transvers cross section of Canterbury Cathedral's nave and the adjoining part of the cloister. 35

Figure 3-5. Generated geometrical model of the nave of Canterbury Cathedral and the adjoining part of the cloister. 36

Figure 3-6. (Left) View of the nave of Canterbury Cathedral looking east. (Right) View of the Gothic lierne quadripartite cross vaults of the nave of Canterbury Cathedral (Photographic survey). 37

Figure 3-7. Gothic cross vault configuration and dimensions (meters) in the nave of Canterbury Cathedral and adjacent clerestory arches, as generated for the 3D CAD model. 37

Figure 3-8. (Left) View of the north aisle of Canterbury Cathedral looking east. (Right) View of the south aisle of Canterbury Cathedral looking east (Photographic survey). 38

Figure 3-9. Gothic cross vault configuration and dimensions (meters) in the south aisle of Canterbury Cathedral with the adjacent arcade arch (left) and the aisle window arch (right), as generated for the 3D CAD model. 38

Figure 3-10. Sections depicting the actual and chosen equivalent dimensions (meters) and area of the piers and buttresses of Canterbury Cathedral (Willis 1845). 39

Figure 3-11. Structural parts of the roof framing in the nave of Canterbury Cathedral and section areas (millimeters). 40

Figure 3-12. Structural parts of the roof framing in the south aisle of Canterbury Cathedral and section areas (millimeters). 40

Figure 3-13. View of the roof void in the south aisle looking west (Photographic survey). 41

Figure 3-14. (Left) External view of the nave clerestory walls of Canterbury Cathedral, depicting the two anchor cross shaped plates on the right side of each transverse section (Morton Partnership Ltd). (Right) Inside view of the roof void in the nave of Canterbury Cathedral, depicting the iron tie in the clerestory walls above the vaults (Photographic survey). 41

Figure 3-15. (Left) View of the iron tie at mid span (Right) Coupling system at the mid span of the iron tie (Photographic survey). 42

Figure 3-16. (Left) 3D representation of the south 3D CAD model of the critical nave section of Canterbury Cathedral, depicting the infill volumes. (Middle) Infill and cross vault system at south aisle roof void. (Right up) Infill and cross vault system at nave roof void. (Right down) Drilled hole in the exterior wall at the level of concrete layer infill, used for drainage (Photographic survey). 42

Figure 3-17. (Left) East view of flying buttress in the south aisle of Canterbury Cathedral, depicting dimensions (meters) on the interface between the clerestory wall and vertical buttress, as well as elevation levels from base. (Right down) View of the south aisle of Canterbury Cathedral, presenting the system of vertical and flying buttresses (Photographic survey). 43

Figure 4-1. Top plan of Canterbury Cathedral depicting the sections and bays of the nave and lateral aisles, consisting the case study area (Morton Partnership Ltd). 44

Figure 4-2. (Left) View of the nave and lateral aisles of Canterbury Cathedral looking east ("Canterbury Cathedral" 2014). (Right) 3D representation of the vaults intrados in the nave and lateral aisles of Canterbury Cathedral. 45

Figure 4-3. Damage map of the intrados of the vault system in the nave and lateral aisles of Canterbury Cathedral. 46

Figure 4-4. (Left) Amplified deformation of Burgos Cathedral cross section. The springing of the aisle vault spreads inwards, while the upper part of the nave deforms outwards. (Right) FEM model representing the large deformation of a vault in St. Francis Basilica under excessive outward movement, leading to the collapse of the vault, caused by the earthquake in September 1997 (Theodossopoulos et al. 2008). 47

Figure 4-5. Damage map of the case study area, which depicts the current and former estimated infill boundaries..... 48

Figure 4-6. Corner detachment of a vault, provoked by differential settlements and rotations at base, in the Monastery of Salzedas, Portugal (Lourenço et al. 2008)..... 49

Figure 4-7. Possible magnified displacement field of a medium-end settlement, induced in the south part of the foundation of Canterbury Cathedral, which affects the vertical abutments of the south part of the nave and aisle by inducing vertical translations and outward leaning. 49

Figure 4-8. (Left) Graphic representation of the nave and lateral aisles of Canterbury Cathedral. The flying buttresses 2 and 3, for which damage maps were prepared, are depicted in red. (Right) View of the flying buttresses of the south aisle looking west..... 50

Figure 4-9. Damage maps of the west and east view of flying buttress 2 at the south aisle of Canterbury Cathedral..... 51

Figure 4-10. Damage maps of the west and east view of flying buttress 3 at the south aisle of Canterbury Cathedral..... 52

Figure 4-11. Crack patterns of joint failure from west view of flying buttress 2 (Left) and 3 (Right) of the south aisle of Canterbury Cathedral. 53

Figure 4-12. Crust formation and flaking in large areas of Caen stone masonry from west views in the flying buttress 3 of the south aisle of Canterbury Cathedral. 54

Figure 4-13. Biological growth in form of algae, mosses and higher plants in the upper surface of flying buttress 3 (east view) in the south aisle of Canterbury Cathedral. 54

Figure 4-14. Cross section 3 depicting the south aisle and half of the nave of Canterbury Cathedral, prepared by the Downland Partnership Ltd and provided by the Morton Partnership Ltd. The inclination of the vertical abutments is depicted in red..... 55

Figure 4-15. Determination of knowledge levels and confidence factors, corresponding to the extent of material testing and on-site inspections (Franchetti 2014). 57

Figure 4-16. Test results from double flat jack tests and sonic pulse velocity, performed in different stone masonry typologies of Campi Alto di Norcia (Perugia, Italy) (Cardani et al. 2013). 57

Figure 4-17.Values of the elastic modulus, obtained by double flat jack tests on different masonry typologies. The results have been grouped in order to allow a comparison of values for regular stonework with thin joints, brickwork, and irregular stone masonry (Binda et al. 2007). 60

Figure 4-18. Stress - displacement diagrams of quasi-brittle materials under tensile (left) and compressive (right) loading (Lourenço 1998). 61

Figure 4-19. Shear stress - displacement diagram of quasi-brittle materials (Lourenço 1998). 62

Figure 4-20. Solid clay brick masonry tests and numerical results are presented in diagrams. (Left) Uniaxial tension - crack displacement diagram. (Middle) Shear stress - crack displacement diagram. (Right) Uniaxial compression - crack displacement diagram (Lourenço 1998). The shaded areas represents the experimental envelope of tests. 62

Figure 5-1. Measuring equipment: (a) accelerometer on the intrados springing of the flying buttresses, (b): accelerometer on the exterior cladding of the nave wall, (c) and (d): data acquisition equipment. 65

Figure 5-2. Disposition of accelerometers in performed Setups of the dynamic identification tests (Reference sensors depict in red colour). 66

Figure 5-3.Data driven with the poles selection through the several test setups of the Stochastic Subspace Identification method. 67

Figure 5-4. Mode shapes obtained from the Setups 1, 3 and 4. 68

Figure 5-5. MAC values obtained from the Setups 1, 3 and 4. 69

Figure 5-6. Averaged Normalized Power Spectral Density for the vertical accelerometers of the Setup 2 and 5. 70

Figure 5-7. Averaged Normalized Power Spectral Density for the horizontal accelerometers of the Setup 5. 70

Figure 6-1. The minimum and maximum thrust line that defines the boundaries of the stability of a pointed Gothic arch. The five hinges for the maximum thrust are depicting (Block et al. 2006). 71

Figure 6-2. Failure mechanism in a circular arch under spreading of the abutments. The three hinges of central part of the arch are depicting (Block et al. 2006). 71

Figure 6-3. The flying arch in Agnicourt church in France is considered to be in state of minimum thrust (Block 2005). 72

Figure 6-4. (Left) Line of thrust in flying buttress of the south aisle of Canterbury Cathedral in corresponding bay 3. (Right) Damage map of the flying buttress of section 3 with the documented hinge, which was used as reference to conduct the thrust analysis. 72

Figure 6-5. Thrust trajectories in cross vaults in three dimensional (Top row) and plan view (Bottom row), targeting the springings with different configurations, which are comprised of (a) parallel and diagonal arches, (b) arches directly from the springings, (c) superposition of first two patterns, (d) quadrilateral arches in plan, directly from the springings, (e) triangulated patterns in each quarter of the vault, parallel to the diagonals (Block et al. 2014). 73

Figure 6-6. A 3D pseudo thrust analysis applied in a Gothic ribbed cross vault, using the sliding technique, in order to obtain the line of thrust (Block 2009). 74

Figure 6-7. Schematic representation of the resultant thrust in the springing of a Gothic cross vault. 74

Figure 6-8. Cross section of the typical bay in the nave of Canterbury Cathedral depicting the macroblocks and the points of application with the force vectors of the transversal structural elements. 75

Figure 6-9. Cross section of the typical bay in the nave of Canterbury Cathedral depicting the line of thrust and the potential hinges, where the thrust line is tangent to the boundaries of the structural elements. 76

Figure 6-10. Stress distribution of a cross section when the resultant force is applied within its middle third (Pela et al. 2014b). 77

Figure 7-1. East view (a) and 3D view (b) of the elaborated FE model of the typical bay in the nave of Canterbury Cathedral, depicting the FE mesh. 78

Figure 7-2. Quality mesh check in relation the aspect ratio of elements. 79

Figure 7-3. (Left) View of a TE12L isoparametric solid pyramid element, with three sides and four nodes. (Right) View of a L2TRU two-node directly integrated (1-point) truss element (DIANA 2014a). 79

Figure 7-4. (Left) Crack stress and strain curve, specifying the tensile behavior of stone masonry with an exponential softening function, beyond the tensile strength. (Right) Crack stress and strain curve, specifying the compressive behavior of stone masonry with a parabolic curve (DIANA 2014b). 80

Figure 7-5. (Left) the Modified Newton-Raphson iteration method. (Right) Convergence under the energy norm (DIANA 2014b). 80

Figure 7-6. 1st mode shape configuration of the typical bay. 81

Figure 7-7. Mode shape configuration of modes 1 to 9, with the natural frequencies. 82

Figure 7-8. Mode shape configuration of modes 10 to 16, with the natural frequencies. 83

Figure 7-9. (Left) Deformed shape (x100) with displacement gradient at last load step. (Right) Distribution of maximum principal strains at last load step. 85

Figure 7-10. (Left) Distribution of maximum principal strains at the 40% of dead load. 85

Figure 7-11. (Left) Distribution of minimum principal stresses at last load step. (Right) Distribution of crack width, depicting widths larger than 0.4 mm. 86

Figure 7-12. Load displacement diagram, depicting the vertical displacements of the crowns in the nave and lateral aisles versus the load steps in which the self-weight is applied. 86

Figure 7-13. Load displacement diagram, depicting the horizontal displacements of the span in the nave and lateral aisles versus the 10 load steps in which the self-weight is applied. .. 87

Figure 7-14. Load displacement diagrams depicting the South aisle and nave span opening, under dead loading. 87

Figure 7-15. Cross section of the FE model of the typical bay, with the infill heights are depicted. 88

Figure 7-16. For the three different infill heights: (a) Load versus vertical displacement diagram of the nave's crown. (b) Load versus vertical displacement diagram of the south

aisle's crown. (c) Load versus horizontal displacement diagram of the nave's crown. (d) Load versus horizontal displacement diagram of the south aisle's crown. 89

Figure 7-17. : Deformed shape (x100) at last load step (Left) and distribution of maximum principal strains at last load step in a slicing plane at the symmetry axis (Right), for the reference infill height (Top row), the past estimated infill height (Middle row) and the current infill (Bottom row). 90

Figure 7-18. Modeling of the foundation soil with springs of vertical and horizontal stiffness coefficients. 91

Figure 7-19. Geometric configuration of a foundation in plan (a) and cross section (b) view. 91

Figure 7-20. Load displacement diagram, depicting the vertical displacements at the base of vertical abutments, under dead loading. 94

Figure 7-21. Load displacement diagram, depicting the span opening and absolute horizontal displacements of the south aisle vault, under dead loading. 95

Figure 7-22. (Left) Deformed shape (x100) with displacement gradient at last load step. (Right) Distribution of maximum principal strains at last load step, in 3D view from above. .. 96

Figure 7-23. (Left) Distribution of minimum principal stresses at last load step. (Right) Distribution of normal strain cracks. 96

Figure 7-24. Deformed shape (x100) with displacement gradient of Model 1 (Left) and Model 2 (Right), at a corresponding load step of a 3 mm crack width at the middle span of the south flying buttress. 98

Figure 7-25. (Left) Distribution of minimum principal stresses of Model 1 (Left) and Model 2 (Right), at a corresponding load step of a 3 mm crack width at the middle span of the south flying buttress. 98

Figure 7-26. Distribution of minimum principal stresses of Model 1 (Left) and Model 2 (Right), at a corresponding load step of a 3 mm crack width at the middle span of the south flying buttress. 99

Figure 7-27. Distribution of crack width distribution at the south flying buttress, at load step 15 in Model 1 (Left) and at load step 22 in Model 2 (Right), with a gradient larger than 3mm. 99

Figure 7-28. Load displacement diagram, depicting the vertical capacity in terms of vertical displacements of the nave crown. 100

Figure 7-29. (Left) Deformed shape (x100) with displacement gradient at last load step of vertical capacity loading. (Right) Distribution of maximum principal strains at last load step of vertical capacity loading. 101

Figure 7-30. (Left) Distribution of minimum principal stresses at last load step at last load step of vertical capacity loading. (Right) Distribution normal strain cracks, depicting cracks larger than 0.3 mm at last load step of vertical capacity loading. 101

Figure 7-31 Load displacement diagram, depicting the lateral capacity in terms of horizontal displacements of the crown of the south aisle vault. 101

Figure 7-32. (Left) Deformed shape (x100) with displacement gradient at last load step of lateral capacity loading. (Right) Distribution of maximum principal strains at last load step of lateral capacity loading. 102

Figure 7-33. (Left) Distribution of minimum principal stresses at last load step of lateral capacity loading. (Right) Distribution normal strain cracks, depicting cracks larger than 0.3 mm at last load step of lateral capacity loading. 102

Figure 7-34. Load displacement diagram, depicting the vertical capacity in terms of vertical displacements of the nave crown. 103

Figure 7-35. (Left) Deformed shape (x100) with displacement gradient at last load step of vertical capacity loading. (Right) Distribution of maximum principal strains at last load step of vertical capacity loading. 104

Figure 7-36. (Left) Distribution of minimum principal stresses at last load step at last load step of vertical capacity loading. (Right) Distribution normal strain cracks, depicting cracks at last load step of vertical capacity..... 104

Figure 7-37. (Left) Distribution of maximum principal strains at last load step under dead loads and the present level of infill, in the interior section of the south aisle vault, under dead loading in the current state. (Right) Corresponding crack surrounding the pier of the south aisle at section 3. 105

Figure 7-38. (Left) Distribution of maximum principal strains at 40% of dead loads and the present level of infill, in the interior section of the south aisle vault. (Right) Corresponding crack in the intersection between the web and the aisle window, at section 3. 105

Figure 7-39. (Left) Distribution of maximum principal strains at last load step, in a slicing plane at the symmetry axis, under differential settlements. (Right) Cracks at the top part and the middle span of the south flying buttress, in section 3. 106

List of Tables

Table 4-1. Reference values of the mechanical parameters and average specific weights for selected types of masonry (extract from Table C8A.2.2. of Circ. NTC08, 2009). 58

Table 4-2.Characteristic shear strength, in absence of vertical load, for masonry with natural stone elements (NTC 08 - Table 11.10.VII) 59

Table 4-3. Mechanical properties of faggoted (wrought) iron rods (Holický et al. 2005). 61

Table 4-4. . Fracture energy of the materials (Lourenco 2014) 62

Table 4-5. Mechanical properties of Caen stone masonry, infill masonry, wrought iron ties and pattress plates. 63

Table 5-1. Frequencies and damping ratios of the first 12 modal shapes (Setups 1, 3 and 4). 67

Table 7-1. Coefficient and variables of vertical stiffness of the foundation soil at the north and south buttress. 93

Table 7-2. Coefficient and variables of horizontal stiffness of the foundation soil at the north and south buttress. 93

Table 7-3. Coefficient and variables of horizontal and vertical stiffness of the foundation soil at the north and south pier. 93

1. INTRODUCTION

The evaluation of the structural behavior and pathology in works of the architectural heritage, stands as the keystone in efficient restoration and conservation studies. The current case study, regarding the "Canterbury Cathedral – Structural Analysis of the South Aisle" had as a main objective to assess and inspect the state and level of damage and to differentiate between various hypotheses responsible for the existing structural damage. In the process of evaluation and reproduction of damage mechanisms, through analytical modelling, several aspects of the structural system of the nave in Canterbury Cathedral were determined by means of the historic survey, in situ inspection and testing.

The nave and lateral aisles of Canterbury Cathedral were reconstructed in the Perpendicular English Gothic style, by Prior Thomas Chillenden, in 1391-1411, out of Caen stone masonry. A system of piers in the central nave, with engraved vertical shafts, supports a system of quadripartite lierne cross vaults, with principal and secondary ribs intersecting in nodes and bosses, reaching a height of 25 meters. The lateral aisle vaults are of the same configuration, with a height of 15 meters. On the exterior, a system of vertical and flying buttresses counteracts the lateral thrusts from the roof and vaults, with a system of wrought iron ties at the level of the nave's roof. An outward lateral movement, accompanied with cracking at the flying buttresses of the south aisle, has been observed, along with a repetitive crack pattern in the intrados of the vaults, which are indicative of active phenomena of structural damage.

In Chapter 1 of the thesis a short introduction of the work is stated.

In Chapter 2 the historic survey is presented, covering the architectural aspects and configuration of Gothic Cathedrals and the English Gothic style, a classification damage pattern in Gothic Cathedrals and the architectural history of Canterbury Cathedral.

Chapter 3 contains the results of the geometrical survey, from data gathered during the onsite inspection and the historic survey. Structural parts of the nave and lateral aisles are defined and a 3D CAD model of a typical transversal cross section is generated.

Chapter 4 presents the findings of the damage survey, conducted in situ, in terms of damage maps of the nave's and lateral aisles vaults intrados and two flying buttresses of the south aisle which suffered the greater damage.

In Chapter 5 the dynamic identification of the south part of the Cathedral is presented, based on ambient vibration tests, performed in situ.

In Chapter 6 the Graphic Statics analysis of the nave's transversal cross section is presented, in order to obtain a line of thrust and indications on how the Cathedral's geometric configuration is related with its structural stability.

Chapter 7 contains the numerical analysis simulations of a built FE model of the nave's typical cross sections in Midas FX+ for DIANA software. After the determination of the materials inelastic behavior and the update of the FE model, from the modal identification tests, various analyses under certain hypotheses were conducted, to reproduce the existing damage and determine levels of structural safety.

Lastly, Chapter 8 contains the conclusion of the thesis, followed by the references' list.

2. HISTORIC SURVEY

2.1 The Gothic Cathedrals: Design and Form – The English Gothic

2.1.1 Introduction

Gothic architecture is mostly a sacred architecture with a significant symbolic function. It was mainly associated with churches, cathedrals and abbeys which were the most prominent works produced. Originated in the 12th century, successor of Romanesque architecture and lasting until the 16th century, the Gothic style has produced many of the most profound works of religious architecture in Europe. Many of the high cathedrals of that time served as a landmark of both faith, wealth, power and distinction in societies under influence of the Catholic Church. A series of Gothic architectural revivals in the 18th century have also contributed in the progression of neo-Gothic buildings or alterations worldwide ("Gothic Architecture" 2014a; "Gothic Revival Architecture" 2014).

Moreover, Gothic ecclesiastic architecture, reflected the idea of a sanctuary served to generate religious emotions, but also inducing a fearful respect for the supernatural entity, through a complex incorporated architectural form (Simson 1988).

2.1.2 Gothic Cathedral – Plan arrangement

The Gothic Cathedral adopts a Latin cross ground plan, but with many alternate variations. The main axis coincides with the east-west orientation, but always in an approximate way. Along the main axis the central nave is formed and in the transverse direction the arms are called transepts. The nave is usually laterally tracked by aisles on both sides, of mostly single, but sometimes double configuration (Figure 2-1). The extension of the nave after the transepts is the choir, containing the sanctuary and the altar. A motif of a semi-circular passageway called ambulatory, with chevette chapels is often present, forming as an extension from the aisles. The nave expanding higher than the lateral aisles allows the forming of clerestory windows. The role of transferring the horizontal thrust is played partly by vertical buttresses along the perimeter and flying buttresses in the aisle roof level. Both systems are crucial parts of the Gothic skeleton structure and extend along the colonnade axis grid, allowing large windows in all facades ("Gothic Architecture" 2014b).

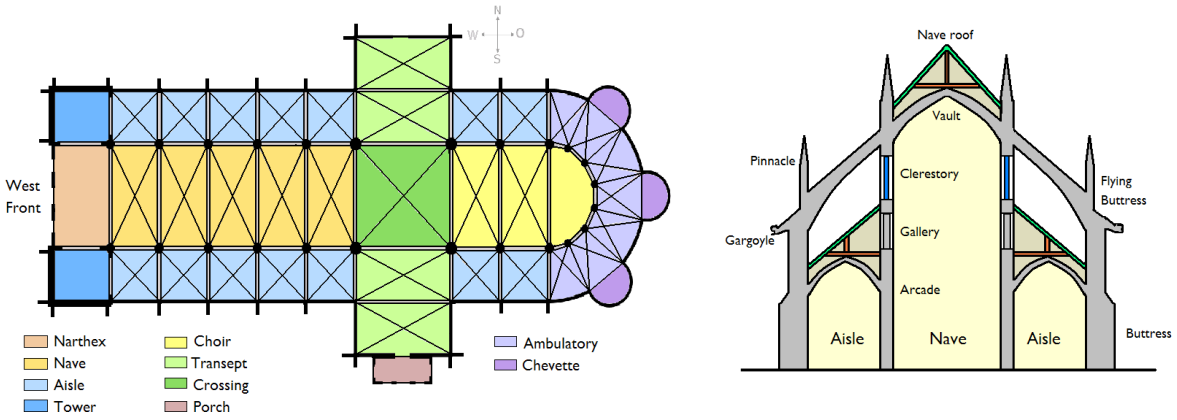

Figure 2-1. Gothic Cathedral's schematic plan (left) and cross section (right) ("Gothic Architecture" 2014b).

2.1.3 Decisive features of Gothic architecture

Gothic architecture is characterized by distinctive architectural, structural and decorative features. Although, many of which have been formerly used, such as the flying arches in the Byzantine period and the cross vaults in Roman and Medieval architecture. Nevertheless, the combination of these elements can be considered unique, mainly due to their serving purpose, their geometric proportions and their overall incorporation of the purely skeletal Gothic style (Figure 2-2). The most relevant building elements and features are addressed next ("Gothic Architecture" 2014a; "Gothic Architecture" 2014b).

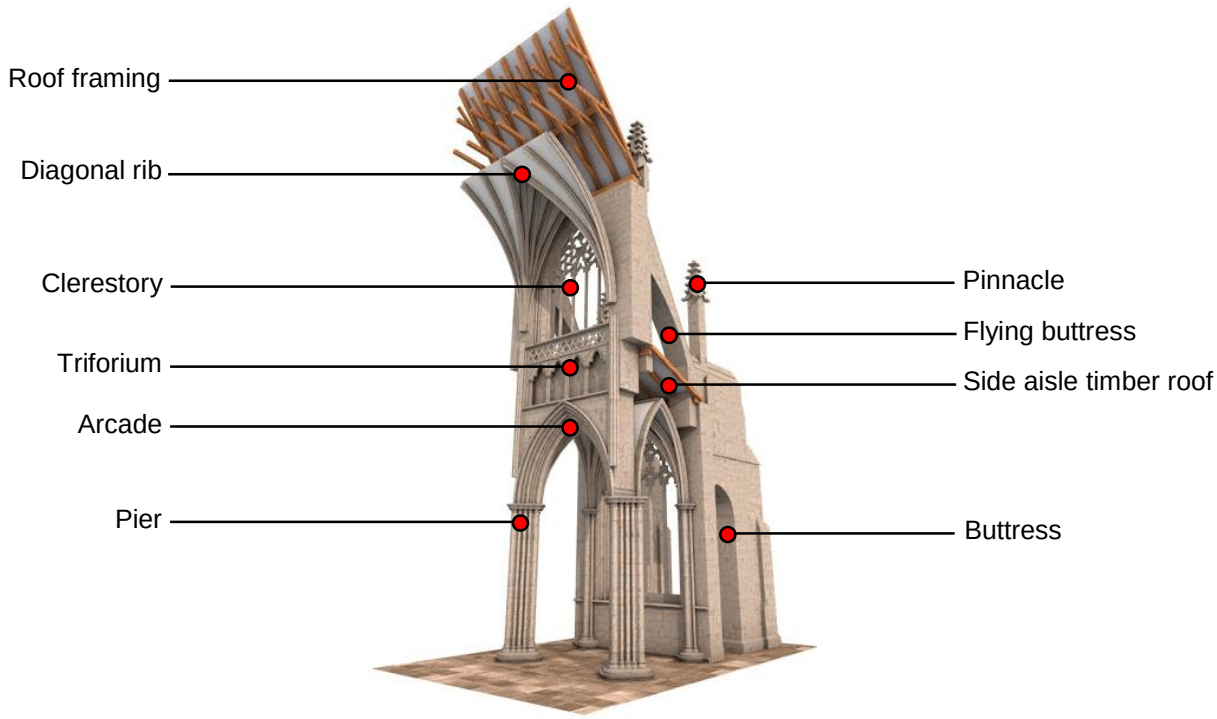

Figure 2-2. Transverse 3D representation based on Exeter Cathedral. Main architectural parts ("Nevertopia" 2014).

Pointed arch: A pointed arch, unlike the semi-circular or segmental one, transfers the horizontal thrust to the vertical abutments at a much steeper angle, thus decreasing the horizontal component. Every opening window and passage is constructed with a pointed arch that can have many shapes or styles (Figure 2-3, 4). This allowed the architects to raise the Gothic vaults at a much higher level, attaining forms with flexibility, verticality and slenderness. Many designs were implemented to fill in these windows with stained glass and stonework supporting frames, called tracery. The Gothic arch can have the main following configurations: ("Gothic Architecture" 2014a; "Gothic Architecture" 2014b)

1. Equilateral arch: Designed upon the equilateral triangle, where the radius of each intersecting arch is equal to the span.
2. Lancet arch: The center of the arc lies outside the opposite arc and is larger than its span. Thus becoming more steeply pointed. The windows are narrower.
3. Depressed arch: A much wider arch, with its span much wider than its height that gives the impression of being compressed under weight. Constructed by four arcs, two of a small radius close to the springs and two with a larger radius close to the rise.

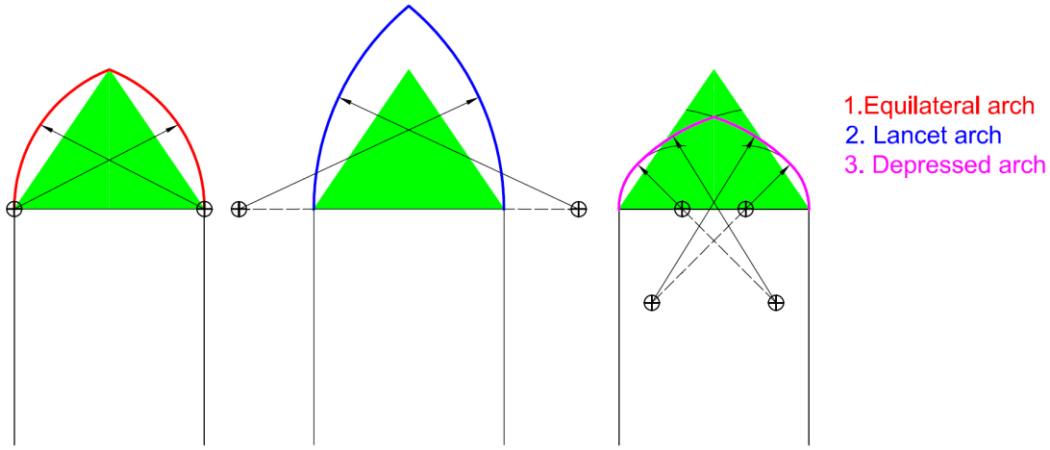

Figure 2-3. Different kinds of pointed arches in Gothic architecture ("Gothic Arches" 2014).

Figure 2-4. (Left) York Minster Cathedral, England, York (1338-1408). Equilateral arches at the east front ("York Minster" 2014). (Right) Gloucester Cathedral, England (1089–1499). Depressed arches at the east front ("Gloucester Cathedral" 2014).

Cross-ribbed vault: The pointed cross-ribbed vault system was introduced in the Romanesque period, evolved and established as the trademark of the Gothic architecture. Basically, the use of a pointed cross vault allows the covering of more irregular and not perfectly squared plans, by altering independently the width and height of the adjoining pointed arches. The vaults were made of ribs, starting from all springing points and intersecting at the center point (boss). The corresponding voids were later filled with brick or stone masonry of a much thinner thickness (Figure 2-5) (Climent 2014).

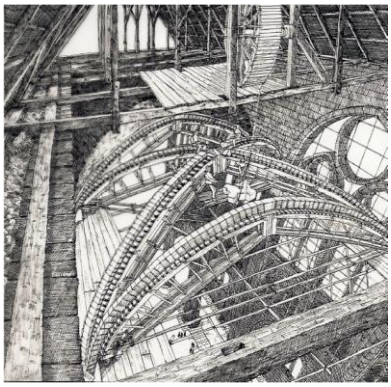

Figure 2-5. Representation of the construction process of a pointed ribbed cross-vault, by means of centering (Climent 2014).

Flying buttress: A significant feature of Gothic architecture is the free standing buttress in a sloping arch shape, attached in between the nave's exterior wall and the vertical buttresses of the aisles, choir and transept walls. In Gothic cathedrals there can be one or two flying buttresses per cross-section on each side. Their main role is to counteract with the outward lateral pressures and bulging effects from the vaults and the roof system, transferring them downwards to the piers and vertical buttresses (Figure 2-6) ("Gothic Cathedral and Church Construction"2014).

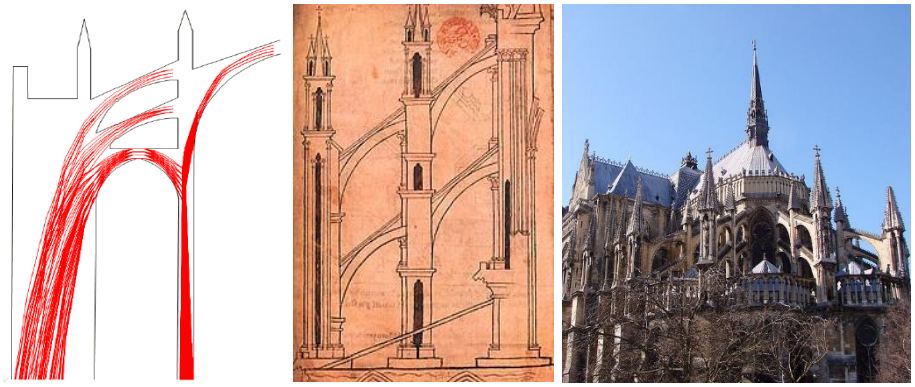

Figure 2-6. (Left) In the appearing typical section of a Gothic Cathedral, the upper flying buttress receives the lateral thrust from the weight of the roof, the wind and the weight of the clerestory wall, whereas the lower one counteracts the lateral outward forces from the weight of the nave vaults. Many possible thrust lines are shown (Luca et al. 2014). (Middle) Villard de Honnecourt's drawing of the flying buttresses system at Reims Cathedral ("Reims Cathedral" 2014). (Right) Exterior view of the east front of Reims Cathedral at Reims, France (1211-1275). System of flying buttresses ("Reims Cathedral" 2014).

Extensive use of light: Gothic cathedrals are much more luminous than the prior Romanesque ones. Light comes through the large stained glass windows from the free spans to the exterior and the formed clerestories, due to the difference of height between the nave and the lateral aisles. The use of pointed ribbed cross vaults lessened the outward thrust, which is redirected in the corners springs and is taken by the vertical abutments, allowing the opening of large windows in between (Figure 2-7) (Simson 1988).

Figure 2-7. Inside view of La Sainte-Chappelle in Paris, France. 1239-1248. Stained glass windows of enormous size cover all the facades, reducing the stone framework to the minimum ("Sainte-Chappelle" 2014).

Immense height: A nave's height is usually higher than its width. Particularly in England the proportion of many cathedrals is 2:1 or even higher ("Gothic Architecture" 2014a).

Towers: One of the most distinctive features of Gothic cathedrals is the presence of towers and spires in the architectural configuration. Their number, form and positioning varies, depending on the leading architectural influences in each country. Some cathedrals have two towers in the west facade, others just one. In England a typical arrangement has two towers in the west facade and another tower of immense size at the crossing (Figure 2-8) ("Gothic Architecture" 2014a).

Pinnacles & Tall spires: The vertical character of Gothic architecture is emphasized by the addition of many vertical decorative components, such as pinnacles and spires. Buttresses, piers and gable ends are prolongated above the roofline with smaller size pinnacles. Milan Cathedral constitutes as an extreme example of this feature (Figure 2-9) ("Gothic Architecture" 2014a).

Majesty: The west front of a Gothic Cathedral, serves as the main gate and is designed to create an overwhelming impression. The central arch (archivault) often contains large sculptural scenes. Above it, a large window or a group of smaller ones is formed. In France there is typically a rose window, whereas in England there is a pointed arch one. The gable is usually richly decorated with statuary (Figure 2-10) ("Gothic Architecture" 2014a).

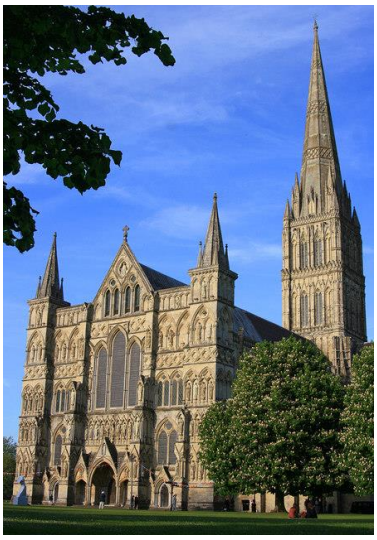

Figure 2-8. Salisbury Cathedral (1220-1258). The spire in the tower of the crossing is the tallest in United Kingdom (123 m in height) ("Salisbury Cathedral" 2014).

Figure 2-9. Milan Cathedral. Advanced use of pinnacles and spires in the vertical arrangement of piers, buttresses and roof gables ("Milan Cathedral" 2014).

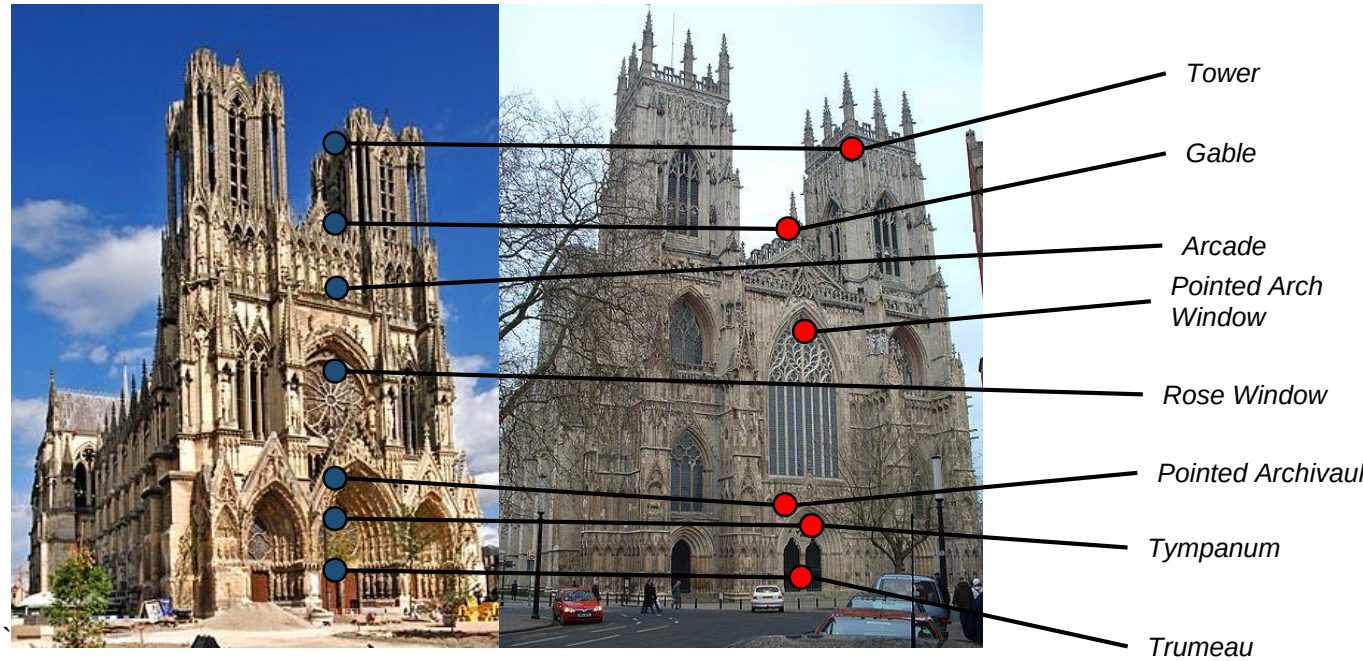

Figure 2-10. (Left) Notre Dame Cathedral, Reims, France (1211). (Right) York Minster Cathedral, York, United Kingdom (1250). Typical arrangement of a Gothic Cathedral's Majesty in France and England ("Gothic Architecture" 2014a).

High pointed roofs: The pitch of the Gothic roofs is rather high (about 55^o), with some extreme cases reaching 60^o and 65^o. In Gothic Cathedrals the roof system was structurally separated from the vaults. The clerestory walls from the nave extended beyond the level of the vaulted ceiling as much as 1.5-2.0 meters. The trusses are then fixed on the top to a ridge board and on the bottom to a wall plate, a timber beam or a set of beams spread along the wall's main axis. Generally the roof trusses were designed as rigid structural elements, cross-pinned, with a resistance to lateral spreading of the two slopes at the base. Metallic-edged blades and a variety of complex joining, were used to ensure the functionality of the hinged joint system. Wind lateral loads were redirected from the system of flying buttresses downwards to the piers and buttresses (Fitchen 1981).

Three main timber truss configurations were implemented in Gothic Cathedrals; the king post, the queen post and the combined type. In the king post the truss consists of a horizontal tie beam, two principal inclined rafters and a vertical member in the center. A common configuration is that the king post is stiffly connected to the tie beam at the mid-span. By two inclined struts, the king post is connected with the rafters. When the covering span is significant (more than 9m), a queen post truss was chosen. The truss consists of two principal rafters and two vertical queen posts connected to the tie beam. Thus, the tie beam is upheld and supported at two points (Figure 2-11). Lastly, in the case of the combined system, the queen post truss above the level of the straining beam is connected to a king post truss. The king post is tied in the straining beam ("Timber Roof Truss" 2014).

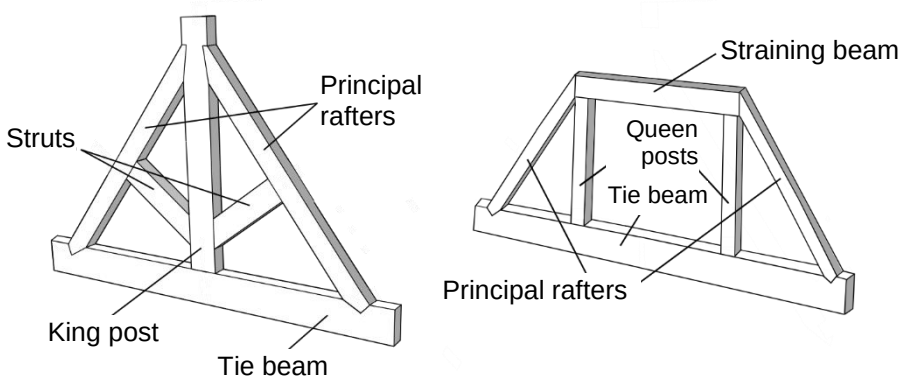

Figure 2-11. Configuration of two main timber roof trusses; King post (Left) and Queen post (Right) and their structural components ("Timber Roof Truss" 2014).

In between the timber trusses, a system of common rafters receives the roof's loading and transfers it through a system of transverse beams called purlins and the ridge board to the trusses (Figure 2-12) ("Timber Roof Truss" 2014).

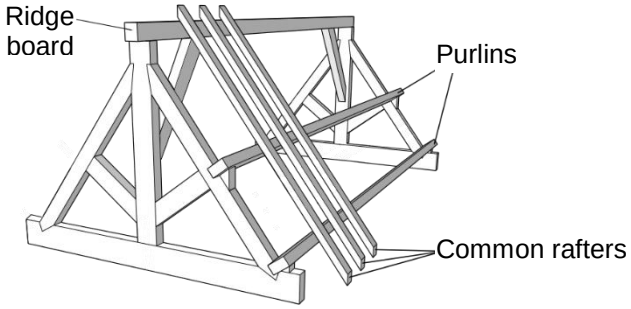

Figure 2-12. Connection of the timber trusses to form the structural roof system ("Timber Roof Truss" 2014).

The timber roofing trusses of great cathedrals were most of times massive and complex, with large configuration diversity (Figure 2-13). Due to fires many of the original timber roofs in Gothic Cathedrals were replaced during the course of time (Figure 2-14) ("Gothic Cathedral and Church Construction" 2014).

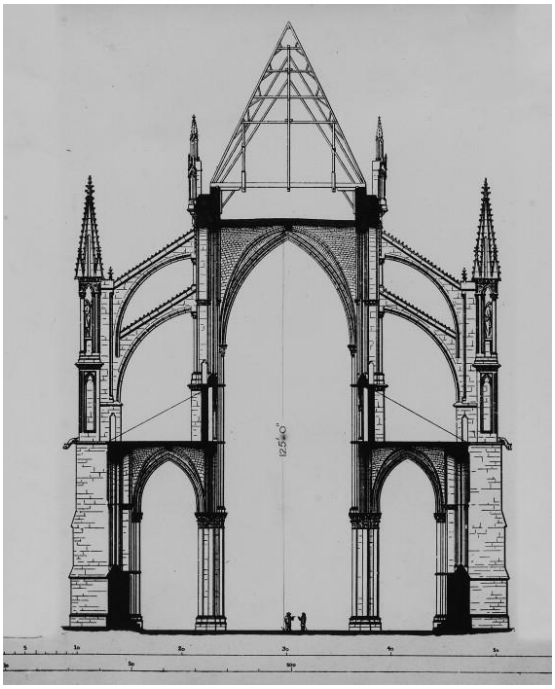

Figure 2-13. Nave section, Cathedral of Notre-Dame de Reims, Reims, France (1211-1417). Timber roof truss configuration ("Cathedral of Notre-Dame" 2014).

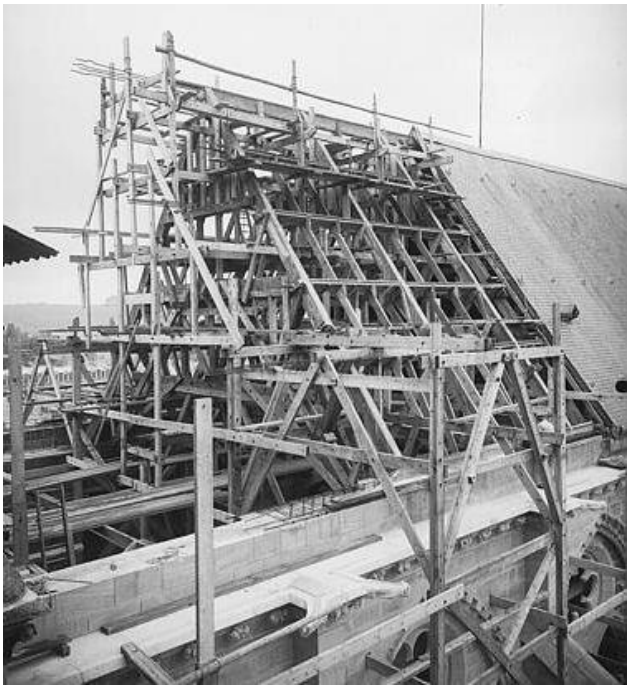

Figure 2-14. Complex timber roof structure of Soissons Cathedral in Soissons, France (1180-1479). Photo from reconstruction during the 18th century ("Gothic Cathedral and Church Construction" 2014).

2.1.4 Other architectural – decorative features

The vertical character of Gothic architecture is also emphasized by sweeping the vertical shafts engraved in structural elements from floor to ceiling, where they meet the ribs of the vaults, giving often the impression of a tree like arrangement with various branches (Figure 2-15) ("Gothic Architecture" 2014a).

The architectural form is based on a clearer structural appearance. The structure of cathedrals in former architectural styles was concealed by ornamental features such as painted stucco. In the Gothic style the form is uncovered and a finer relationship between architectural and structural appearance is established. This type of architectural approach can be compared with the simplicity of the Greek temple ("Gothic Architecture" 2014a).

Coatings are rarely used, leaving the bare joints, emphasizing a great deal on a more qualified craftsmanship, a finer material quality and above all a tribute to a tight geometric entity (Simson 1988).

Figure 2-15. (Left) View of the central nave of the Canterbury Cathedral (1070-1834) in the UK. The pier molds are incorporated with the arch molds, resulting in a vertical continuity, thus creating a series of tree-like patterns ("Canterbury Cathedral" 2007). (Right) Pier section in the nave (center section), additional portion of the pier next to tower (left section) and arch mold (right section) (Willis 1845).

2.1.5 The English Gothic

2.1.5.1 Distinctive characteristics

The English Gothic structures emphasize on the horizontality, as wider plans of Gothic Cathedrals exist. The transepts project more widely and there can be two of them. Along with the historic evolution and the close monastic interference, most of the English cathedrals internal configuration is fragmented in between the barrier of one or two transepts. This division allowed the parts of the nave and the choir to evolve independently over time, to undertake different kind of reconstructions and alterations, leading to a variety of architectural styles and influences. Canterbury Cathedral is a characteristic example of this kind of independent approach, as it can be seen in detail in a next section (Theodossopoulos 2006).

The west front is not particularly used as the basic portal. Mostly the entrance is on the side, through a porch. Lastly, the choir can either be square or rounded with a number of Chapels dedicated to the Virgin Mary (Figure 2-16) ("English Gothic Architecture" 2014).

Figure 2-16. (Left) East end in York Minster Cathedral, showing the typical square configuration ("York Minster" 2014). (Right) East end of Canterbury Cathedral, having a semi-circular plan with three chapels ("Canterbury Cathedral" 2014).

2.1.5.2 Pointed ribbed cross vault variables

In England, the architects invested in the decorative alteration by adding small ribs in between the main ones, thus producing a richful complexity of patterns. Different kind of Gothic ribbed vaults in England, many of which served as transition stages are presented in Figure 2-17, 18, 19, 20 and 21 ("English Gothic Architecture" 2014).

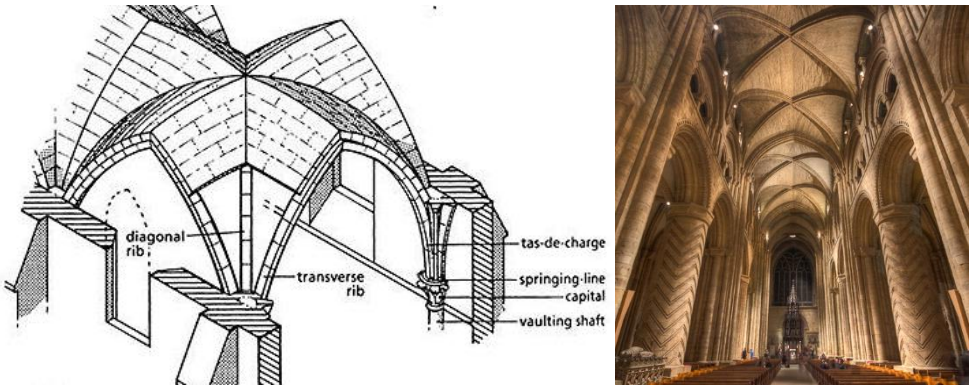

Figure 2-17. (Left) Quadripartite pointed crossed-ribbed vault with transverse, diagonal and wall ribs, with no ridge ribs ("Medieval Construction" 2014). (Right) Durham Cathedral, England (1093-1133), Romanesque Style ("Durham Cathedral" 2014).

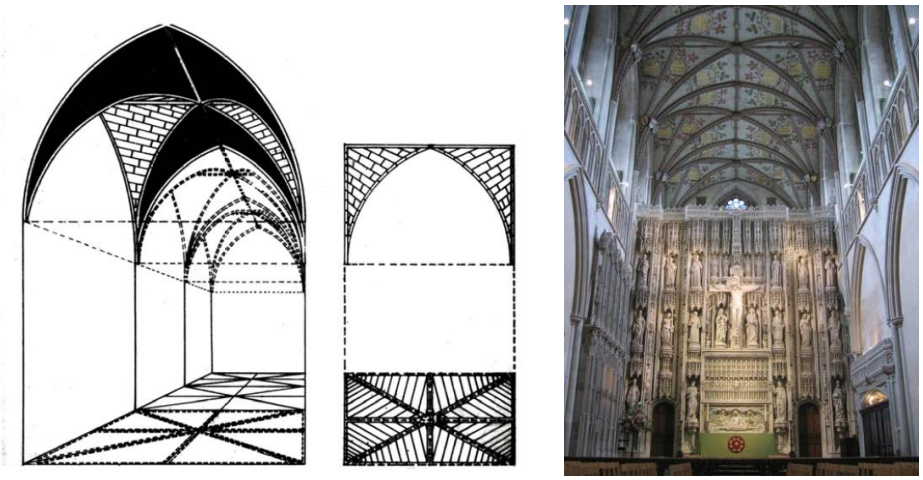

Figure 2-18. (Left, middle) Quadripartite pointed crossed-ribbed vault with ridge ribs ("Medieval Construction" 2014). (Right) St. Albans Cathedral, England (1077-1893), Romanesque/Gothic Style ("St. Albans Cathedral" 2014).

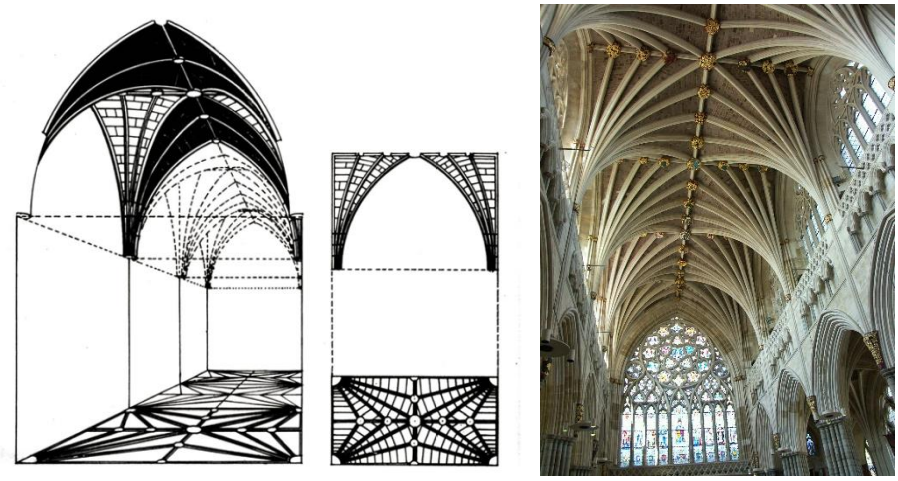

Figure 2-19. (Left, middle) Tierceron vault. Consists of additional secondary diagonal ribs, called tiercerons, extended from the springers to the transverse ridge ribs ("Medieval Construction" 2014). (Right) Exeter Cathedral, England (1112-1400), Norman/Gothic Style ("Exeter Cathedral" 2014).

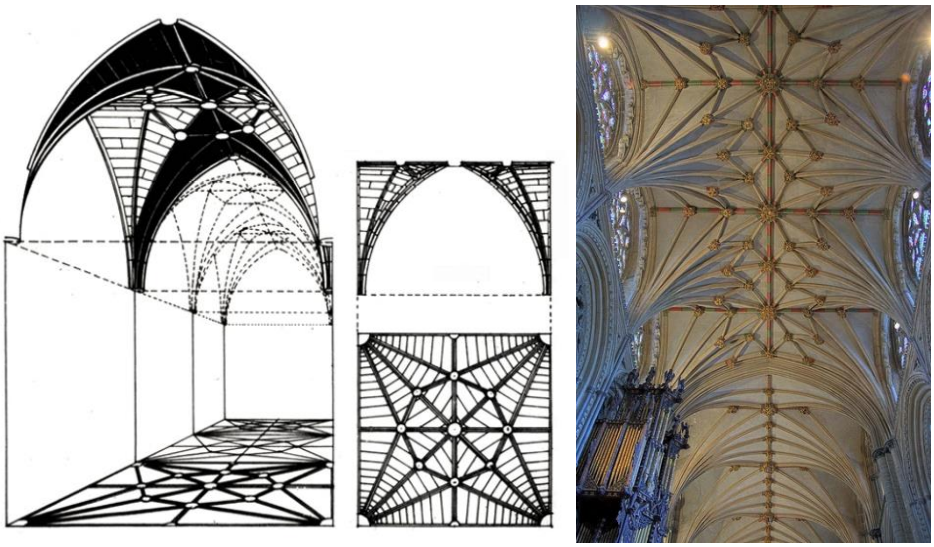

Figure 2-20. (Left, middle) Lierne vault. The main and secondary diagonal ribs intersect in nodes around the boss perimeter and additional tertiary ribs span between those nodes and the boss. In more complicated connections between liernes Stellar vaults are produced ("Medieval Construction" 2014). (Right) Ely Cathedral, England (1083-1375), Romanesque /Gothic Style ("Ely Cathedral" 2014).

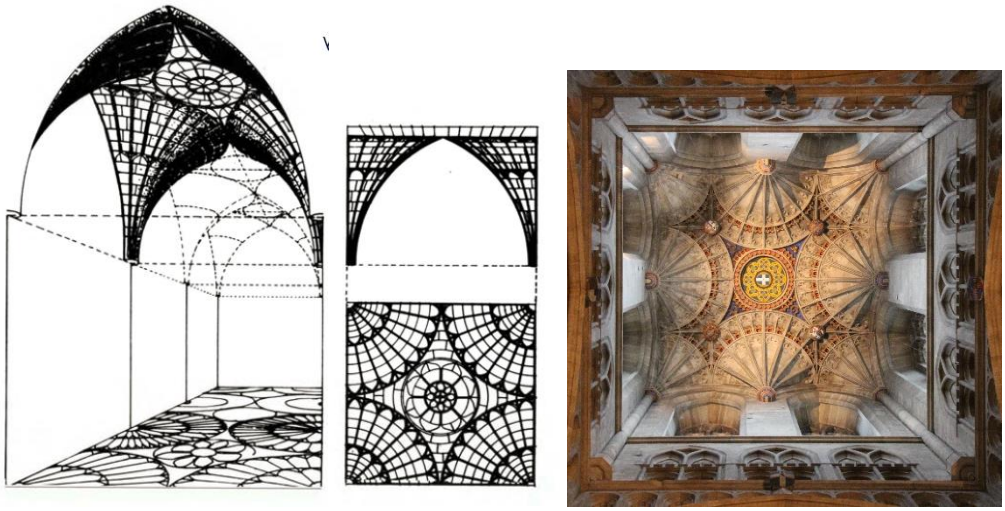

Figure 2-21. (Left, middle) Fan vault. Many ribs, having the same curvature, extend from the springers, thus forming fan-conical shaped vaults. Flat central spandrels fill the voids. Depending on the type of bay (square or rectangular) the shape of the central spandrel changes. In a more complex design, these vaults were combined with lierne ribs ("Medieval Construction" 2014). (Right) Canterbury Cathedral, England (1070-1834), Romanesque /Gothic Style. Fan square vault at the tower in the crossing ("Canterbury Cathedral" 2014).

2.1.6 Use of materials

The construction materials of Gothic Cathedrals depend mainly on the availability of stones and quarries in each region, but there have also been many documented material imports. In the high majority of Gothic structures, masonry was the main structural material, composed either of stone or brick units. Considering the mortar joints, they were generally weak and the interactions of the adjoining structural elements was through compressive forces. Also the level of homogeneity can only be established through surveying and testing on each case ("Gothic Architecture" 2014a).

Furthermore, regarding the regional diversity of material use for the construction of Gothic Cathedrals it can be noted in France, an extensive use of limestone took place. Caen limestone was used, due its particularly good quality and white color, producing very fine carvings. In England coarse limestone, red and dark green Purbeck marble was used. In Italy, the main building materials where limestone and brick. Marble was also used, but mainly for coatings and coverings. Lastly, in central Europe, due to scarcity of good quality building stone, the main construction material was considered brick ("Gothic Architecture" 2014a).

2.1.7 Gothic Revival of 19th – 20th century

The Neo-Gothic revival began in England in the second quarter of the 19th century, spreading in the western world after the second half of the 19th century, concerning buildings of ecclesiastical, civic and institutional type. Many new buildings were constructed, but also many attempts of restoration of Gothic structures have taken place. An extensive Gothic survival practice was performed in France, mainly under the Stylistic Restoration movement (1814-1879). Ideals of an established and specifically applied Gothic style were raised, with the introduction of new materials, such as cast iron. This movement resulted in many aggressive alterations in Gothic Cathedrals (Figure 2-22) ("Gothic Revival Architecture" 2014).

Figure 2-22. (Right) Notre Dame in Paris (1163-1345). From 1845-1870 the monument undertook a controversial restoration, resulting in many additions and reconstructions, such as the chimeras that were extracted from other Gothic buildings (Left) ("Notre Dame de Paris" 2014).

2.2 Damage in Gothic Cathedrals

2.2.1 Introduction

Damage patterns in Gothic Cathedrals have often similar causes and can either occur under single events or long term processes. The most significant damage patterns in Gothic Cathedrals are related to large deformations and cracking due to tensile or compressive failure, which can be linked with various causes, explained in the current section.

Damage identification and cause differentiation can only be feasible through a multi-approached methodology, involving structural modelling, analysis and inspection. Many of the effects can act in an accumulating way, increasing damage and deformation.

2.2.2 Large deformations

Large deformations can involve the whole structure, in terms of outwards rotations of macro-elements due to differential settlements, changes in the structural behavior, overloading, eccentricities, earthquakes etc. The deformation at failure usually includes the failure of buttresses, piers and flying buttresses against lateral thrust. As deformation increase, the structure experiences fragmentations (longitudinal cracks) and a hinge line is usually formed in the transverse direction. Structural members that are mainly affected are piers and buttresses, as shown in Figure 2-23 (Binda et al. 2008; Roca et al. 2005).

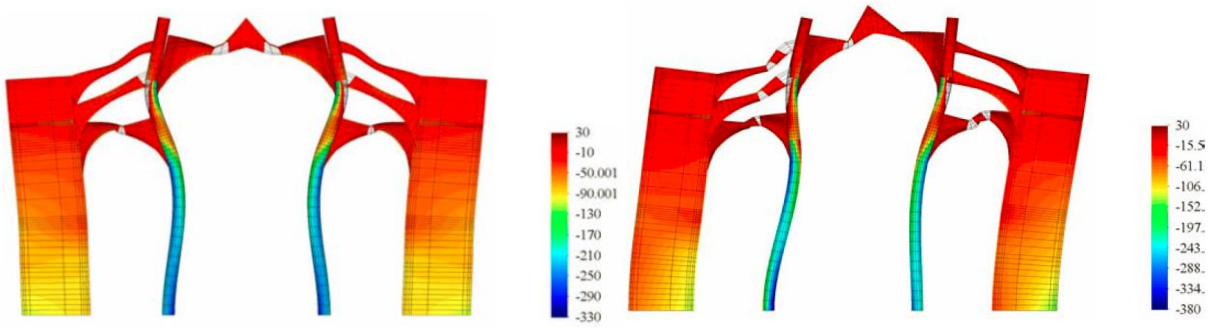

Figure 2-23. Deformation patterns in a transverse section of Mallorca Cathedral. Chromatic scale distribution of normal stresses. The white color represents cracking. (Left) Deformation under dead load. (Right) Deformation under seismic loads (Roca et al. 2005).

2.2.3 Cracks under tensile failure

Cracks caused mainly under tensile or shear failure in masonry structures can propagate in a uniform way and can either form a continuing fragmentation in large areas of structural elements (longitudinal cracks running through the nave's or aisle's main axis) or in a distributed way, but of a smaller scale (cracks related to a repeated structural or material detail, such as Sabouret's cracks, which are near the vaults springing due to the high stiffness, caused from excessive infill volumes). The elements mainly

experiencing tensile cracks are structural components used to redirect lateral forces (vaults, arches, buttresses and piers) (Binda et al. 2008; Roca et al. 2005).

2.2.4 Cracks under compressive failure

Cracks under compressive failure of masonry can lead to sudden overall structural failure and can propagate in concentrated areas, such as longitudinal cracks in columns due to high compressive stresses. Creep phenomena is also of relevance for crack propagation, sometimes induced by load redistribution. Damage can occur even under moderate compressive stresses (Figure 2-24) (Binda et al. 2008; Roca et al. 2005).

Figure 2-24. Pier of Tarazona Cathedral. Under excessive compressive stresses stone crushing and detachment occurred (Roca et al. 2005)

2.2.5 Material deterioration

Material deterioration under certain environmental conditions can affect the mechanical and physical properties of structural elements, either from long term environmental influence (freeze-thaw cycles, thermal effects, corrosive agents, moisture infiltration, raising damp, salts efflorescence, etc.) or under short term weathering (fires, floods, earthquakes, etc.) (Figure 2-25). The level of influence, exposure and deterioration can determine the level of damage and if the structure is affected at a local or global scale (Roca et al. 2005).

Figure 2-25. In 1984 a great fire, believed to have been caused by a lighting strike, destroyed the timber roof of the south transept of York Minster. Additional damage was caused by the vast quantities of water used to put out the fire. ("An Introduction to the History of York" 2014)

2.2.6 Other parameters related to damage in Gothic Cathedrals

Other aspects that can induce damage in Gothic Cathedrals are related with the construction process, alterations and reconstructions. Gothic Cathedrals had many construction periods, accounting for several decades, as well as many alterations, demolitions and reconstruction phases, during which many deformations were likely to have been imposed, due to lack of supporting provisions that provided enough lateral confinement and bracing.

2.2.6.1 Construction process

A commonly used construction sequence for Gothic Cathedrals consists first of the erection of piers, buttresses and lateral aisles, along with their vaults and nave timber roof. The next stage involves the construction of the nave's vaults. During the intermediate stage a system of horizontal pole fittings is implanted and wedged on the top and bottom of the vertical elements. This system together with nave's roof trusses provided a temporary support, centering and protection against tilting of the inner piers, counteracting also the inward lateral trust from the vaults (Figure 2-26). In case of early removal of the centering or the temporary support system, significant large deformations were introduced in the structure (Roca et al. 2005).

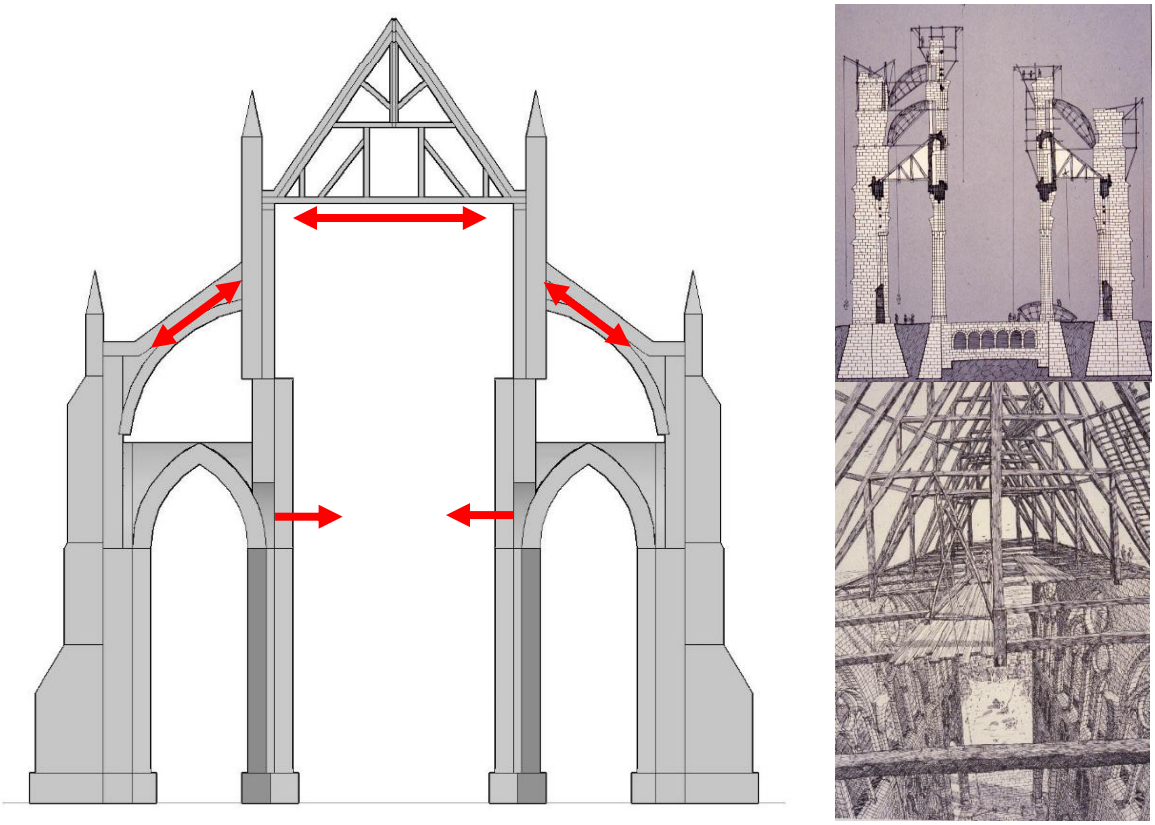

Figure 2-26. (Left) Typical cross-section of a Gothic Cathedral at an intermediate construction stage, prior to the construction of the nave's vault. Arrows showing the counteracting lateral forces. (Right-up) Construction phase involving the erection of piers and buttresses and the centering of flying buttresses. (Right-down) Sketch showing the system of timber trusses. The nave's vault is not yet constructed ("Index of /URBS110/Gothic" 2014).

2.2.6.2 Additions – alterations

Problems related with the overall stability and differential settlements were caused by the addition of new structural elements in Gothic Cathedrals, many of which were not accounted as loading in the initial design of the foundations. The most common additions responsible for structural damage are the erection of new towers and vertical additions in existing ones, in the west front or in the crossing (Figure 2-27).

Furthermore, structural substitutions and additions of new structural elements, such as reinforced concrete beams and ties, often introduce excessive or eccentric loading in the structure, changing the previous structural behavior. They often lack of sufficient connection and under extreme dynamic conditions can cause sudden failures (D'Ayala et al. 2003).

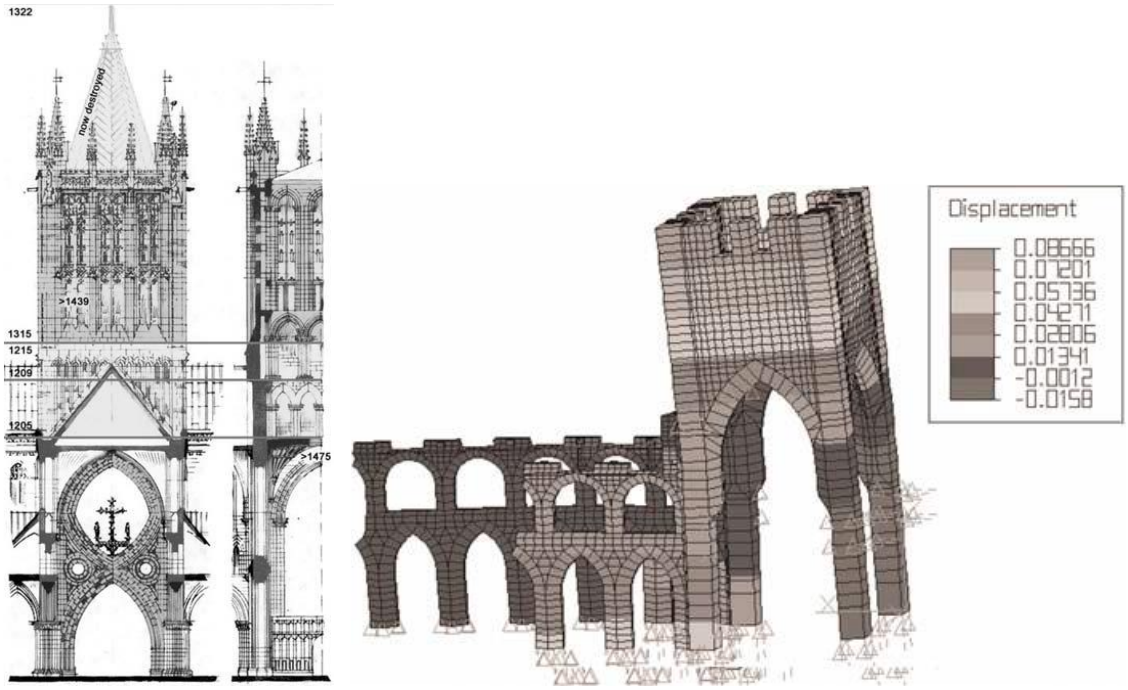

Figure 2-27. (Left) Chronological construction phases hypothesis and additions in elevation of the central crossing tower in Wells Cathedral in UK (1176-1490). Settlements and foundation failure have occurred. (Right) FEM model of the tower showing westward leaning (D'Ayala et al. 2003).

2.2.6.3 Accidental loading

Many Gothic Cathedrals undertook immense damage from accidental actions, such as blast waves or even direct hits from shelling during the warfare combats. Devastating effects such as sudden collapses of the roof structure under fire, loss of equilibrium of the lateral walls, partial collapse of the vaults was the outcome in many great Gothic Cathedrals across Europe (Figure 2-28) (Theodossopoulos et al. 2008).

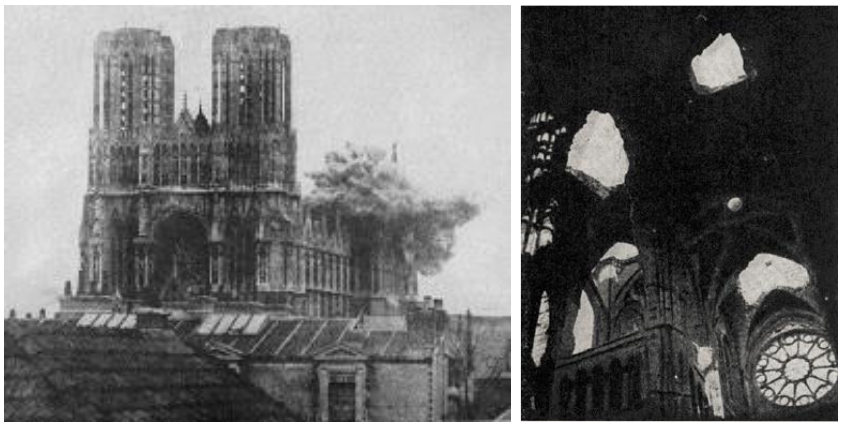

Figure 2-28. Reims Cathedral, Reims, France. (Left) Picture at the time of struck from German shellfire in September 1914. (Right) Inside view. Holes in the vault system from the bombarding (Theodossopoulos et al. 2008).

2.2.7 Specified damage in structural elements

2.2.7.1 Cracks in Gothic cross-vaults

Gothic masonry vaults can have different crack patterns due to a variety of reasons (building sequence, foundation and/or soil settlements, old seismic events, inadequate consolidation works etc.), which have to be considered in the analysis. It is therefore important to observe and document the crack pattern and deformations on historic masonry vaults in the process of investigation of the cause of damage (Figure 2-29) (Roca 2014).

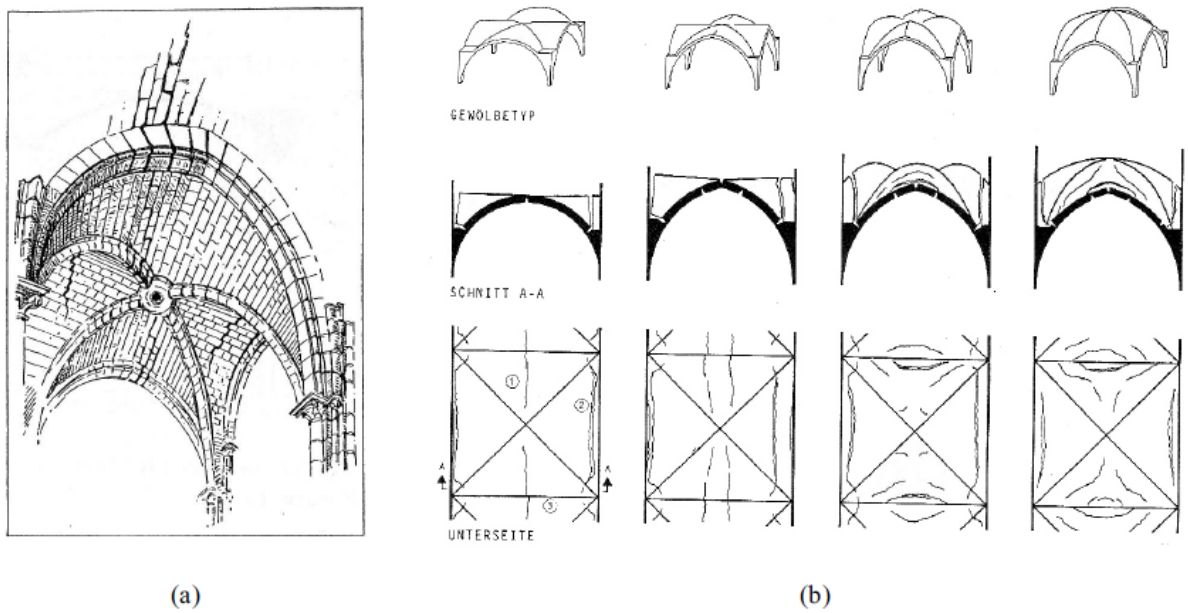

Figure 2-29. Typical crack patterns for masonry vaults. (a) Cracks running parallel with the side walls (Sabouret's cracks). (b) Typical pathologies for some common vaults (Roca 2014).

2.2.7.1.1 Compatibility cracks

A cross vault can experience cracks parallel to the side walls, known as Sabouret's cracks. Due to the high levels of stiffness in confined spans or infills with materials of high stiffness, the vault is constrained, unable to deform, cracks occur and create a discontinuity in the lateral vault-wall connection (Theodossopoulos 2008).

2.2.7.1.2 Cracks from lateral instability

The structural behavior of the Gothic cross-vault system is vulnerable to large lateral thrusts and excessive lateral displacements. The nave might become unstable for a lateral relative displacement of around 1/30 of the span's length (Theodossopoulos 2008). The failure mechanism considering only the nave vaults consists of three hinges, one in each springing (extrados), which are usually formed first, and one in the surrounding area near the crown and the tip of the arches (intrados). These cracks cannot

be mixed with the Sabouret's cracks that are merely compatibility cracks and are formed only as a result of high confinement (Figure 2-30) (Theodossopoulos 2008).

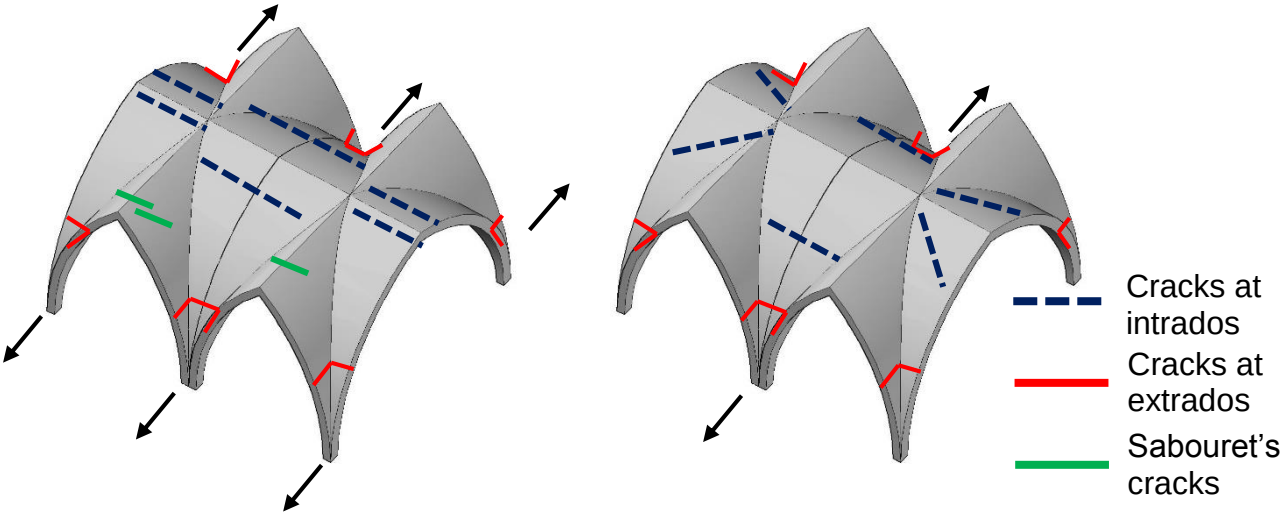

Figure 2-30. Crack pattern in Gothic vaults under outward movement of the supports. (Left) Outward movement of all supports. (Right) Relative movement of middle abutments. Hinges form in the area of springing and in the proximity of the crown. Higher compressive stresses concentrate near the supports (Theodossopoulos 2008).

2.2.7.2 Collapse mechanisms of macroelements

Many failure modes in Gothic Cathedrals, particularly under seismic loading consist of separation of large rigid elements that experience out of plane rotation. This type of kinematic mechanism can involve the rotation of whole facades and towers, or parts of them. Investigation of various potential failure mechanisms under specific ground excitation can also provide information about the most critical failure modes (Figure 2-9) (Roca et al. 2010).

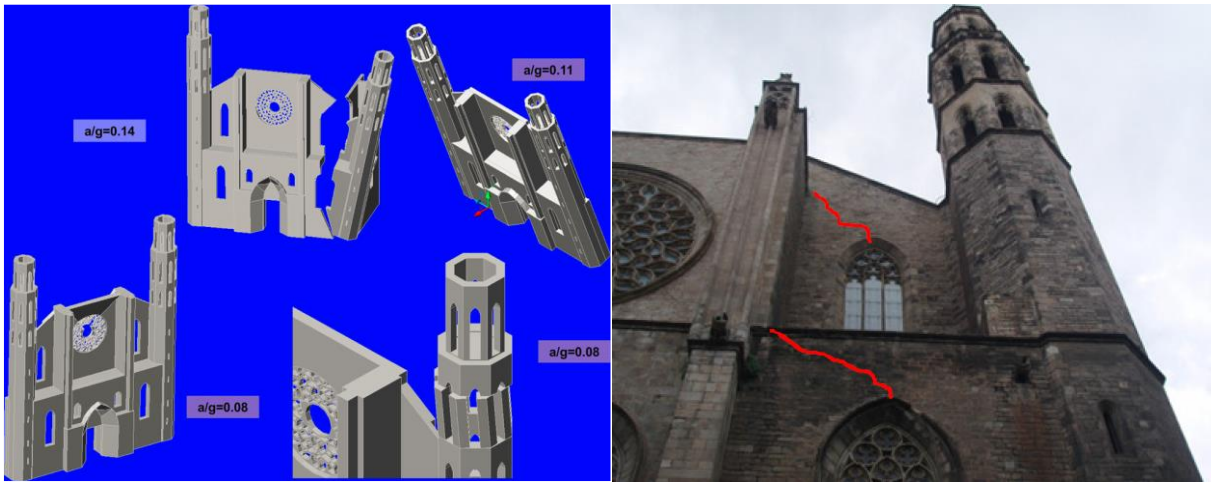

Figure 2-31. (Left) Kinematic failure mechanisms applied on the facade of Santa Maria del Mar, Barcelona, Spain (1329-1383) (Roca et al. 2010). (Right) Photo revealing fragmentation cracks due to uneven settlements and the tower's rotation (Roca 2014).

2.3 History of Canterbury Cathedral

2.3.1 Introduction

Christ Church Cathedral at Canterbury, Kent, or shortly Canterbury Cathedral is considered one the most prestigious and prominent ecclesiastic structures in United Kingdom (Figure 2-32). It is the seat of the Archbishop of Canterbury, head of the Anglican Church for more than five centuries and an established Unesco World Heritage site since 1988. Under a long sequence of construction phases, alterations, distractions and total rebuilding of parts, Canterbury Cathedral has reached the present time as a mixture of Romanesque, Early Gothic and Decorated Gothic styles, dated from 1070 until 1834 ("Canterbury Cathedral" 1992; "Canterbury Cathedral" 2014).

Figure 2-32. (Left) Aerial view of Canterbury Cathedral from southeast ("Canterbury Cathedral Aerial" 2013). (Right) Northwest view of Canterbury Cathedral ("Britain's Greatest Cathedrals" 2012).

2.3.2 The Anglo – Saxon period (597 – 1070)

St Augustine, who arrived in Kent from Rome in 597, along with a group of missionaries, was consecrated as the first Archbishop of Canterbury. At his arrival he established the Christ Church, the first Cathedral of Canterbury, located in a north-east part of the city. From that point, until 1070 the Cathedral of Canterbury evolves under four specific phases: ("Canterbury Cathedral" 2008; Collinson et al. 2002), as discussed next.

Phase I: The original Church of St Augustine was constructed soon after his arrival in 597 and was likely to have had a Roman core. The church consisted of a simple nave and an apsidal altar, gradually surrounded along the west, north and south sides by porches (porticus), which were later added by successive Archbishops. The style is likely to have been typical Kentish, built out of re-used Roman materials.

Phase II: The Cathedral comprises partly of additions on the existing Church and of a separate building, which served perhaps as baptistery-church and mausoleum for the archbishops, near the south-east corner of the nave (740-60).

Phase III: During the 9th or 10th century a massive enlargement of the Cathedral takes place, involving the widening of the foundations, serving for a likely increase of the walls in height, along with rebuilding and restoring the existing Cathedral-monastic complex. The whole process was a part a reorganization of the Christ Church of Canterbury in order to include monastic buildings. The porticoes were incorporated into side-aisles and the cathedral was doubled in length (49m by 23m).

Phase IV: This last phase of the Anglo-Saxon period involves mainly the demolition of the squared west front of the cathedral and its replacement with a major west polygonal apse (The Oratory of St Mary), making the Cathedral bipolar, having apses and altars both in the east and west front. Additionally, flanking hexagonal stair towers were built in the west front. The arcade walls were strengthened and two towers were added at the eastern corners. From the excavated remains of Phase IV, it was concluded that the Cathedral was 75m in length and about 31m in width, making it one of the largest in Northern Europe in the beginning of the 11th century.

No structure from the Anglo – Saxon period survived until the present day. The monastic complex, along with the church, was burned by a great fire in 1067. Any remains were soon after demolished by Archbishop Lanfranc for the new Norman Cathedral in 1070. In 1993, during the replacement of the marble floor at the nave, an archaeological excavation project took place and remains of the western apse foundations of the latest Anglo-Saxon Cathedral phase were revealed (Figure 2-33). During the project the identification of the four historic phases of the Anglo – Saxon Cathedral was possible. The successor Norman Cathedral was placed more to the south, so as to avoid the former foundations.

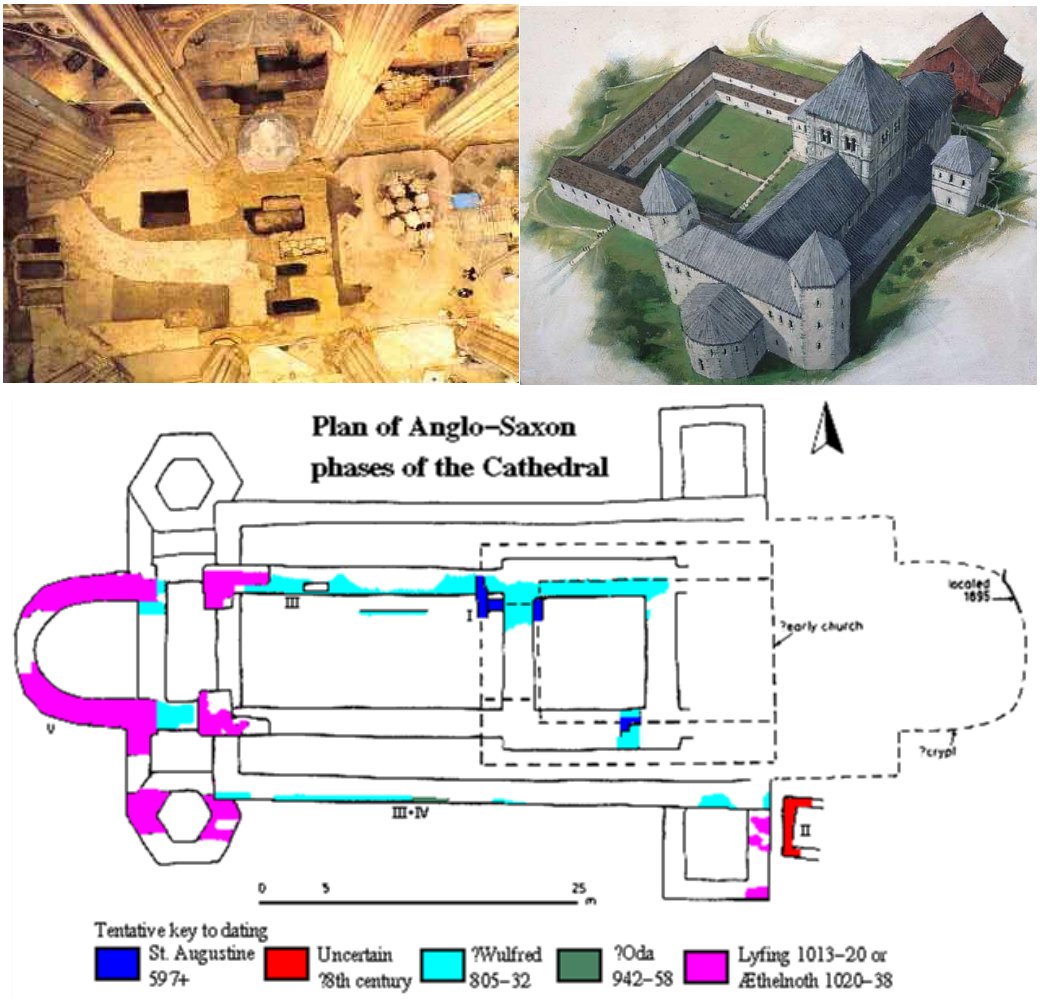

Figure 2-33. (Above left) Photo taken from the nave's ceiling, showing the western apse foundation of the Saxon Cathedral ("Canterbury Cathedral" 2008). (Above right) Imaginary representation of the Anglo-Saxon Cathedral, as believed during the final phase IV (1025), comprised by the Cathedral and many additional buildings ("AD 1000 - Canterbury Cathedral" 2007). (Below) Plan of the Anglo-Saxon Cathedral showing parts from the four different phases, as identified from the archaeological excavation in 1993 ("Canterbury Cathedral" 2008).

2.3.3 The Church of Archbishop Lanfranc

In times of Archbishop Lanfranc, a major reconstruction project was conducted as stated above, and the monastery complex was replaced by a building of greater volume (cloisters, offices, refectories and dormitories). In 1077 a new Norman Cathedral was erected in its place from the very foundations. Lanfranc's Cathedral had one transept and at its crossing a tower was constructed, raised on four pillars with a steeple terminated by a golden angel. The nave was arranged in eight bays and on the west front two twin towers were raised, terminated with gilded pinnacles (Figure 2-34) (Dudley 2010; Collinson, Ramsay and Sparks 2002).

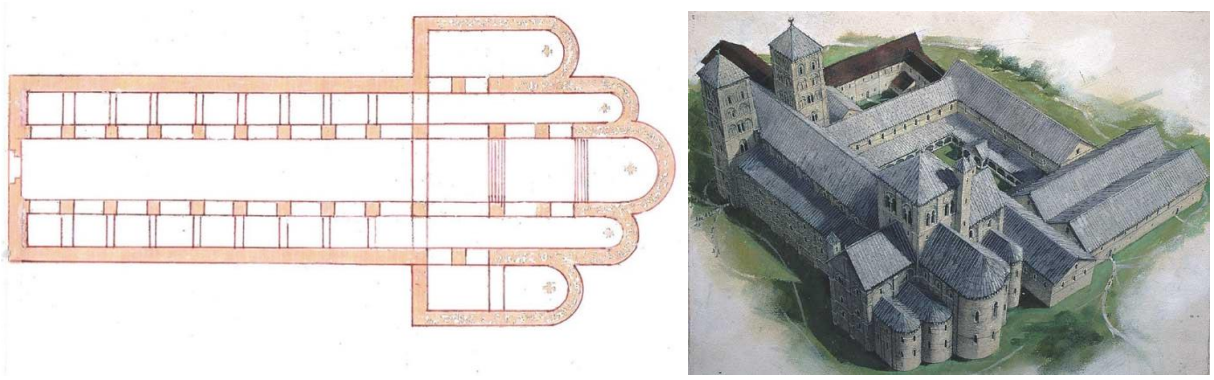

Figure 2-34. (Left) Ground plan of Lanfranc's Canterbury Cathedral (1070-1077). The exact form of the apses is uncertain, as only remains of their foundations were uncovered. The plan and proportions were based on Lanfranc's abbey in Normandy (Dudley 2010). (Right) Imaginary representation of Canterbury's Norman Cathedral under Archbishop Lanfranc (1077), comprised by the Cathedral and many additional buildings ("Canterbury Cathedral" 2007).

2.3.4 The new Choir of Archbishop Anselm (1096-1130)

In 1096, Archbishop Anselm, being Lanfranc's successor, under notifications that the recently completed Choir was inadequate to serve the processional demands of the monastic worship, decided for the part of the Choir and the underground crypts to be demolished, so as to be replaced with larger ones. Many of the Lanfranc's stonework (columns – capitals) may have been used, but due to the extensive new design they had to be placed in different positions. The new choir included an ambulatory passage with chevette chapels, new altars in three levels and an attaching chapel of the Holy Trinity. This choir extended 58m from the crossing to the east (Figure 2-35) (Willis 1845; Collinson, Ramsay and Sparks 2002).

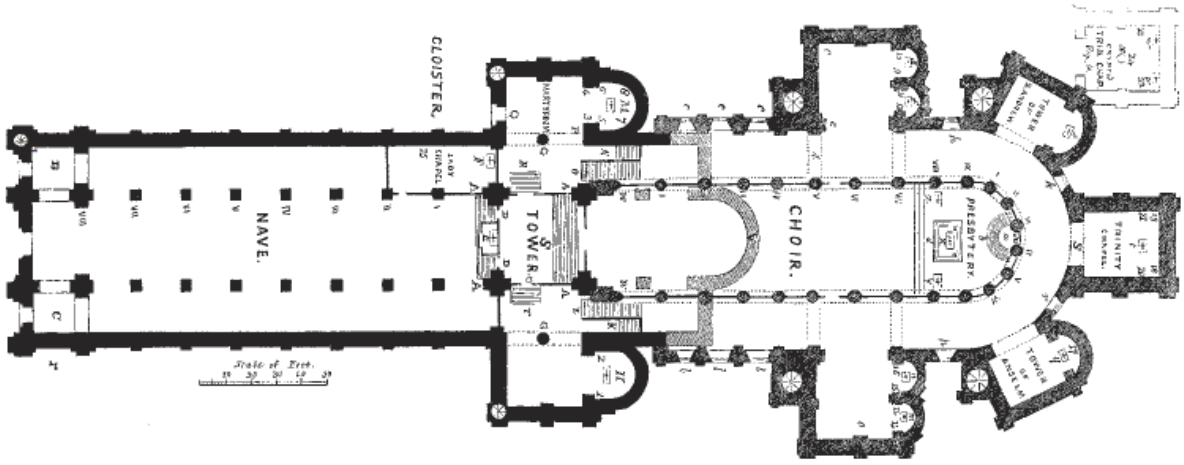

Figure 2-35. Plan of Canterbury Cathedral in 1174. The lighter shading pattern in the crossing of the new Choir is the intersecting termination of Lanfranc's Cathedral on the eastern front (Willis 1845).

2.3.5 The New Cathedral (1175 -1184)

Archbishop Anselm's new Choir was destroyed in 1174 by fire and soon after the third Choir reconstruction begun by William of Sens. In the forthcoming reconstruction many sound structural elements were maintained and incorporated to the new Gothic Choir, such as the foundations, the exterior walls up to the part of the Triforium base and the crypt. The new Choir had increased in height by 3.7m. The Trinity Chapel was completely reconstructed, widened to the east and served as a shrine of the archbishop Thomas Becket, who was murdered in the cathedral in 1170. After the retirement of William of Sens because of an injury, the implementation of the new Choir was taken over by William the Englishman, who incorporated the transition from the Romanesque to the Gothic style (Figure 2-36) (Willis 1845; Collinson, Ramsay and Sparks 2002).

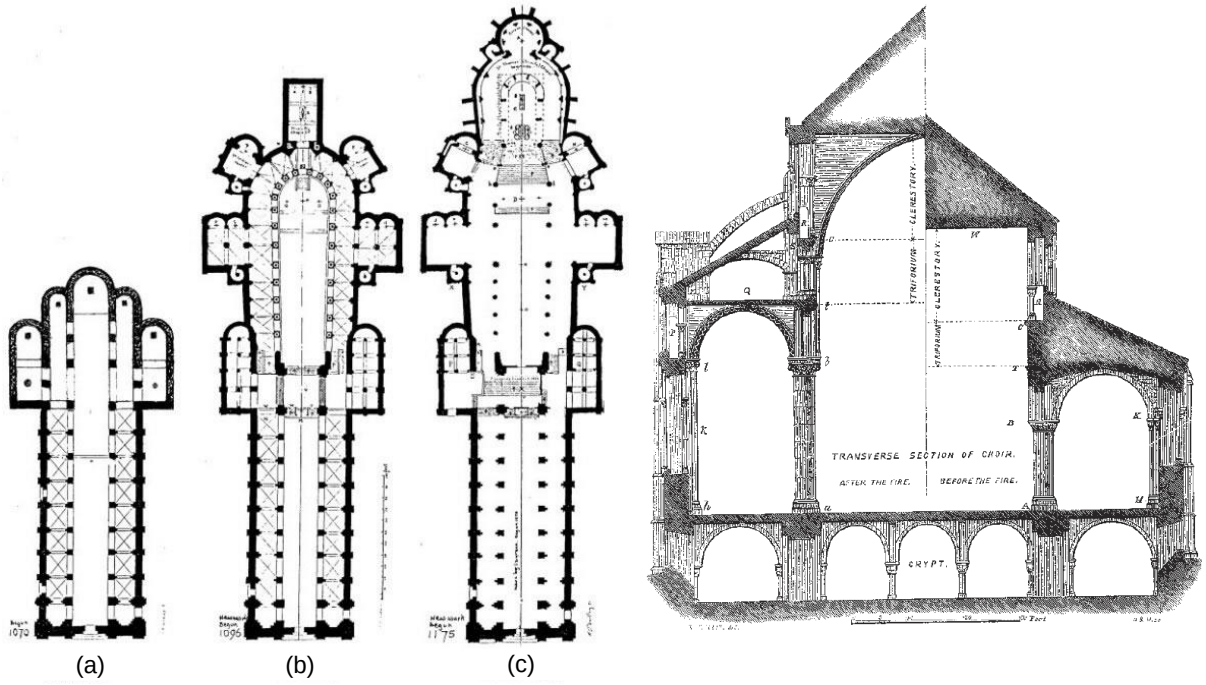

Figure 2-36. (Left) Ground plans of Canterbury Cathedral as it evolved over time, from 1070 to 1175. (a) The Cathedral of Lanfranc, (b) the Cathedral of Anselm, (c) the Cathedral of William of Sens ("Canterbury Cathedral" 2007).(Right) Transverse section of the choir. In the left cross section the new Gothic Choir after the reconstruction is presented. In the right part of the cross section Archbishop Anselm's Choir before the fire is depicted. (Willis 1845).

2.3.6 14th – 19th Centuries

In 1378 Archbishop Sudbury started the demolition and total rebuilding of Lanfranc's nave, accounting for its bad state, but the attempt was terminated because of his death in 1381. An earthquake in 1382, estimated at 5.8 on the Richter scale damages severely the Cathedral's bell tower and cloister. The reconstruction project of the nave and transepts in the Perpendicular English Gothic style was later on assigned to Prior Thomas Chillenden (1391-1411). All piers were removed and replaced with more slender ones, while the side walls in the aisles were demolished and rebuilt. The vaults were constructed as lierne vaults with bosses. Some of the original fabric was retained, mainly in the eastern walls of the transepts. The nave roof was raised, so as to align with the choir roof, which was raised by 3.7m in the 12th century. Regarding the towers of the west front, the south-west tower was replaced in 1459 (Willis 1845; Collinson, Ramsay and Sparks 2002).

As far as Lanfranc's square tower in the crossing, it was demolished in 1430 and its supporting piers were reinforced, so as to support the new bigger one. The reconstruction only started 50 years later in 1490 and completed in 1504, when the central tower was erected at its complete height of more than 70m (Collinson, Ramsay and Sparks 2002).

Regarding the north-west tower, it was retained until 1834, when it was demolished due to structural deficiencies and replaced with a twin of the south-west tower. The north-west tower's spire was maintained until 1705. The north-west tower's reconstruction is considered the last major structural alteration implemented in Canterbury Cathedral, which formed the monument until the present time. In Figure 2-37 is depicted the building sequence of the west front, along with the erection of the bell tower ("Canterbury Cathedral" 2014).

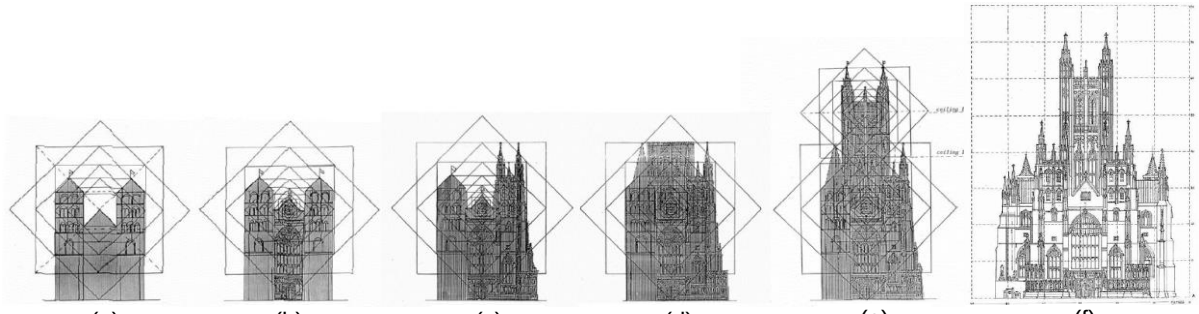

Figure 2-37.(Above) Geometrical representation of Canterbury Cathedral's west front in different time phases (Dudley 2010): (a) The geometry of Lanfranc's west front 1070-1077, (b) Prior's Thomas Chillenden west front completed in 1401, (c) Completion of southwest tower in 1459, (d) First construction phase of central tower (1470-1490) after demolition in 1430. Architects: R. Beck & J. Wastell, (e) Second construction phase of central tower completed in 1504 by J. Wastell, (f) Aspect of the west front as it exists in present time. (Below left) The west front aspect of Canterbury Cathedral in 1821 before the completion of the north-west tower ("Canterbury Cathedral" 2014). (Below right) West front configuration of Canterbury Cathedral at present time ("Canterbury Cathedral" 2005).

2.3.7 20th century's intervention & conservation works

2.3.7.1 1946 - 1968

In Canterbury Cathedral the walls consist of a three leaf masonry. The two external leaves are from Caen stone masonry and the intermediate void is filled with lime mortar and small fragments of rubble. The connection between the three leaves is ensured with long tie stones, placed transversely. During World War II the city of Canterbury was severely bombarded. Fortunately none of the bombs hit Canterbury Cathedral. Still, the monument suffered from the resulting negative pressure caused by the blast waves from nearby exploding shells, as well as from the resulting heat of the caused fire, which led to the bond weakening and separation of the outer masonry wall layer. Any partial or insufficient connection between the wall's claddings is potentially dangerous for the structural stability of the building

and propagates through freeze-thaw cycles (Foyle, Newton and Greshoff 2013), other environmental actions and wind.

In an attempt to reestablish the former condition of the wall, under Harold Anderson (Surveyor to the Fabric from 1946 to 1968) the masonry exterior walls were grouted using a strong Portland cement. The use of Portland cement had negative effects for the soft limestone by being a potential source of sulphates, thus accelerating the stonework's decay and by changing the migration of moisture. ("Canterbury Cathedral: Great South Window" 2013).

For the repairing works in the Bell Harry tower (central tower at crossing) and pinnacles Bath stone was used, which seems incompatible with the original Caen stone, as being more coarse and grainy in texture and darker in color (Foyle, Newton and Greshoff 2013).

2.3.7.2 1968 - 1991

In 1968 the architect Peter Marsh was appointed as the new Surveyor to the Fabric of Canterbury Cathedral. A good quality limestone from the south west of France, known as Lepine, was chosen for repairing works, given that Caen stone was hard to find in the desired quantity or quality at that time (Foyle, Newton and Greshoff 2013).

During his service Peter Marsh undertook the following projects (Foyle, Newton and Greshoff 2013; "Stained Glass Studio" 2013; Filippoupolitis 2011):

1. Reconstruction of the gable of the south west transept: A reinforced concrete cantilever beam was built in order to connect the gable back with the rest of the building.
2. Conservation of the south window's glass: The glass panels were removed, conserved and were installed in the back, behind new protective glazing.
3. Large scale repairs concentrated in the cathedral's west end: Rebuilding the oculus and gable, as well as stone replacements at the twin towers of the west front took place.

2.3.7.3 1991 - 2013

In 1991 John Burton was appointed as the new Surveyor of the Fabric and undertook the subsequent repairing and restoration projects.

In 1991 the floor in Cathedral's nave and south west transept was replaced. A Portland concrete slab floor was laid over a lime screed together with an under floor heating system, thus using the stone floor as a huge radiator. The task was completed in 1992 (Filippoupolitis 2011).

During the 1990s and under a fire resistance enhancement strategy, soon after the fire in the roof of York Minster in 1984, a concrete layer was added in the infill of the aisles and nave. The additional concrete layer serves as an impermeable surface in order to drain more effectively the amount of water that would be used to extinguish a potential fire, through drilled holes in the lateral walls (Figure 2-38).

The evident cause was to avoid the water infiltration through the vault system, which can cause additional damage (Deeming 2014).

Figure 2-38.View of the interior nave roof void, depicting the concrete infill layer and the drilled hole for drainage.

A monitoring system was installed in the Canterbury cathedral in the year 2010. The system is gathering information on temperature, relative humidity and movement in the roof spaces, ground floor, crypt, Bell's Harry interior, south west transept and flying buttresses on the south side of the nave.

From 2006 until 2012 the restoration of the Corona chapel took place. The stone masonry of the Corona chapel at the east front of the Cathedral was cleaned, conserved and restored. The pinnacles on the top of the corona chapel were reconstructed. For the restoration works Lepine stone as well as Caen stone were introduced. Parts of the stained glass windows of the Corona Chapel were also conserved ("Completed Corona Is Finally Revealed" 2012).

In 2009 the conservation project of the South East Transept was on track. The stained glass panels from the 12th century South Oculus window, of the south east transept, were removed in order to be treated for glass and glass paint corrosion. The wrought iron *ferramenta* frame, which supports the stained glass window, dates to 1180 and is denoted as the world's oldest space frame, underwent mechanical cleaning with scalpels and wire brushes in order to remove rust and wax coating, with rust inhibitors applied as a final treatment. Additionally, the timber roof of the South East Transept, being the oldest part of the Cathedral's roof system, underwent timber repairs and replacement of its lead tiles covering. The exterior cladding of the stone masonry was treated in order to remove the black sulfate crust. Cement mortar was replaced with lime mortar and damaged stones were replaced. The project was concluded in 2012. ("The World's Oldest Space Frame" 2011; "ACNS - Anglican News Service" 2007).

2.3.7.4 2013 - present

In October 2013 the new appointed Surveyor of the Fabric was Jonathan Deeming. The Great South Window of the South West Transept tracery experienced extensive damage (cracks and fracturing), mainly due to embed iron rusted bars and outward tilting. Given the widespread damage and after all the stained window panels have been removed, the tracery is being currently repaired in all its extent, by stone replacement of damaged parts (Figure 2-39). The project is bound to be completed by summer 2015 ("The Great South Window" 2014).

Figure 2-39. (Left) The Great South Window of the South West Transept behind scaffolding. (Right above) Inside view of the Great South Window tracery of the South West Transept. The glass panels have been removed and stone parts are been taken off piece by piece. (Right below) Process of removal of damaged stone masonry in the Great South Window tracery of the South West Transept which will later be replaced by replicas. View of the tracery at top level. ("The Great South Window" 2014).

3. GEOMETRICAL SURVEY

3.1 Introduction

As mentioned extensively in the historic survey, the nave and lateral aisles of Canterbury Cathedral are mainly part of a major reconstruction project conducted in the late 14th century by Prior Thomas Chillenden (Willis 1845). The conducted geometrical survey was partly based on drawings, which were gathered during the historic survey (Figure 3-1 and 2), on the in situ geometrical inspection and on the geometrical survey of the south half cross section and the corresponding part of the south façade, as prepared by the Downland Partnership Ltd and provided by the Morton Partnership Ltd (Figure 3-3).

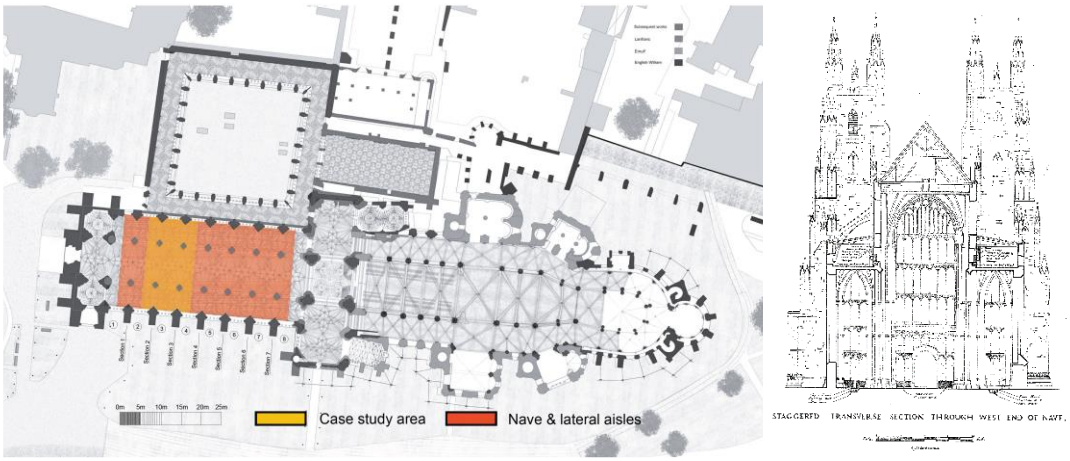

Figure 3-1. (Left) Top plan of Canterbury Cathedral depicting the nave and lateral aisles area, as well as the case study area of the critical cross sections. (Right) Transverse cross section of the nave and lateral aisles of Canterbury Cathedral looking west (Morton Partnership Ltd).

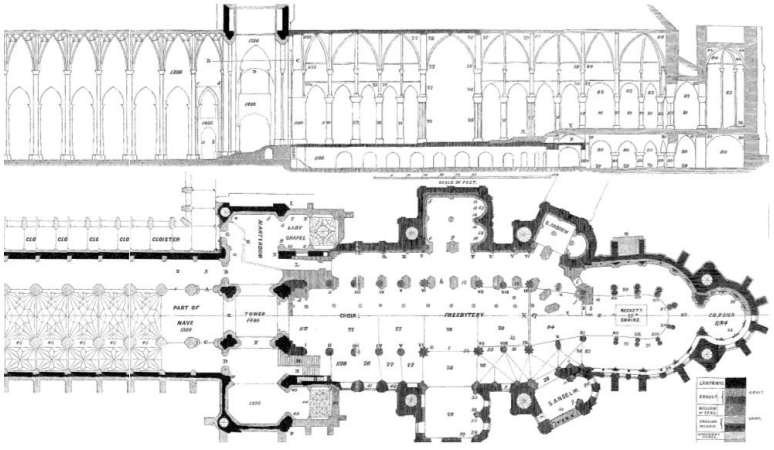

Figure 3-2. Longitudinal cross section and top plan of the nave, transepts and choir of Canterbury Cathedral (Willis 1845).

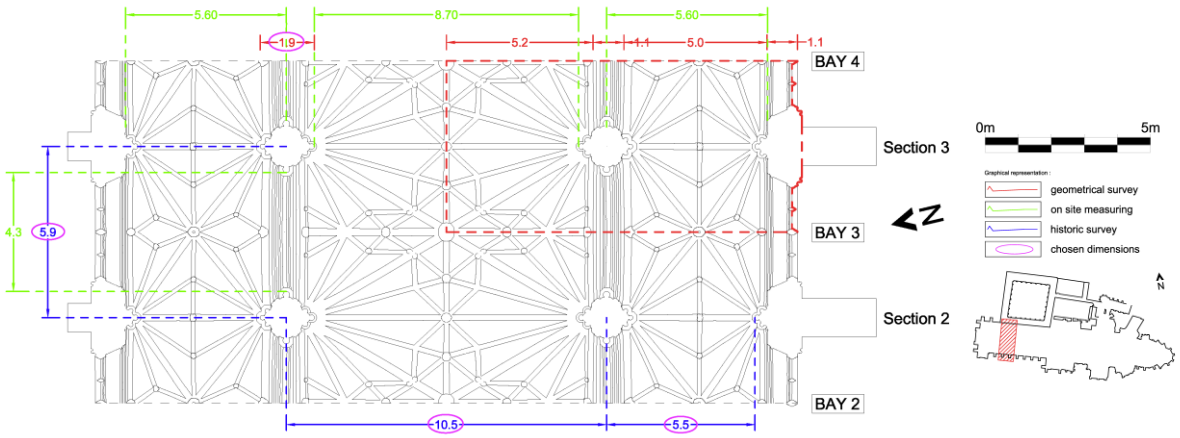

Figure 3-3. Top plan of the vertical abutments and vault configuration of the critical area of the nave, depicting dimensions (meters) based on the historic survey, the in situ inspection and the geometrical survey provided by Morton Partnership Ltd.

The main objective of this part of the work was to identify the structural components of the structural skeleton and to construct a 3D CAD model of the critical transverse cross section with its corresponding bays, which will serve to initiate a 3D FE model (Figure 3-4). A repetitive sequence of the geometrical model of the critical section was also used to generate a 3D CAD model of the entire nave and lateral aisles, for preparation of the damage maps and for presentation purposes (Figure 3-5).

Figure 3-4. Generated geometrical model of the critical transvers cross section of Canterbury Cathedral's nave and the adjoining part of the cloister.

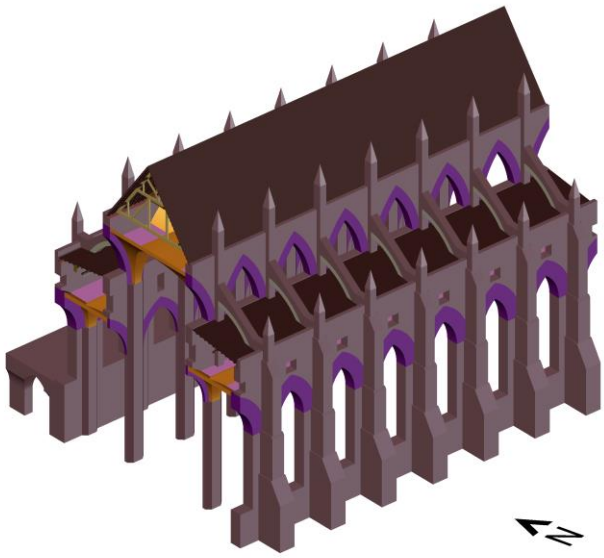

Figure 3-5. Generated geometrical model of the nave of Canterbury Cathedral and the adjoining part of the cloister.

3.2 Nave configuration

The plan configuration of the nave of Canterbury Cathedral, measured from the axis of the transversal ribs and the centre axis of the piers has 48.6 m of length, 10.5 m of width and 24.6 m of inner height. The nave is organised in 8 bays with an inscribed plan, measured from the axis of the nave arches and the transversal ribs respectively, of 11.1 x 6.1 m, covered with Gothic lierne quadripartite cross vaults and equilateral pointed arches. The main diagonal and transverse ribs intersect in bosses, whereas the secondary ones intersect in nodes around the perimeter of the central boss (Figure 3-6). The vaults have a clear span of 9.4 m and 5.2 m in the transverse and longitudinal direction, respectively, and a rise of 6.3 m. During the geometrical survey, the thickness of the nave vault, as measured from a cylindrical void in boss was 0.8 m. Taking in to account a portion of the boss and the intersecting diagonal ribs that project below the web of the vault, the design shell thickness of the vaults was accounted as 0.4 m. The ribs are considered an essential part of the vault's structural system, providing safe enclosure of the web masonry (Theodossopoulos 2006). Nevertheless, for simplicity of the generated 3D CAD and FE model and due to the limited information regarding their size and configuration, the diagonal and transversal ribs were not accounted for in the model. Adjacent equilateral pointed nave arches of 4.0 m clear span, 5.4 m rise and 0.9 m width are the structural elements of the clerestory walls. The nave vault and adjoining arches are depicted in Figure 3-7.

Figure 3-6. (Left) View of the nave of Canterbury Cathedral looking east. (Right) View of the Gothic lierne quadripartite cross vaults of the nave of Canterbury Cathedral (Photographic survey).

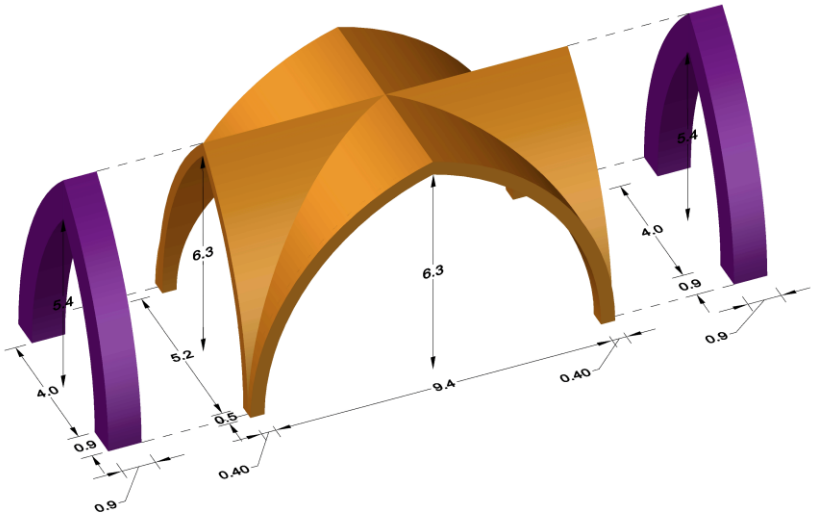

Figure 3-7. Gothic cross vault configuration and dimensions (meters) in the nave of Canterbury Cathedral and adjacent clerestory arches, as generated for the 3D CAD model.

3.3 Lateral aisles configuration

The lateral aisles of Canterbury Cathedral comprise 8 bays with compartment dimensions, measured from the axis of the arcade arches and the transverse ribs, respectively, of 6.6 x 5.9 m and 15.1 m in height. The vaults are Gothic lierne quadripartite cross vaults, drawn from equilateral pointed arches. The adjacent arcade arches have a clear span of 4.0 m, 3.5 m rise and 0.9 m width, whereas the arches

of the aisles windows have a clear span of 2.9 m, with 2.9 m rise and 1.4 m width. The thickness of the vaults in the lateral aisles was considered equal to that of the nave, i.e. 0.4 m. The lateral vault configuration and the adjoining arches are depicted in Figure 3-8 and 9.

Figure 3-8. (Left) View of the north aisle of Canterbury Cathedral looking east. (Right) View of the south aisle of Canterbury Cathedral looking east (Photographic survey).

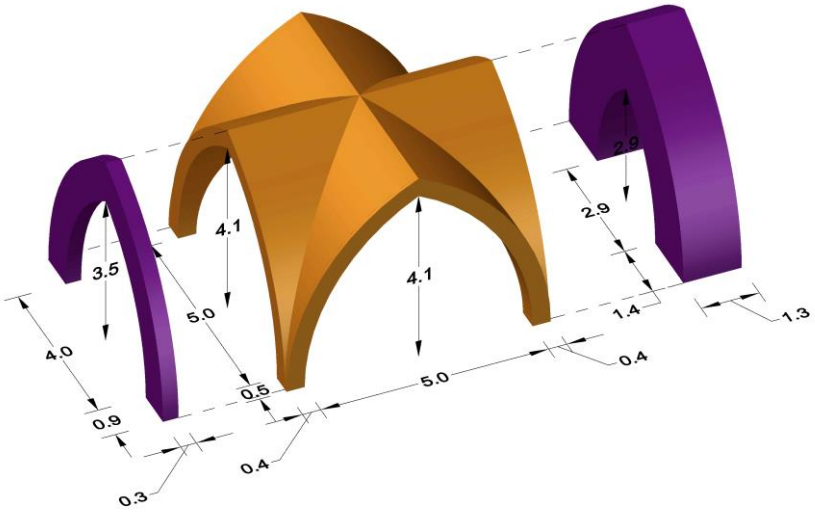

Figure 3-9. Gothic cross vault configuration and dimensions (meters) in the south aisle of Canterbury Cathedral with the adjacent arcade arch (left) and the aisle window arch (right), as generated for the 3D CAD model.

3.4 Vertical abutments

The vertical abutments in the nave consist of a colonnade of 7 piers on both sides, of 18.3 m height, measured from the base to the springing of the nave vaults. The level of the springing of the lateral vaults is 11 m. Their section has an area of 1.8 m^2, is symmetrical and follows an ornamental pattern with engraved shafts that can be inscribed in a square. The piers slenderness ratio (height over circumscribed diameter) is around 9.6 and considered normal, as in many other Gothic Cathedrals this value normally stays between 7 and 9 (Roca et al. 2013). For the geometrical model, an equivalent pier mould was chosen which inscribes the springings of the lateral vaults. For the lateral buttresses an equivalent section was also chosen, as shown in Figure 3-10.

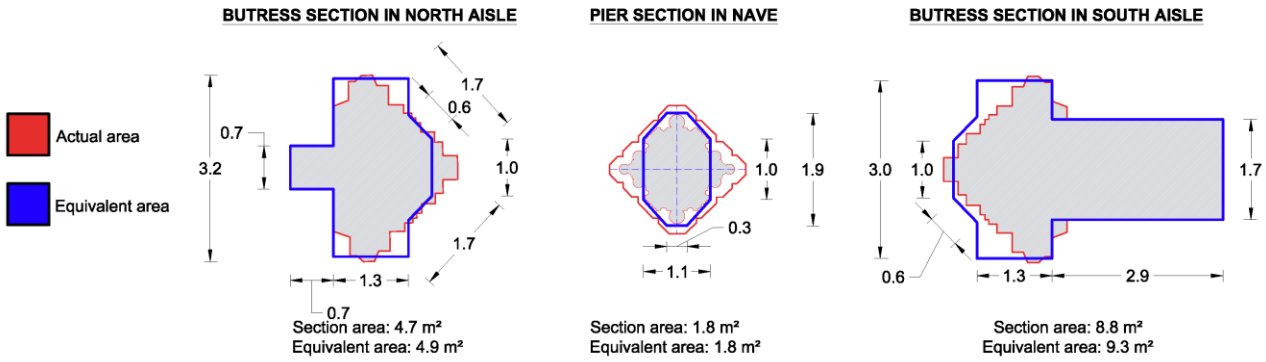

Figure 3-10. Sections depicting the actual and chosen equivalent dimensions (meters) and area of the piers and buttresses of Canterbury Cathedral (Willis 1845).

3.5 Roof trusses in nave and lateral aisles

The nave roof of Canterbury Cathedral can be defined as a classic high pitched Gothic roof of about 54º, with a covering span of 11.1 m. The timber trusses are a combined configuration of a queen post on the lower level and a king post placed over the level of the straining beam. A series of diagonal and vertical compressive elements called struts are used to redirect the stresses to lower beam elements. The trusses are placed with a spacing of 3.5 m (centre axis) and are fixed over timber wall plates, which extend on top of the clerestory walls. They form a rigid timber framing system with hinged joints of timber connections and metallic-edged blades. The whole system appears to be structurally independent from the nave vaults as the clerestory walls extend over the extrados of the vaults by 0.8 m. The external roof coating is large size lead sheets, attached on a system of timber roof battens (Figure 3-11).

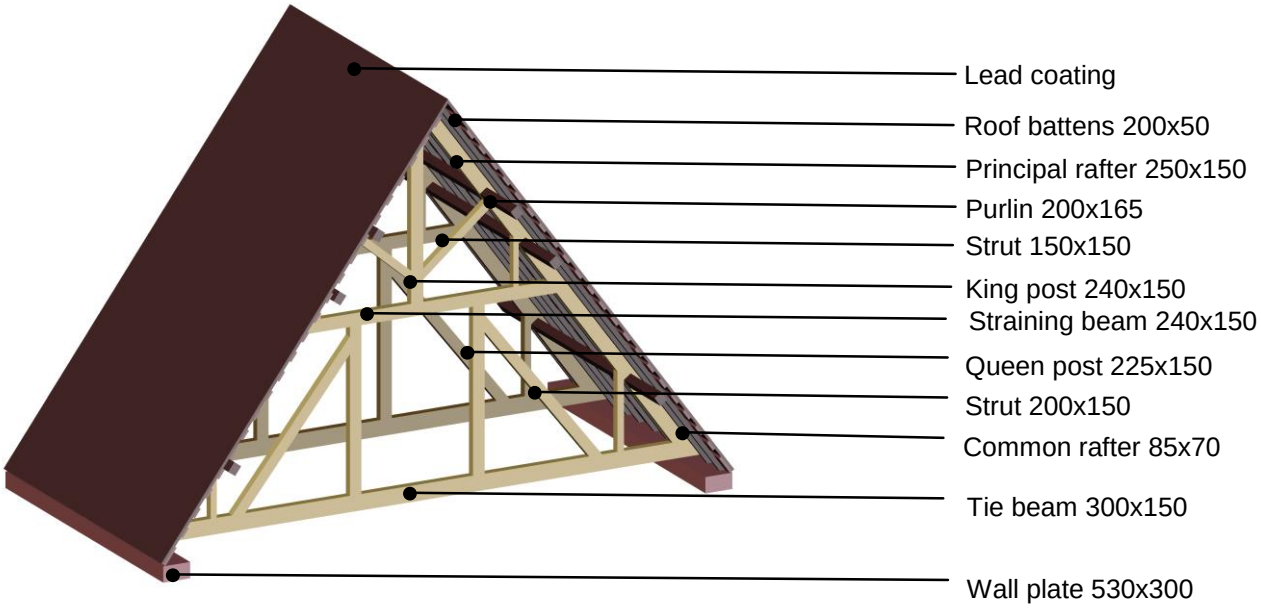

Figure 3-11. Structural parts of the roof framing in the nave of Canterbury Cathedral and section areas (millimeters).

The roof of the south aisle of Canterbury Cathedral is single pitched of about 8º, with a covering span of 5.0 m. The timber trusses are placed with a spacing of 2.7 m (centre axis) and on the side of the buttresses the tie beams rest on wall plates over the upper surface of the buttresses. An adjoining post and curved brace timber elements, fixed on a small cantilever, counteract the bending and vertical forces. From the inner side, the tie beam and principal rafter are attached separately to the walls of the triforium. Thus, the trusses of the lateral aisles are not considered a hinged truss system. The external roof coating is large size lead sheets, attached on a system of timber roof battens (Figure 3-12 and 13).

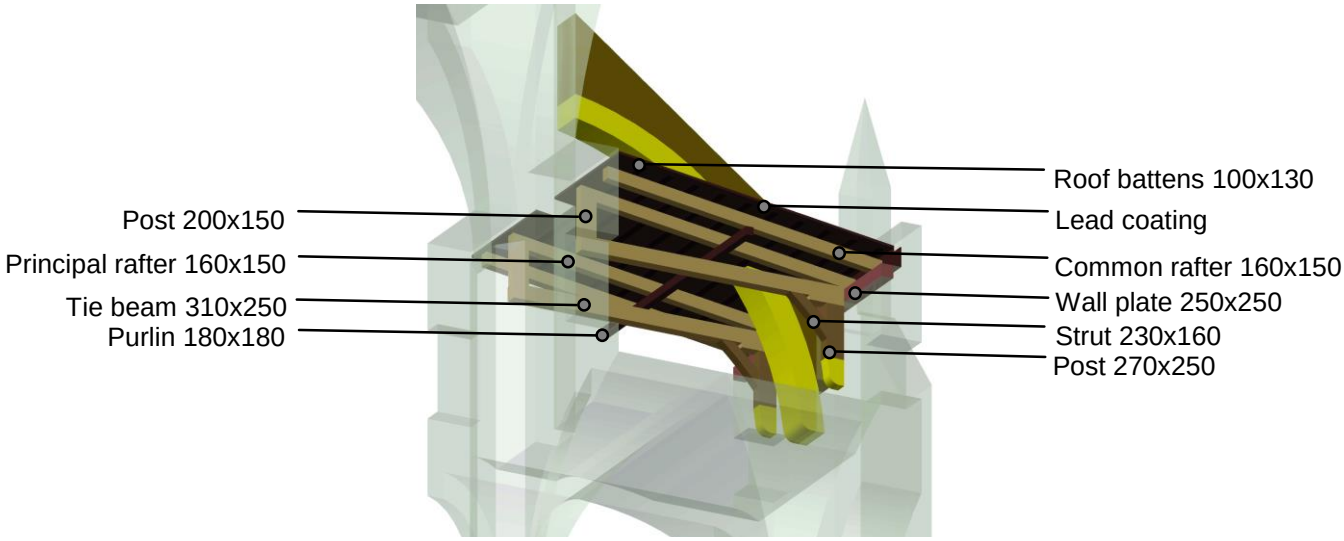

Figure 3-12. Structural parts of the roof framing in the south aisle of Canterbury Cathedral and section areas (millimeters).

Figure 3-13. View of the roof void in the south aisle looking west (Photographic survey).

3.6 System of ties

A system of wrought iron ties is present in each section of the nave of Canterbury Cathedral. The ties run along the nave span, placed on the right side after each corresponding section, 0.9 m below the level of the adjacent clerestory walls and their diameter is 0.043 m. Most probably an initial post tensioning force was applied to the ties, through the coupling system at mid span. The ties were externally anchored to the clerestory walls, through a cross shaped pattress plate on either side (Figure 3-14 and 15). During the visual inspection it was noted that the ties corresponding to case study area (Figure 3-1) were under tension, whereas the others were loose, when they were induced to vibrate.

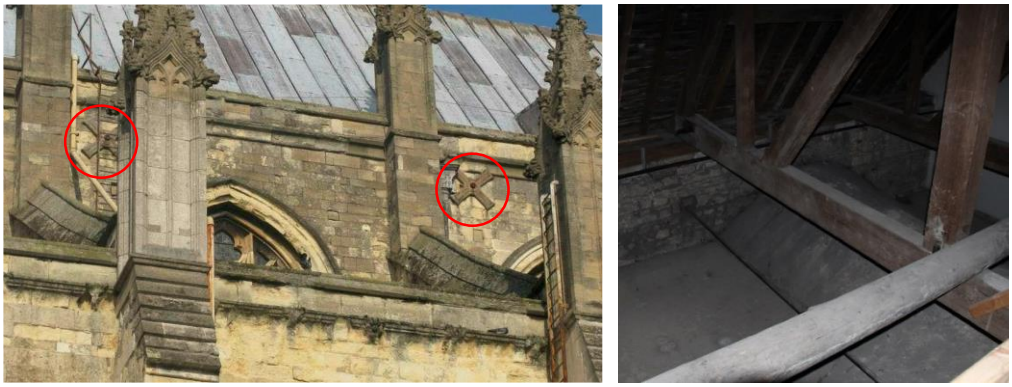

Figure 3-14. (Left) External view of the nave clerestory walls of Canterbury Cathedral, depicting the two anchor cross shaped plates on the right side of each transverse section (Morton Partnership Ltd). (Right) Inside view of the roof void in the nave of Canterbury Cathedral, depicting the iron tie in the clerestory walls above the vaults (Photographic survey).

Figure 3-15. (Left) View of the iron tie at mid span (Right) Coupling system at the mid span of the iron tie (Photographic survey).

3.7 Infill

The infill consists of a part of rubble masonry of unknown consistence and an exterior coating of concrete of unknown thickness, which serves as an impermeable surface for water drainage and water infiltration protection of the vaults system in the event of fire. This drastic measure was imposed in many cathedrals in the United Kingdom in the 1990's, after the fire in York Minster in 1984, as a part of an overall fire proofing intervention. Thus, in case of a fire in the cathedral's roof the disposed water from putting out the fire would not infiltrate the vaults, instead it will drain through drilled holes in the exterior wall system (Figure 3-16) (Deeming 2014).

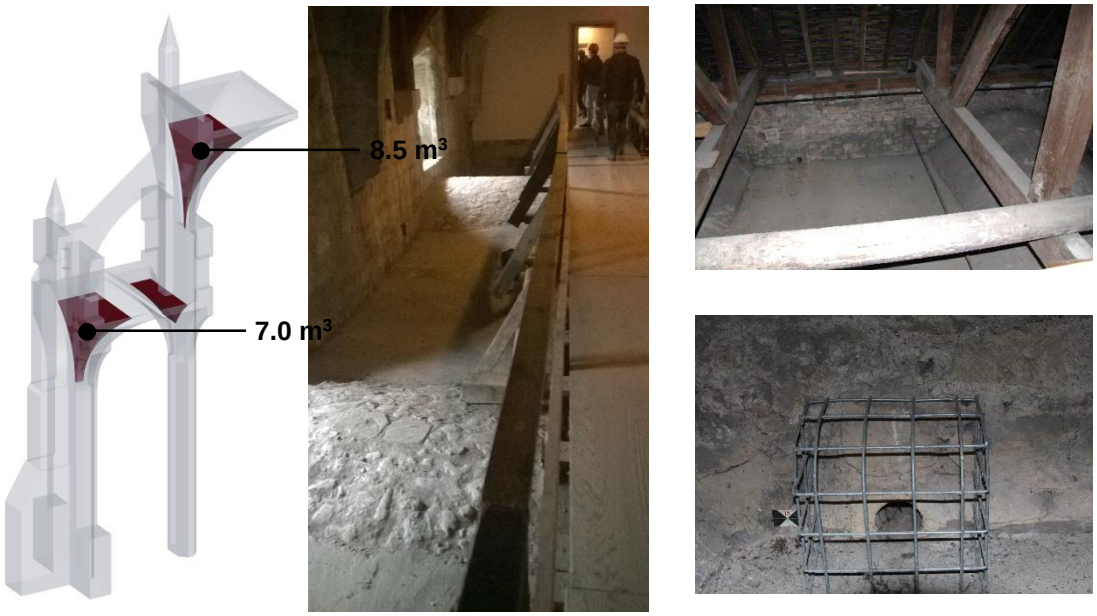

Figure 3-16. (Left) 3D representation of the south 3D CAD model of the critical nave section of Canterbury Cathedral, depicting the infill volumes. (Middle) Infill and cross vault system at south aisle roof void. (Right up) Infill and cross vault system at nave roof void. (Right down) Drilled hole in the exterior wall at the level of concrete layer infill, used for drainage (Photographic survey).

In the central nave the infill height, from the springing level, is 5.3 m and corresponds to the 84% of the vault's rise. Regarding the south aisle the infill height is 3.87 m and corresponds to the 95% of the vault's rise. As far as the infill in the vault system of north aisle, it has been removed during an ongoing process of disposing materials with asbestos from parts of the cathedral. Due to the toxicity, access to the north aisle roof void was not possible.

3.8 Flying buttresses

The nave of Canterbury Cathedral has 7 pairs of flying buttresses, attached in between the nave's clerestory wall and the vertical buttresses. Their thickness is 0.7 m and their geometric characteristics are depicted in Figure 3-17.

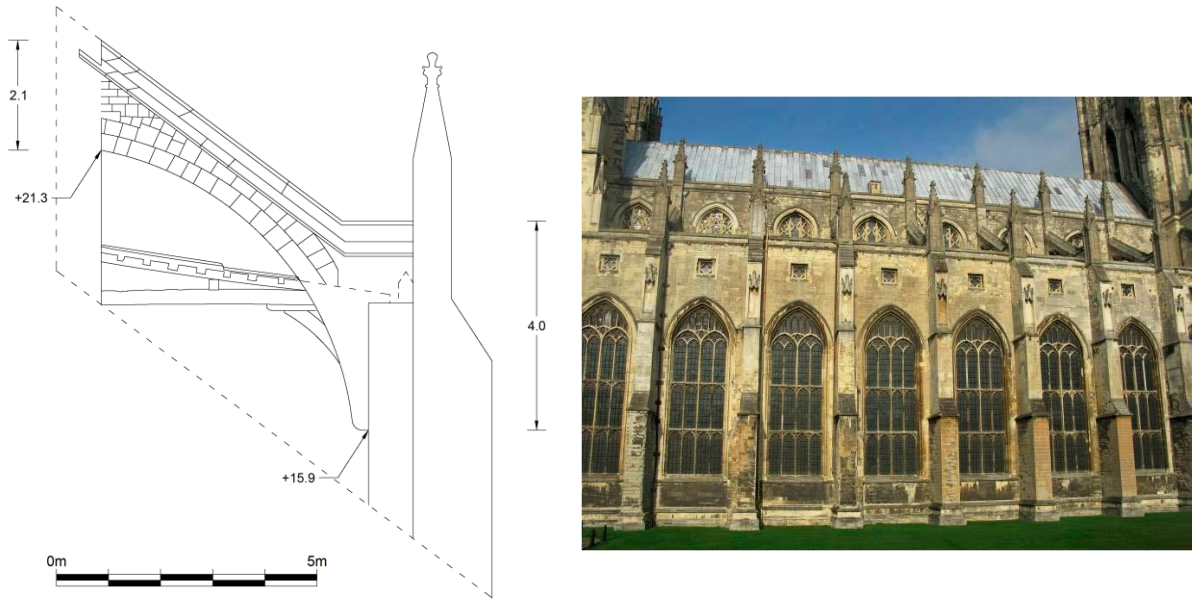

Figure 3-17. (Left) East view of flying buttress in the south aisle of Canterbury Cathedral, depicting dimensions (meters) on the interface between the clerestory wall and vertical buttress, as well as elevation levels from base. (Right down) View of the south aisle of Canterbury Cathedral, presenting the system of vertical and flying buttresses (Photographic survey).

4. INSPECTION AND INVESTIGATION SURVEY

4.1 Visual inspection plan

A visual inspection and damage survey was carried out in the central nave and lateral aisles of Canterbury Cathedral during the 1st and 2nd of May 2014, from the Civil Engineering Department of University of Minho, Portugal. The study emphasised on the detailed geometric and damage documentation of the transversal cross sections 2 and 3 and the corresponding bays 2, 3 and 4, as shown in Figure 4-1.

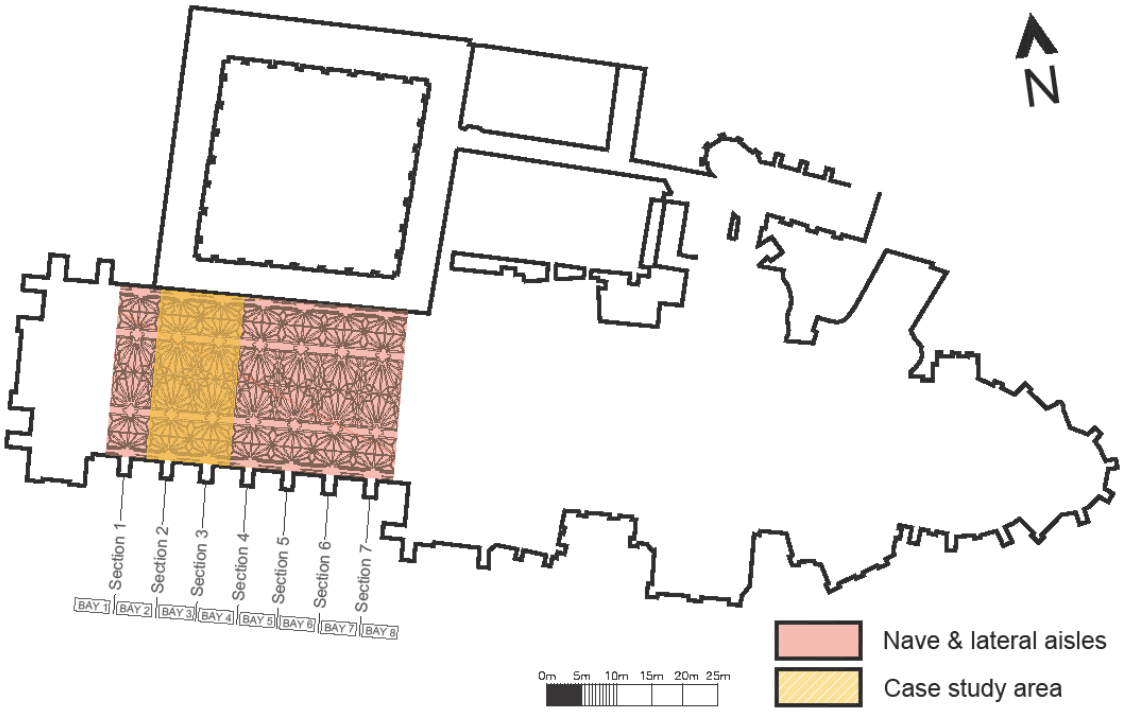

Figure 4-1. Top plan of Canterbury Cathedral depicting the sections and bays of the nave and lateral aisles, consisting the case study area (Morton Partnership Ltd).

The main objective of the visual inspection survey was to identify and document the damage patterns in structural elements and specifically the crack pattern. The crack survey and interpretation is of immense importance as it can be directly related to the structural damage and can indicate significant structural movements. Thus, by identifying the crack pattern it is possible to differentiate the existing damage with plausible causes of damage and deterioration (Ramos et al. 2014a).

In particular, damage maps were prepared for the vault's intrados of the nave and lateral aisles as well as for the flying buttresses in section 2 and 3 of the south aisle, in which the greater damage was

observed. Lastly, an outward tilting initial investigation was conducted from the geometrical survey prepared by the Downland Partnership Ltd and provided by Morton Partnership Ltd.

Through the visual inspection, and despite the damage, the overall condition of the vault system in the nave and lateral aisles, as well as in the flying buttresses of Canterbury Cathedral could be considered satisfactory. The main damage documented in the intrados of the vault system was a distributed crack pattern in the webs and moisture stains and discoloration areas on both the nave and lateral aisles crossed vault system. As for the flying buttresses in sections 2 and 3, the most significant damage was the tensile and shear failure of joints, the deterioration of large surface areas of the stone units and the extended biological growth.

4.2 Damage survey in nave and aisles vaults

This damage survey was conducted in the entire area of the intrados of the main nave and lateral aisles, rather than the area of study, which inscribes the cross sections 2 and 3 and the corresponding vaults, in order to identify and obtain the damage sequence in a greater area (Figure 4-2). Indeed the cracks followed a distributed and repetitive pattern throughout the whole nave and lateral aisles, but without resulting to uniform or continuing fragmentations. Still, a potential fragmentation of large structural parts is evident. Also, the number, length and width of the cracks intensifies in sections 2 and 3.

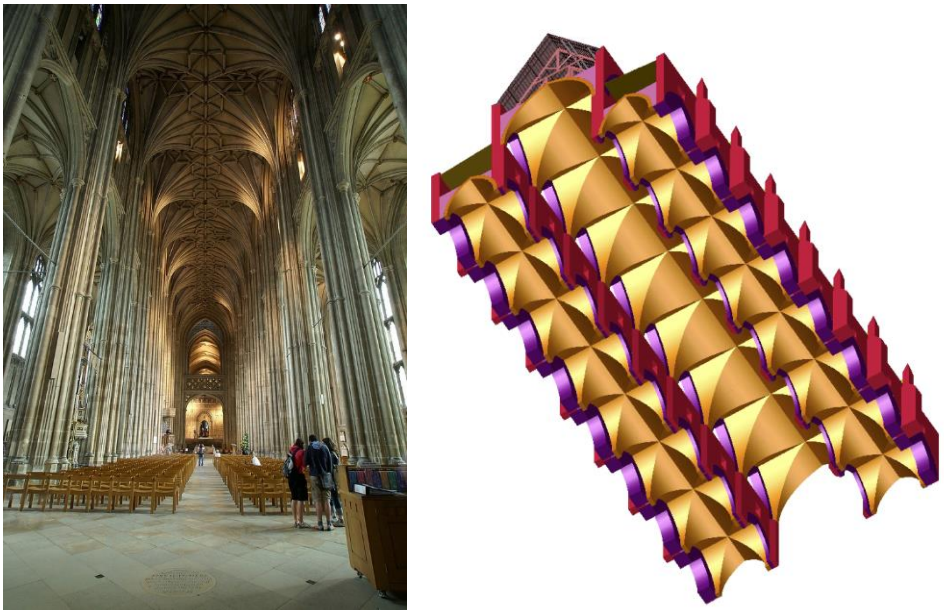

Figure 4-2. (Left) View of the nave and lateral aisles of Canterbury Cathedral looking east ("Canterbury Cathedral" 2014). (Right) 3D representation of the vaults intrados in the nave and lateral aisles of Canterbury Cathedral.

The nave and lateral aisles structural system experiences many individual cracks, as shown in the damage map (Figure 4-3). The width of the cracks could not be obtained, due to the absence of approaching means.

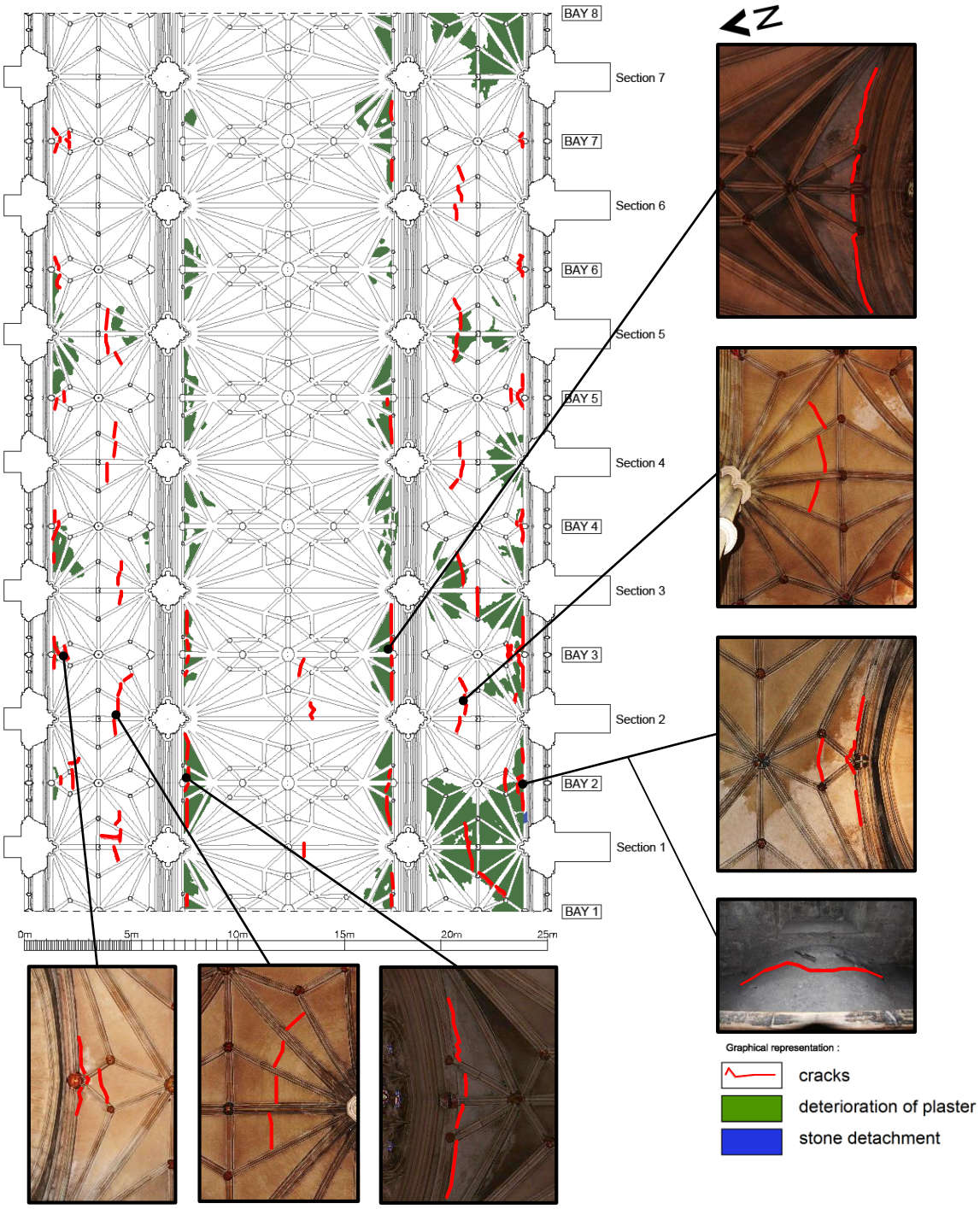

Figure 4-3. Damage map of the intrados of the vault system in the nave and lateral aisles of Canterbury Cathedral.

4.2.1 Crack pattern

As it can observed in Figure 4-3, in the south aisle, large cracks, parallel to the south side walls are observed in bays 2 and 3, whereas in bays 4, 5, 6 and 7 the cracks are less in length. The same crack pattern is evident mainly in bays 2 and 3 of the nave, in both interfaces between the north and south side walls and the vault. Taking into account the high level of infill, which with the added concrete layer reaches 95% and 84% of the vault's rise in the south aisle and nave respectively, it can be concluded that the attaching spans are highly confined and undeformable, and eventually the vaults got separated from the side walls, by forming Sabouret's cracks (Theodossopoulos 2008).

Another set of cracks (intrados), following a repetitive pattern, is observed above the springings of the inner adjacent span in both the north and south aisle and mainly in sections 1, 2, 3, 4 and 5 (Figure 4-3). The cracks are formed in between the ribs and follow a circular arrangement around each capital. This type of cracks can be induced by several different phenomena, such as lateral thrusts that lead to large deformations. A common mechanism of lateral instability in Gothic Cathedrals, comprised off a nave and lateral aisles, is the spreading of the supports; inwards at the aisles and outwards for the nave and is mainly triggered by excessive thrusts, overloading or insufficient flying buttresses. By taking into account the excessive infill volume of the aisles vaults, any large deformation would be highly influenced by the infill mass, resulting to high tensile stresses in the intrados of the web, close to the level of the infill (Figure 4-4) (Theodossopoulos et al. 2008).

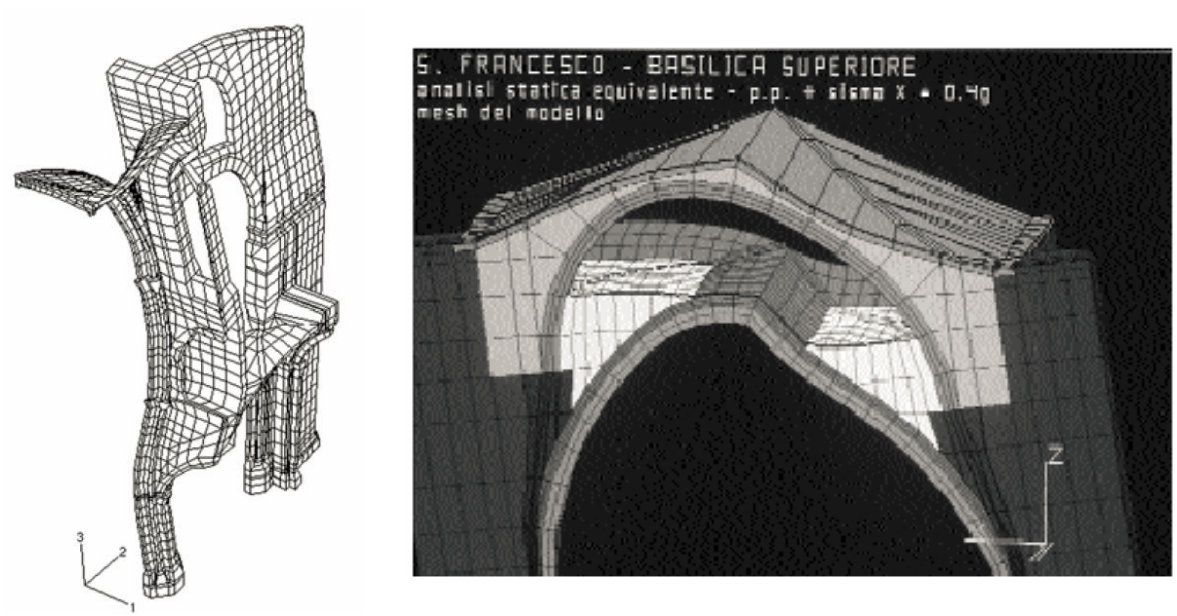

Figure 4-4. (Left) Amplified deformation of Burgos Cathedral cross section. The springing of the aisle vault spreads inwards, while the upper part of the nave deforms outwards. (Right) FEM model representing the large deformation of a vault in St. Francis Basilica under excessive outward movement, leading to the collapse of the vault, caused by the earthquake in September 1997 (Theodossopoulos et al. 2008).

Focusing on the case study area, as shown in Figure 4-5, the surface of the infill, being classified from the geometrical survey, is correlated with the damage map and depicted in purple. In order for the crack pattern, which surrounds the capital of the piers, to be consistent with the infill boundaries and taking into account that the present infill level is higher, due to the addition of the concrete layer, an estimated former infill level is chosen. The estimated former infill upper surface, depicted in green, was chosen so as to approximately correspond to the cracks in the springings and is 40 cm lower than the current level in both the aisles and the nave vaults.

Figure 4-5. Damage map of the case study area, which depicts the current and former estimated infill boundaries.

Another possible cause related to the documented damage is the imposition of differential settlements in some part of the foundation soil of the structure. Matching crack patterns, induced by differential settlements are detachments of corners and outward leaning of structural elements, resulting in a redistribution of stresses and resetting the structural system in a new state of equilibrium (Figure 4-6). Local soil failures that cause differential settlements can be triggered by modifications in the foundation soil, caused by vibrations from civil works, dead load increase, water leakage of underground pipes, changes in underground water level etc. (Figure 4-7).

Figure 4-6. Corner detachment of a vault, provoked by differential settlements and rotations at base, in the Monastery of Salzedas, Portugal (Lourenço et al. 2008).

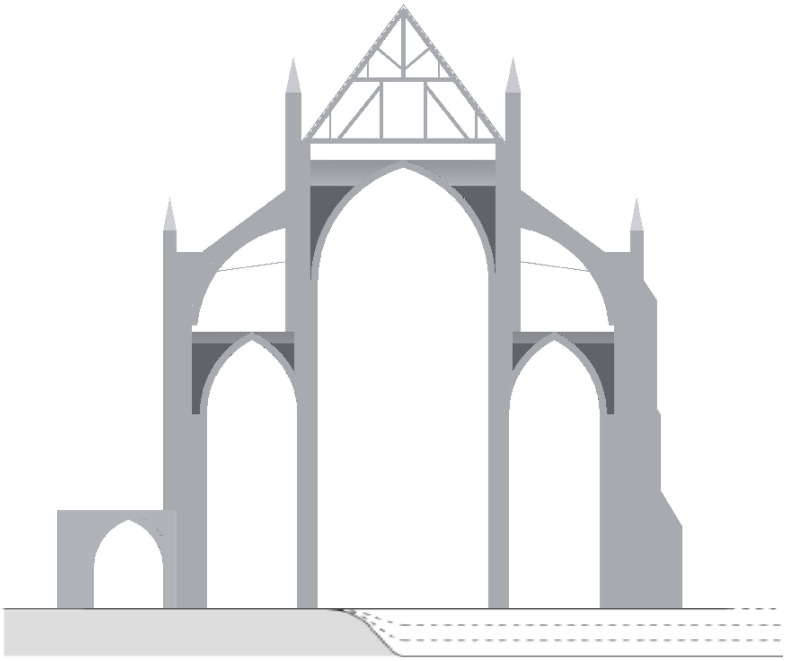

Figure 4-7. Possible magnified displacement field of a medium-end settlement, induced in the south part of the foundation of Canterbury Cathedral, which affects the vertical abutments of the south part of the nave and aisle by inducing vertical translations and outward leaning.

4.2.2 Deterioration of plaster

Another damage located on the plaster surface of the vault's intrados, in areas close to the interface between the vaults and the exterior walls of both the nave and lateral aisles, is a discoloration of the plaster surface, which can also be regarded as staining (Figure 4-3). Water penetration in the vault structure, through the pore system, even amplified by the present cracks can be regarded as the triggering mechanism (Ramos et al. 2014b).

The previously mentioned degradation mechanism, can be also combined with the presence of the concrete infill layer, causing the formation of efflorescence (calcium carbonate, calcium silicate) in the

plaster surface. Through the presence of pore water, the dissolved soluble salts in the concrete mass get transferred in the vault's system, were they crystalize. This can lead to a potential future deterioration through spalling and loss of joint adhesion of the vault system. Further investigation and testing is needed in order to determine the presence of soluble salts, such as sulphates and nitrates, or even chlorides (Ramos et al. 2014c).

4.3 Damage survey in flying buttresses of south aisle

A detailed damage survey was conducted in the flying buttresses of the south aisle in sections 2 and 3. Their location can be shown in Figure 4-8.

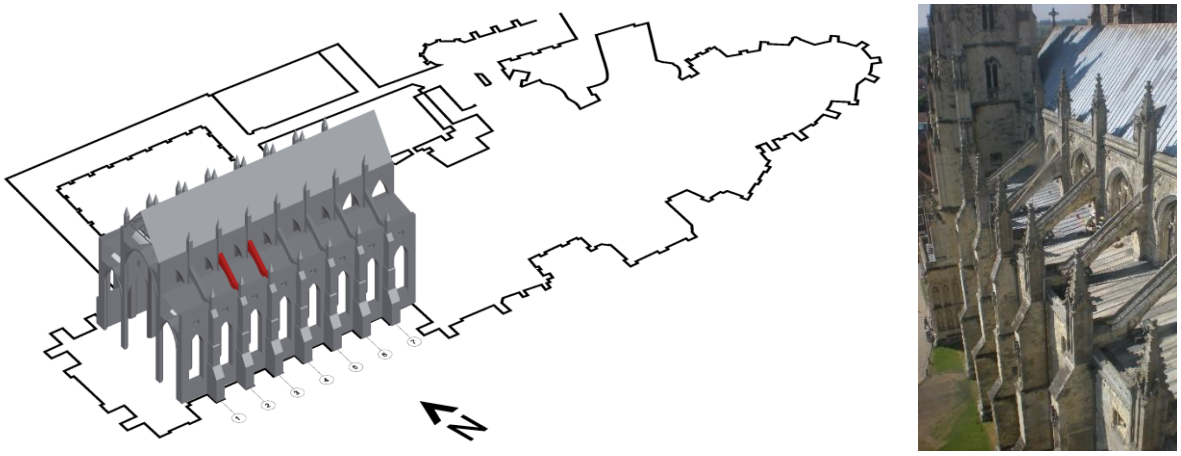

Figure 4-8. (Left) Graphic representation of the nave and lateral aisles of Canterbury Cathedral. The flying buttresses 2 and 3, for which damage maps were prepared, are depicted in red. (Right) View of the flying buttresses of the south aisle looking west.

The flying buttresses 2 and 3 of the south aisle show significant deflection, following the global deformation of the structure, which appears to be rotating outwards. The failure of many joints was classified and large areas experience crust formation and biological growth, as shown in Figures 4-9 and 4-10.

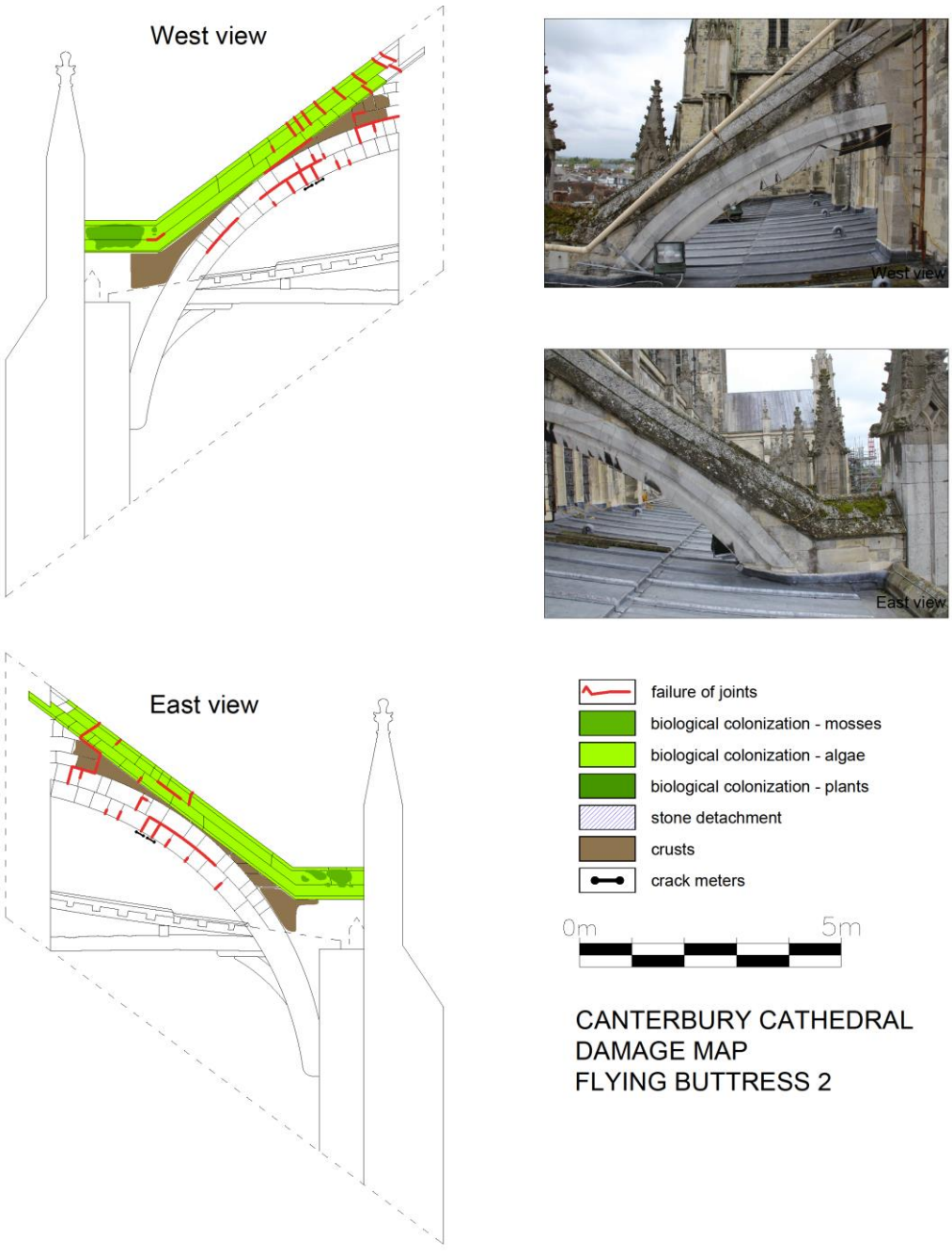

Figure 4-9. Damage maps of the west and east view of flying buttress 2 at the south aisle of Canterbury Cathedral.

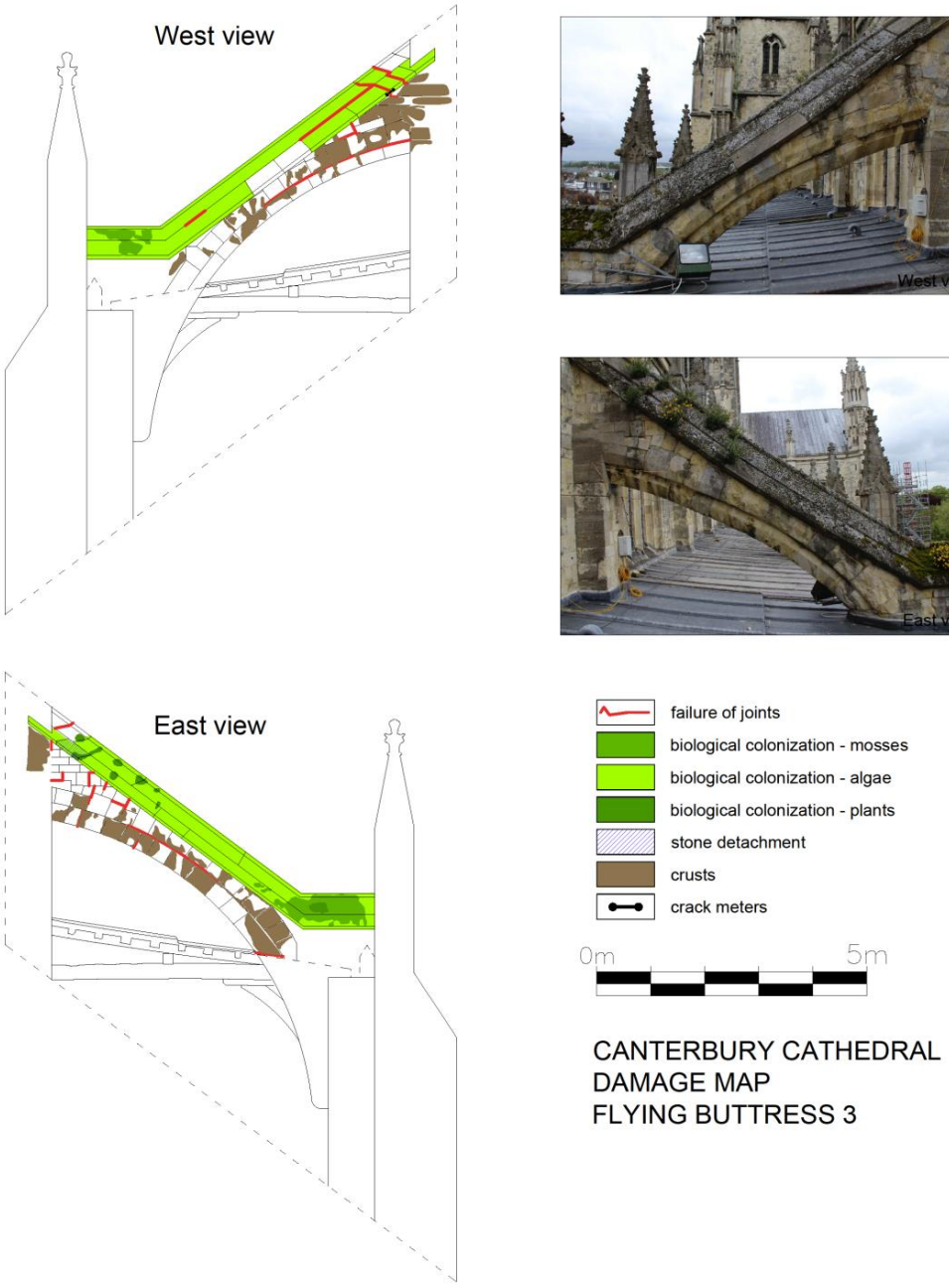

Figure 4-10. Damage maps of the west and east view of flying buttress 3 at the south aisle of Canterbury Cathedral.

4.3.1 Joint failure

As it can be observed in the damage maps of the flying buttresses 2 and 3 of the south aisle, many of the joints close to the intrados of the arch have failed under tensile and shear stresses. The crack width is moderate (lower than 1 mm) (Figure 4-11).

This type of damage pattern corresponds to an outward rotation and spreading of the vertical abutments, as the cracks seem to have occurred in recent decades. This type of deflection and joint failure can also come from the construction process, due to the deformation of the centerings. Some loss of mortar from the joints can also be activated from weathering or chemical reactions (Roca et al. 2013). Through the correlation with the response from the monitoring data, which will be presented in a following chapter, a stronger notion of the triggering mechanism can be obtained.

Figure 4-11. Crack patterns of joint failure from west view of flying buttress 2 (Left) and 3 (Right) of the south aisle of Canterbury Cathedral.

4.3.2 Crust formation

Large parts of the stone units of the flying buttresses have evident signs of ageing and weathering that can be classified as crust formation with exfoliation. During this process layers of the outer stone surface were subject to a chemical material transformation. Further testing could determine the responsible mechanism and the specific pollutants, such as carbons, chlorides and fluorides, and solid particles (dust, soot, ashes, etc.) (Ramos et al. 2014a).

The typical physical mechanism responsible for the deterioration and weathering of limestone is the presence of pollutant gases SO_2 and NO_x, which by reaction with air moisture produce a black crust, which later exfoliates and produces flaking (Figure 4-12). The rate of deterioration of limestone blocks differs according to the local environmental conditions over the course of time and would have certainly been more intense in the coal burning urban economy of the 19th century in UK. Freeze-thaw cycles can escalate the level of damage, as entrapped water freezes and expands, causing material disintegration and/or due to salt crystallization, in the presence of soluble salts (Blows et al. 2003).

Figure 4-12. Crust formation and flaking in large areas of Caen stone masonry from west views in the flying buttress 3 of the south aisle of Canterbury Cathedral.

4.3.3 Biological growth

Biological growth consists mainly of minute biological organisms such as mosses and algae, which cover large surfaces of the upper part of the flying buttresses and of higher plants, but only in small areas, as shown in Figure 4-13.

Figure 4-13. Biological growth in form of algae, mosses and higher plants in the upper surface of flying buttress 3 (east view) in the south aisle of Canterbury Cathedral.

4.4 Outward tilting of the vertical elements

From the cross section 3 produced in the geometrical survey prepared by the Downland Partnership Ltd and provided by the Morton Partnership Ltd, the outward leaning of the vertical abutments of the nave and south aisle was graphically investigated (Figure 4-14).

The vault of the south aisle is depicted clearly deformed, suppressed by an outward tilting of the vertical abutments. The outward leaning of the pier is around 1% and 1.4% in the level of the aisle and nave vaults respectively and is a direct indication of the incapacity of the vertical elements to counteract the lateral thrusts (Theodossopoulos et al. 2002). The greater inclination of the upper part of the pier corresponds to the residual thrust from the nave vault and reveals that it spreads more outwards than its lower part.

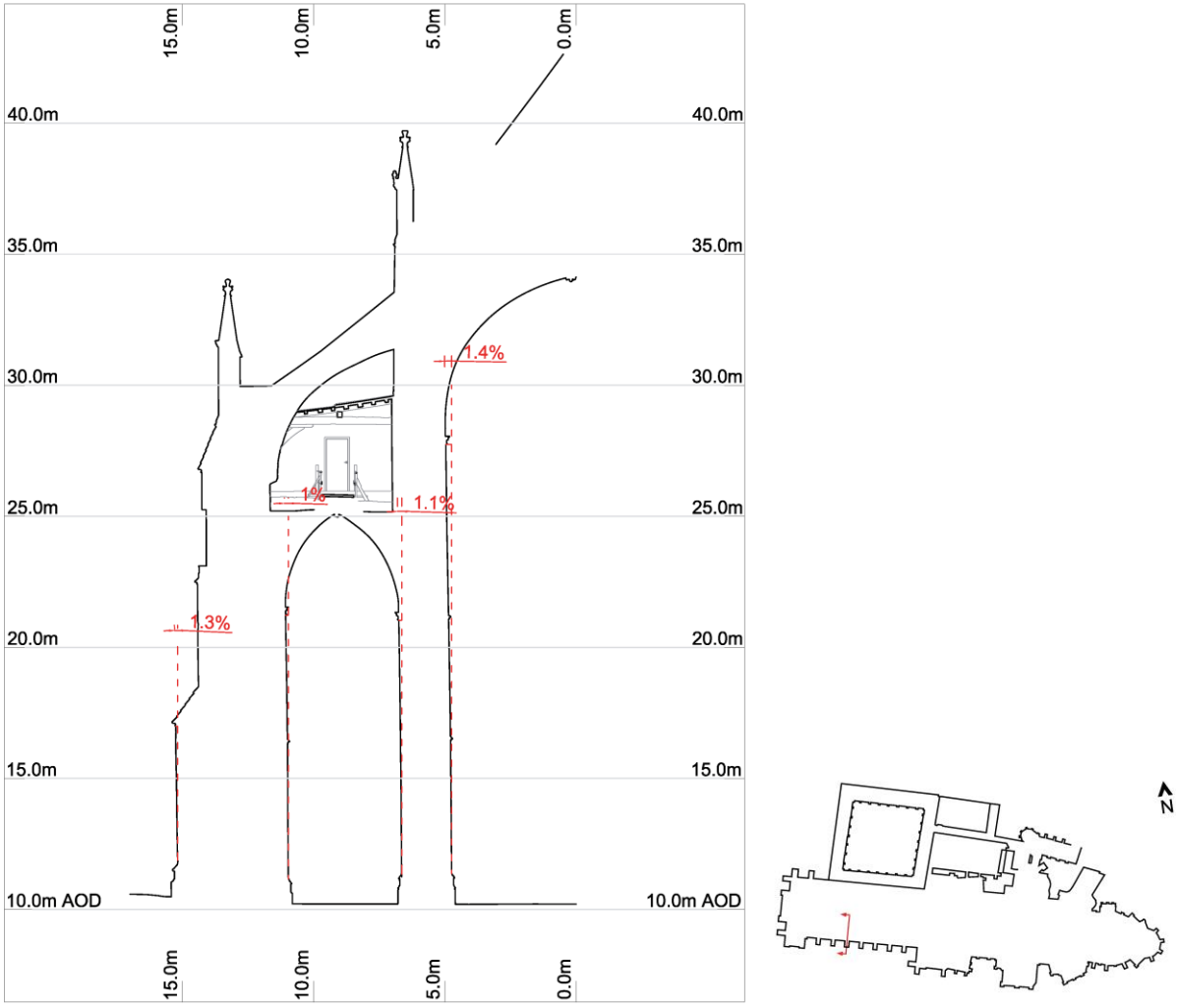

Figure 4-14. Cross section 3 depicting the south aisle and half of the nave of Canterbury Cathedral, prepared by the Downland Partnership Ltd and provided by the Morton Partnership Ltd. The inclination of the vertical abutments is depicted in red.

4.5 Material properties

In the current study the experimental in situ tests were limited to dynamic identification, and the material properties were determined according to bibliographic resources and the Italian standards (NTC-2008), because it gives the possibility of determining the mechanical characteristics of masonry structures by means of prescribed classified values.

Through NTC-2008, specific criteria and characteristics are assigned in masonry, according to different knowledge levels (LC1, LC2, LC3) (Figure 4-1). In many case studies it is often difficult or unfeasible to obtain the material properties from direct in situ testing, whereas in other cases can be proven unreliable. Additionally, an important aspect that can increase the level of knowledge, accountable in the Italian norms is the option of experimental results from other buildings of a proven similar typology and regional proximity (Franchetti 2014).

Nevertheless, material in situ testing is the only objective way to obtain values that can approximate the actual material properties. Specifically for accurately determining the material properties, an integrated procedure is suggested: (Binda et al. 2007; Cardani et al. 2013)

1. Detailed visual inspections in order to determine issues related to structural characteristics, such as the actual quality of connections between walls, typology and level of damage in masonry.
2. Superficial and internal sampling from specific points (of sound masonry) in order to distinguish the type of masonry.
3. Characterization tests of the type of mortar, type and ratios of binding agents and aggregates, and physical and mechanical characteristics of units (stone or brick).
4. Single and double flat jack tests to verify the overall behavior of the masonry, by acquiring the level of stresses and the modulus of elasticity.
5. Complementary non-destructive tests (sonic pulse velocity test, ground penetrating radar, boroscopic camera, infrared camera) that can correlate with the minor destructive and destructive test results (Figure 6-2). Where single and double flat jack test are not applicable or give questionable results, due to low level of stresses in masonry and in highly irregular, inhomogeneous or damaged masonry, then ND tests are considered the only feasible approach to obtain material properties. Yet, a quantitative substantial correlation between sonic pulse velocity tests and double flat jack tests is still under investigation.
6. All the above steps have to be repeated for every different type of masonry present in the structure.

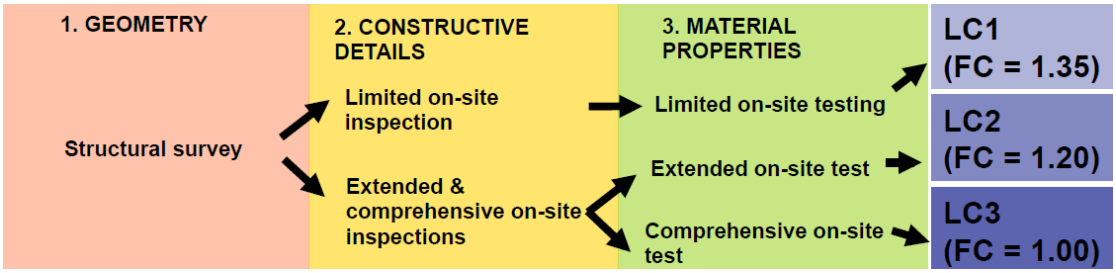

Figure 4-15. Determination of knowledge levels and confidence factors, corresponding to the extent of material testing and on-site inspections (Franchetti 2014).

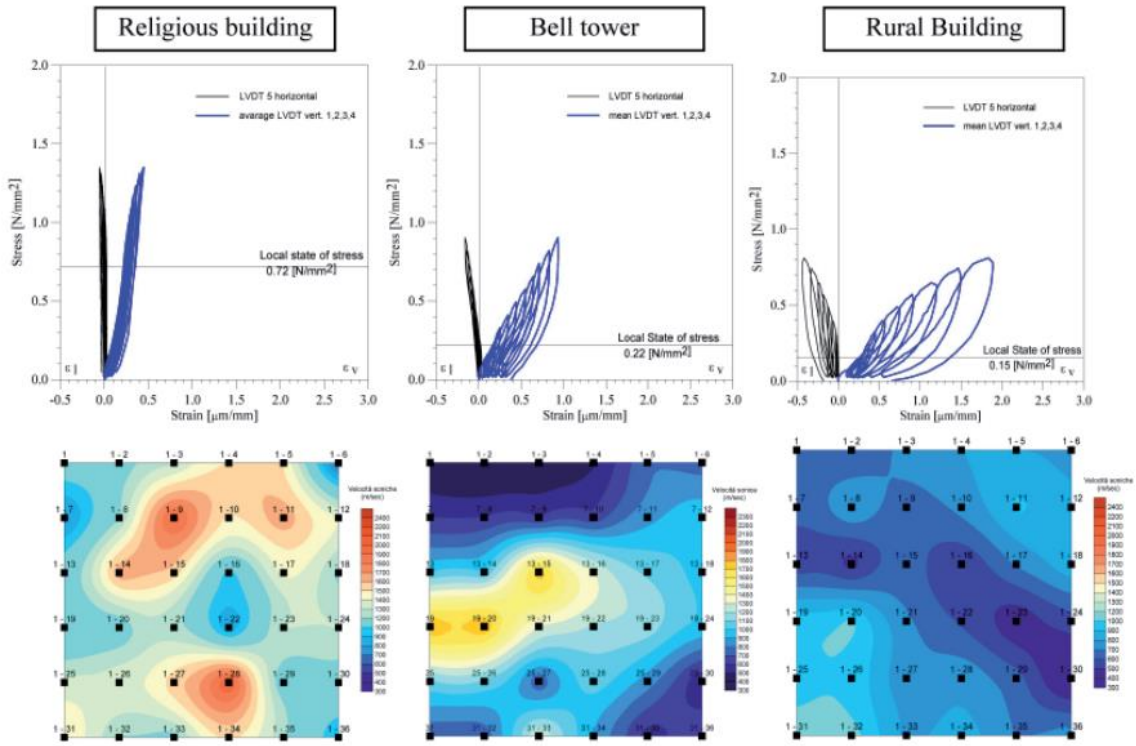

Figure 4-16. Test results from double flat jack tests and sonic pulse velocity, performed in different stone masonry typologies of Campi Alto di Norcia (Perugia, Italy) (Cardani et al. 2013).

In the current study, three different types of materials are defined in the FEM model; Caen limestone masonry, describing the entire skeleton of the cathedral, irregular and inhomogeneous masonry used as infill, wrought iron ties in the level of the nave vaults and wrought iron pattress plates, used as projecting boundaries for the ties.

The Italian code NTC08 provides ranges of material properties for different masonry typologies and material qualities (Table 4-1). According to the differentiation of masonry typologies, the infill material can be defined as irregular stone masonry. As for the Caen stone masonry two kinds are eligible; the cut stone masonry with good bonding and the dressed rectangular (ashlar stone) masonry. In that case, the range of values presented in Table 6-1 would be considered as a reference and the mechanical

properties would be validated through their additional components; i.e. unit blocks and mortar joints (Magenes et al. 2009; Foti et al. 2012).

Table 4-1. Reference values of the mechanical parameters and average specific weights for selected types of masonry (extract from Table C8A.2.2. of Circ. NTC08, 2009).

Masonry typology	f_m (N/mm^2)	τ_o (N/mm^2)	E (N/mm^2)	G (N/mm^2)	W (kN/m^3)
	min-max	min-max	min-max	min-max	
Irregular stone masonry (pebbles, erratic, irregular stone)	1.0 1.8	0.020 0.032	690 1050	230 350	19
Uncut stone masonry with facing walls of limited thickness and infill core	2.0 3.0	0.035 0.051	1020 1440	340 480	20
Cut stone with good bonding	2.6 3.8	0.056 0.074	1500 1980	500 660	21
Soft stone masonry (tuff, limestone, etc.)	1.4 2.4	0.028 0.042	900 1260	300 420	16
Dressed rectangular (ashlar) stone masonry	6.0 8.0	0.090 0.120	2400 3200	780 940	22
Solid brick masonry with lime mortar	2.4 4.0	0.060 0.090	1200 1800	400 600	18

Infill material Sound stone masonry - possible identification

4.5.1 Caen limestone masonry

Caen stone is a light yellow quarried in northwestern France near the city of Caen and is regarded as the original stone used in the masonry of Canterbury Cathedral ("Caen Stone" 2014). According to validated technical information for stone industrialized products (according to BS EN 1936:2006), the compressive strength and mass density of Caen limestone are 25.9 MPa and 2.050 kg/m^3 respectively ("Anglo-European Stone" 2014). The mortar joints were assumed to be of pure lime mortar, of the weakest compressive strength f_m, according to the Italian code; M2.5 (f_{mk}=2.5 MPa). According to the Italian code (NTC 08-TABLE 11.10.VII), the characteristic compressive strength of masonry, composed by natural squared stone elements and mortar joints of thickness 5-15 mm, can be validated by the average compressive strength of its components. Thus, the characteristic compressive strength of Caen stone masonry is f_{bk}=6.7 MPa (Magenes et al. 2009; Foti et al. 2012).

According to the definition of the knowledge level (LC1, 2, or 3), a specific confidence factor is applied to the mean material properties of the masonry. Thus, the material properties are considered smaller, due to the uncertainty imposed by the lack of experimental tests. In the current case study, due to the

lack of material testing, the Knowledge level considered is LC1, corresponding to a Confidence factor of 1.35 (Franchetti 2014). Thus, the reduced compressive strength of Caen stone masonry is:

$$\mathrm{f_{bk,red}} = \frac{\mathrm{f_{bk}}}{\mathrm{FC}} = 5.0\ [\mathrm{MPa}] \qquad \text{(Eq.4.1)}$$

The pure shear strength of masonry, composed by natural elements or squared artificial elements, can be obtained as a relation of the compressive strength of the units and the class of the mortar (Table 4-2) (Magenes et al. 2009; Foti et al. 2012).

Table 4-2.Characteristic shear strength, in absence of vertical load, for masonry with natural stone elements (NTC 08 - Table 11.10.VII)

f_{bk} (N/mm^2)	Type of mortar	f_{vko} (N/mm^2)
$f_{bk} > 15$	M10 ≤ M ≤ M20	0.20
$7.5 < f_{bk} \leq 15$	M5 ≤ M ≤ M10	0.15
$f_{bk} \leq 7.5$	M2.5 ≤ M ≤ M5	**0.10**

Regarding the tensile strength of Caen stone masonry, a specific relation between the tensile strength and the compressive strength is difficult to be established, due to high variability of shapes, scatter in materials and diversity of construction processes. The flexural strength of composite masonries, as stated in EC6, ranges from f_{xk1}=0.05-0.2 N/mm^2 for plain failure parallel to bed joints and f_{xk2}=0.10-0.4 N/mm^2 for plane failure perpendicular to bed joints (EN 1996-1-1 §3.6.3).

Given to the low tensile bond strength in the unit mortar interface, which is typically in range of 0.1 to 0.2 MPa, the chosen value for the tensile strength of Caen stone masonry is considered equal to 0.2 MPa (Lourenço 2008).

Taken into account extensive experimental double flat jack testing performed on various masonry typologies, both regular and irregular, depicted in the diagram of Figure 4-3, there is a dispersion on the acquired values of modulus of elasticity. The obtained average values are around 4500 MPa, 1800 MPa and 1700 MPa for regular stonework, brick and stone masonry and irregular stonework respectively (Binda et al. 2007). Given the lack of experimental testing on site and the uncertainty of the level of regularity of the Caen stone masonry in Canterbury Cathedral, the value of modulus of elasticity provided by usual formulas is considered rather high. Thus, a value of 3000 MPa is estimated, from the range of values in the diagram. Regarding the shear modulus, it can be determined as a relation of the elastic modulus (Eq.4.2).

$$\mathrm{E_m} = 3000\ \mathrm{MPa} \qquad \text{(Eq.4.2)}$$

$$G_m = 0.4 * E_m = 0.4 * 3000 = 1200\ MPa\ (11.10.3.4\ \mathrm{of\ NTC} - 2008)$$

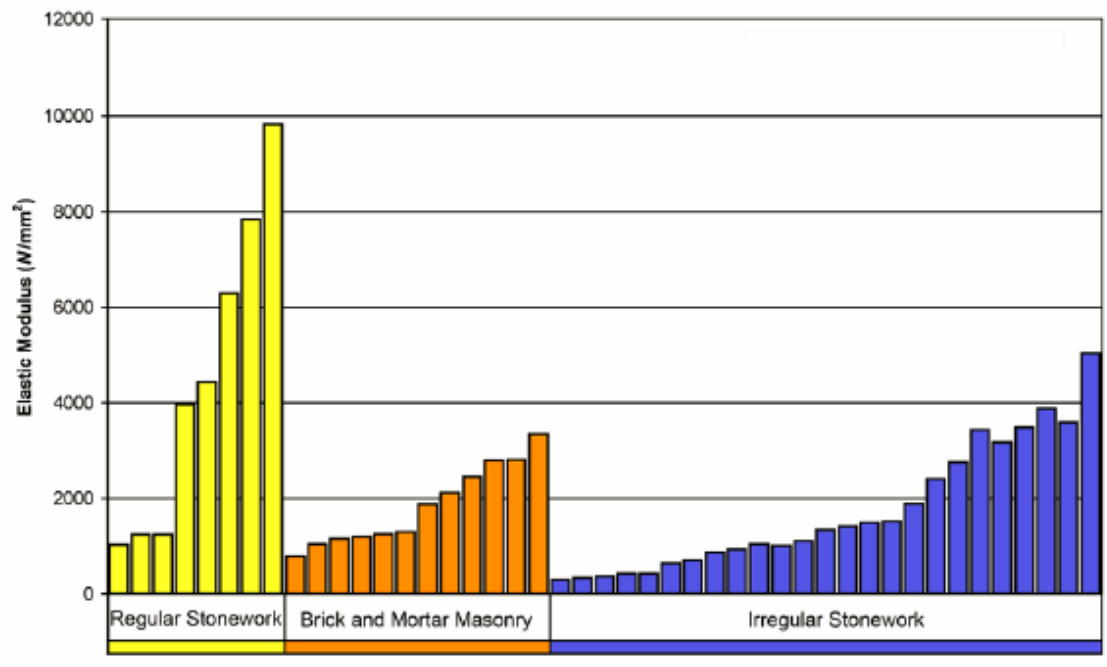

Figure 4-17.Values of the elastic modulus, obtained by double flat jack tests on different masonry typologies. The results have been grouped in order to allow a comparison of values for regular stonework with thin joints, brickwork, and irregular stone masonry (Binda et al. 2007).

4.5.2 Infill material properties

As described in the geometrical survey, the ribbed cross vaults of both nave and the south aisle have a significant volume of infill; approximately 8.5 m^3 and 7.0 m^3, respectively. Due to the high level of heterogeneity of the infill and the unknown depth of the observable concrete layer on top, the mechanical characteristics will be taken from reference values for irregular type of stone masonry in Table 4-1. Due to the lack of experimental tests, the level of knowledge is set to LC1 and the minimum of the range values is chosen, as 1.0 MPa for the compressive strength, 690 MPa for the modulus of elasticity and 19 kN/m^2 for the mass density. The tensile bond strength was chosen as 0.1 MPa (Lourenço 2008).

4.5.3 Wrought iron ties and pattress plates

The mechanical properties of wrought iron ties and wrought iron pattress plates are determined as given in Table 4-3.

Table 4-3. Mechanical properties of faggoted (wrought) iron rods (Holický et al. 2005).

Characteristic tensile strength (MPa)	207
Tensile design strength (MPa)	180
Compressive strength (MPa)	Equal to tensile strength
Elastic modulus (GPa)	100
Shear modulus (GPa)	30
Density (kN/m^3)	76

4.5.4 Softening behavior and fracture energy

Masonry can be described as a quasi-brittle, heterogeneous material, of many different typologies, regarding the geometry, consistency and construction process. Despite its high diversity, masonry elements have in common a very low tensile strength. The weak and decisive point for the structural behaviour and gradual failure of masonry is the bond between the unit and the mortar (Lourenço 1998).

The objective of an accurate simulation, through numerical models, of the quasi brittle behaviour of masonry is to represent the transition from the elastic stage to the quasi brittle behaviour that involves cracking, leading eventually to failure. This can be defined as the softening behaviour of masonry. Mechanical resistance decreases under a continuous increase of deformation, by the formation of cracks that progress gradually. The process evolves from the state of a diffused pattern of micro-cracks to localized macro-cracks, and the accumulated tensile or compressive stresses are released, as presented in Figure 6-4 (Lourenço 1998).

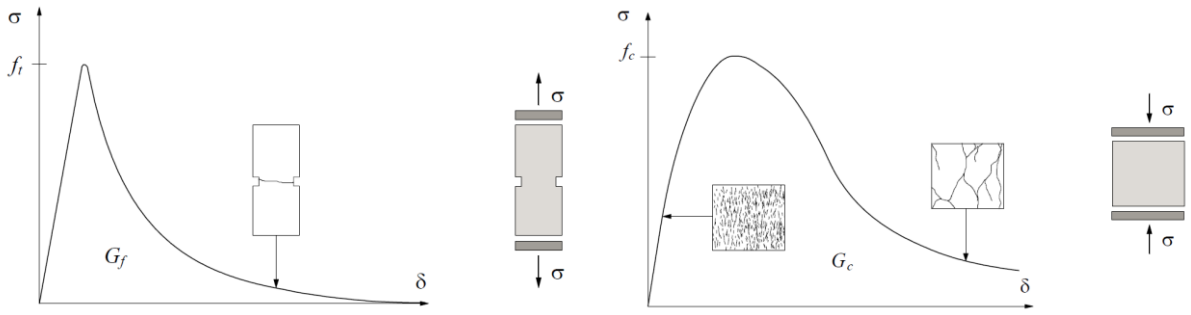

Figure 4-18. Stress - displacement diagrams of quasi-brittle materials under tensile (left) and compressive (right) loading (Lourenço 1998).

The above inelastic quasi-brittle behavior is quantified by the integral of the *σ-δ* diagram, denoted as fracture energy G_f for tension and G_c for compression, quantities that are considered material properties and describe the inelastic response of the material, usually considered as mode I. In masonry, an additional failure mechanism is present that depends on the shear resistance of the unit-mortar interface, denoted as mode II fracture energy G_f^{II} and is the integral of the *τ-δ* diagram in the absence of confined loading (Figure 6-5) (Lourenco 1996).

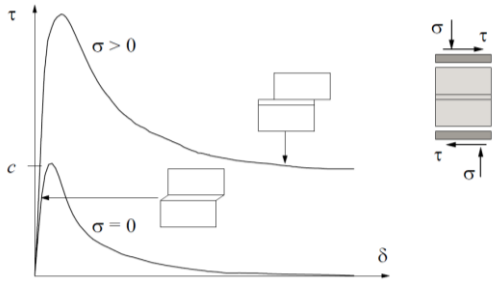

Figure 4-19. Shear stress - displacement diagram of quasi-brittle materials (Lourenço 1998).

For the numerical determination of the fracture energy values, different kind of tests associated with the unit-mortar interface are required that measure the strains in terms of displacement versus stresses. The tensile and shear stresses diminish exponentially, while compression combines a hardening and a softening phase (Figure 6-6) (Lourenço 1998). The recommended fracture energy values for all materials are presented in Table 4-4 (Lourenco 2014).

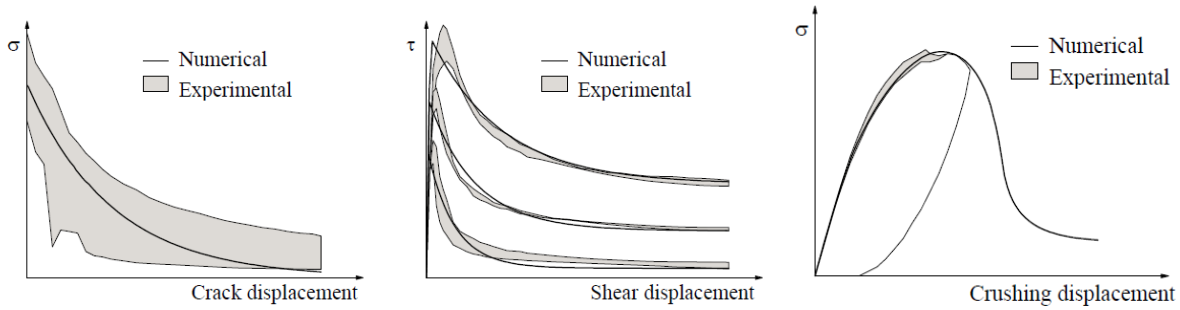

Figure 4-20. Solid clay brick masonry tests and numerical results are presented in diagrams. (Left) Uniaxial tension - crack displacement diagram. (Middle) Shear stress - crack displacement diagram. (Right) Uniaxial compression - crack displacement diagram (Lourenço 1998). The shaded areas represents the experimental envelope of tests.

Table 4-4. . Fracture energy of the materials (Lourenco 2014)

Material	**f_{tk} (MPa)**	**f_{tk} (MPa)**	**Mode I Fracture Energy - G_f for tension (N/mm)**	**Mode I Fracture Energy - G_{fc} for compression (N/mm)**
Caen stone masonry	5.0	0.2	0.012	8
Infill brittle masonry	1.0	0.1	0.012	1.6

4.5.3 Implemented material properties

The material properties, as previously defined, are summarized for the different materials in Table 4-5.

Table 4-5. Mechanical properties of Caen stone masonry, infill masonry, wrought iron ties and pattress plates.

Mechanical properties		Caen stone masonry	Infill loose stone masonry	Wrought iron pattress plate & ties
Compression strength	f_c (MPa)	5.00	1.0	207
Modulus of elasticity	E (MPa)	3000	690	100000
Poisson's ratio	v (-)	0.2	0.2	0.2
Shear modulus	G (MPa)	1200	230	30000
Tensile strength	f_t (MPa)	0.2	0.1	207
Fracture energy Mode I (tension)	G_f (N/mm)	0.012	0.012	-
Fracture energy Mode I (compression)	G_{fc} (N/mm)	8	1.6	-
Specific weight	ρ (kN/m^3)	21*	19**	76

*** Cut stone masonry with good bonding - TABLE 4-1**
**** Irregular stone masonry - TABLE 4-1**

5. DYNAMIC IDENTIFICATION TESTS

5.1 Introduction

The determination of the actual structural and mechanical behaviour of historic structures, which consist of inhomogeneous and quasi-brittle materials, such as stone masonry, is a task of great difficulty and of a high level of uncertainty.

The unavoidable restrictions and limitations on testing implementation in buildings of the architectural heritage (destructive or minor destructive testing), along with the high structural diversity, in terms of collapse mechanisms, damage, alterations, connections and confinements, lead to the decrease of the accuracy and reliability of the obtained structural data. Several carried out tests, such as the dynamic identification tests, the sonic tests and flat jack tests, provide a substantial validity on the obtainment of the actual structural behaviour characteristics and response of a structure.

Specifically the ambient vibration tests (output-only tests), take into account the ambient or operational excitation in order to obtain modal parameters (natural frequencies, mode shapes and damping ratios). This type of tests is a tool of high efficacy, easily performed in historic structures, without causing any damage and with a considerable low performance cost. Besides, the obtainable results are directly related to the dynamic behaviour, which can be often more favourable than specific mechanical or structural characteristics (stiffness, mass, connections between members, boundary conditions), which can be difficult to be assigned accurately in structures of high mechanical and physical diversity (Ramos 2007).

Additionally, the dynamic identification tests are considered as an efficient tool for the validation and calibration of the numerical models. The mechanical and physical parameters of numerical models can be calibrated in order that the numerical dynamic properties match the ones obtained from dynamic identification tests.

Moreover, the results obtained from the ambient vibration tests can be used to estimate the occurrence and localization of damage, the degradation of mechanical properties and any type of effect that can cause modifications on the dynamic behaviour of a structure (Ramos 2007).

5.2 Test preparation and setup

Dynamic identification tests (ambient vibration) were carried out in May 2014 in the nave and South aisle of Canterbury Cathedral, by the University of Minho, in order to obtain the natural frequencies and mode shapes in a specific area of interest, so as to be used later for the update of the boundary conditions and mechanical properties of a specified FE model.

The critical nave sections 2 and 3 (Figure 3-1), which present the greater documented damage, correspond to the areas of interest, in which the acceleration transducers were placed. Structural

elements chosen as dynamic monitoring points were flying buttresses, interior and exterior claddings in the South aisle and nave, as well as points on the extrados of vaults. The dynamic identification tests were carried out through five setups with one reference accelerometer and three accelerometers positioned in several points of the area of interest, with the exception of the Setup 5 in which all the accelerometers were changed of position. The transducers correspond to piezoelectric accelerometers with a frequency range of 0.15 to 1000 Hz, measurement range ± 0.5 g and a sensitivity of 10 V/g. The signals were recorded by an acquisition system of 24-bit resolution, where the accelerometers are connected. The accelerometers were bolted to wooden cubes with aluminium plate faces and fixed to the stones (Figure 5-1). The sensors disposition in each setup is presented in the Figure 5-2. Setups 1, 3 and 4 aim to obtain the mode shape configuration along the y-y axis, while setup 2 was used for the vertical components along the z-z axis. Setup 5 was implemented in the roof void of the nave and was used for the mode shapes of the nave's vault system in the y-y and z-z axis.

(a)

(b)

(c)

(d)

Figure 5-1. Measuring equipment: (a) accelerometer on the intrados springing of the flying buttresses, (b): accelerometer on the exterior cladding of the nave wall, (c) and (d): data acquisition equipment.

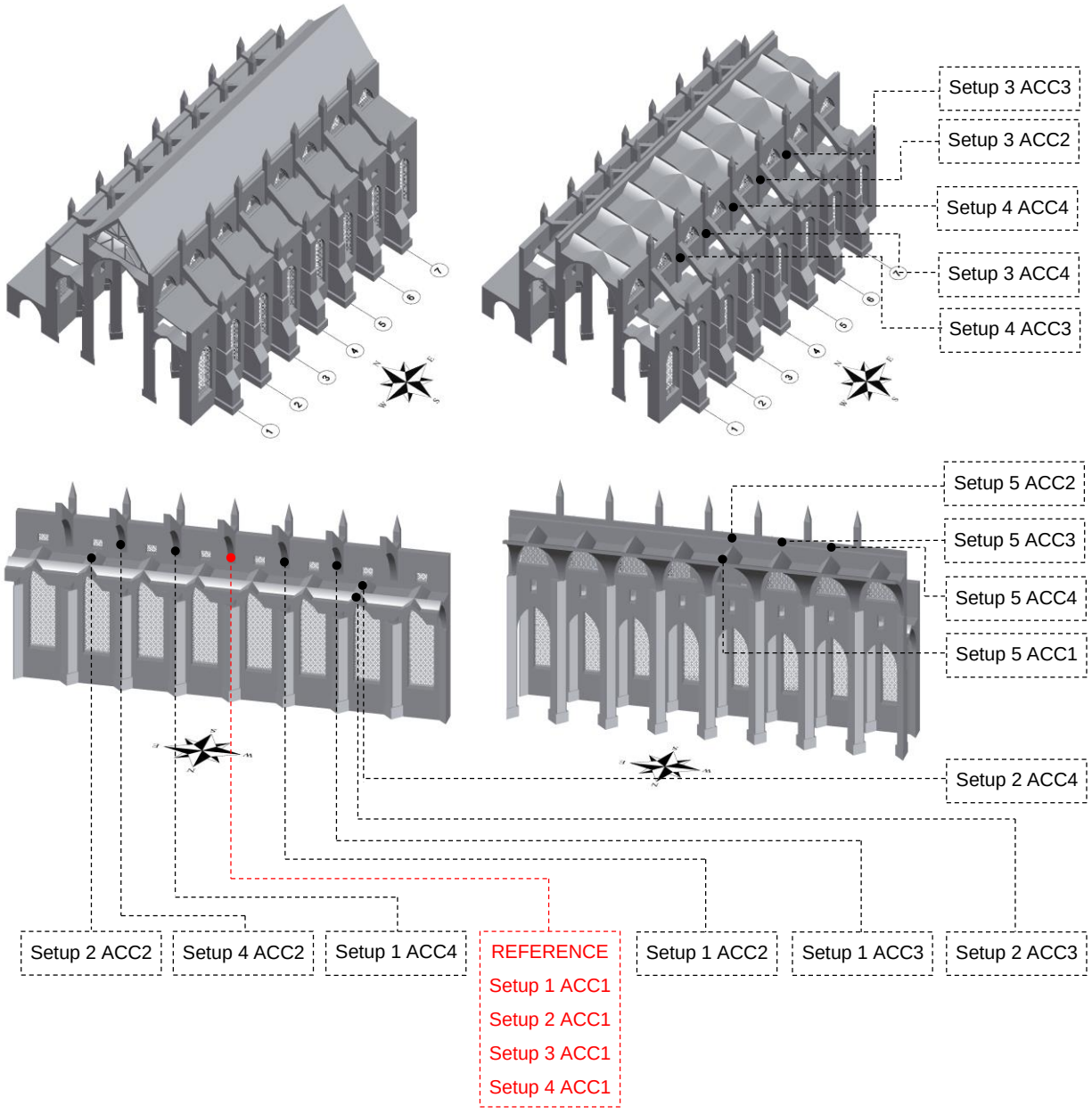

Figure 5-2. Disposition of accelerometers in performed Setups of the dynamic identification tests (Reference sensors depict in red colour).

5.3 Experimental results

Ambient vibrations, mainly induced by wind, were measured in all monitoring points in every setup. The signals were recorded with frequency sampling equal to 200 Hz and duration equal to 15 min. The signals were processed in the ARTeMIS software (SVS, 2006), in which the Stochastic Subspace Identification Method (SSI), namely the Unweighted Principal Components (UPC) Method, was used, aiming at determining the dynamic properties of the structure.

Figure 5-3 presents the poles selection and link of modes for the Setups 1, 3 and 4. Table 6-1 presents the natural frequencies and damping coefficients of the first 12 modes. The frequencies and damping ratios of the first 12 modes ranges between 1.29 Hz and 4.27 Hz and between 1.87% and 6.99%, respectively. Figures 6-4 and 6-5 present modes shapes and the Modal Assurance Criterion (MAC) values. A MAC value equal to 1 implies perfect matching between the two mode shapes, while a value of 0 indicates uncorrelated (orthogonal) vectors.

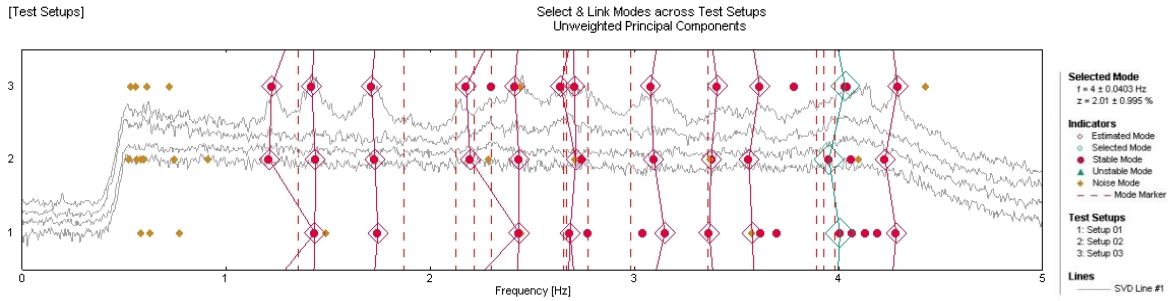

Figure 5-3.Data driven with the poles selection through the several test setups of the Stochastic Subspace Identification method.

Table 5-1. Frequencies and damping ratios of the first 12 modal shapes (Setups 1, 3 and 4).

Mode	Frequency [Hz]	Std. Frequency [Hz]	Damping Ratio [%]	Std. Damping Ratio [%]
1st Mode	1.29	0.13	2.04	0.90
2nd Mode	1.43	0.01	2.47	1.04
3rd Mode	1.73	0.02	2.14	0.28
4th Mode	2.27	0.14	3.42	1.51
5th Mode	2.43	0.01	2.56	1.33
6th Mode	2.68	0.04	3.81	2.75
7th Mode	2.70	0.01	3.62	2.91
8th Mode	3.11	0.04	2.18	0.52
9th Mode	3.38	0.02	6.99	7.06
10th Mode	3.58	0.03	5.42	4.88
11th Mode	4.00	0.04	2.02	1.00
12th Mode	4.27	0.03	1.87	1.39

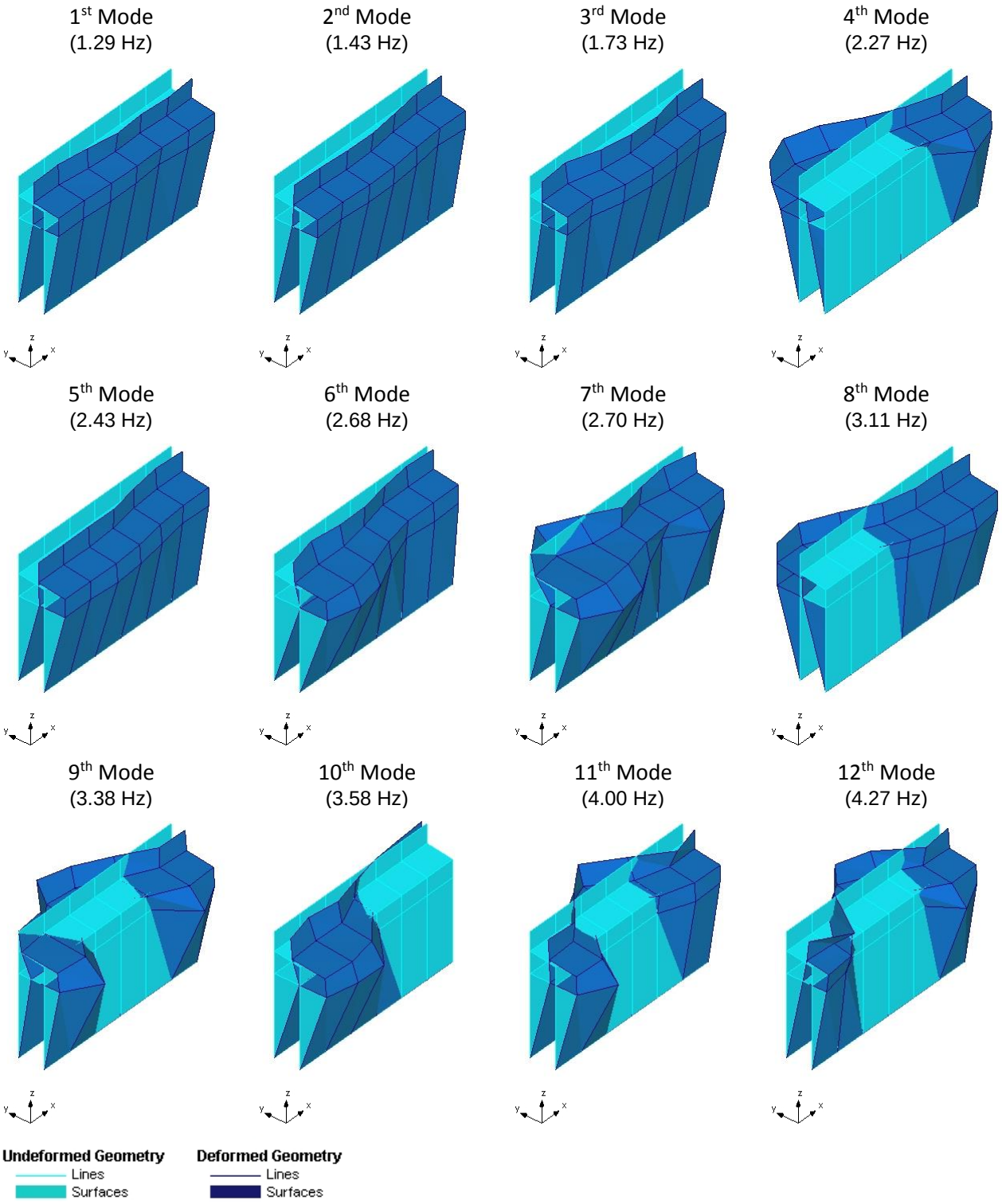

Figure 5-4. Mode shapes obtained from the Setups 1, 3 and 4.

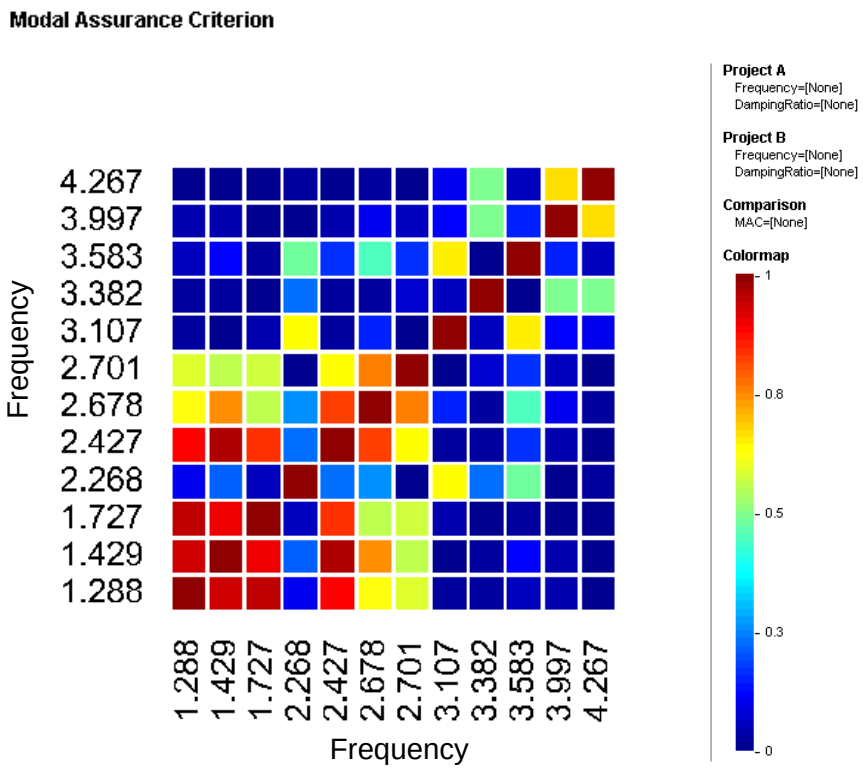

Figure 5-5. MAC values obtained from the Setups 1, 3 and 4.

The 1st mode (1.29 Hz) corresponds to the first mode in the transversal direction of the Cathedral and presents a mode shape similar to the ones of the 2nd, 3rd and 9th modes, which is in agreement to the MAC values for these modes. The mode shapes of the 1st, 2nd and 3rd modes have MAC values higher than 0.95, which denotes a high similarity. Furthermore, the first three modes present very close frequencies (1.29 Hz to 1.73 Hz). It is noted that the obtained mode shapes correspond to a small part of the Cathedral and these frequencies can be associated to different modes of the entire structure.

The 4th and 8th modes present similar mode shapes (2nd curvature), in which the main differences are related with the inflection point. Furthermore, the 9th, 11th and 12th modes present similar modes shapes, corresponding in general to a mode of 3rd curvature with two infection points.

Finally, the Figures 5-6 and 5-7 present the Averaged Normalized Power Spectral Density (ANPSD) graphs for the vertical accelerometers of the Setup 2 and 5, and the horizontal accelerometers of the Setup 5. The ANPSD's of the vertical accelerometers present peaks around the 11 Hz and 16 Hz. However, it is not clear that they correspond to the vertical modes of the structure. On other hand, the ANPSD's of the horizontal accelerometers of the Setup 5 presents clear peaks with frequencies equal to 1.25 Hz, 1.42 Hz, 1.71 Hz and 4.00 Hz, showing that the estimated modes for the nave's vault are in agreement to the modes estimated from the Setup 1, 3 and 4. Furthermore, the frequency of 1.42 Hz in the horizontal accelerometer of Setup 5 corresponds to a similar high energy peak in all three accelerometers, which indicates a plane mode, whereas for the frequencies of 1.25 Hz, 1.71 Hz and 4.00 Hz the additional energy spectral densities are different, specifying a 3D mode.

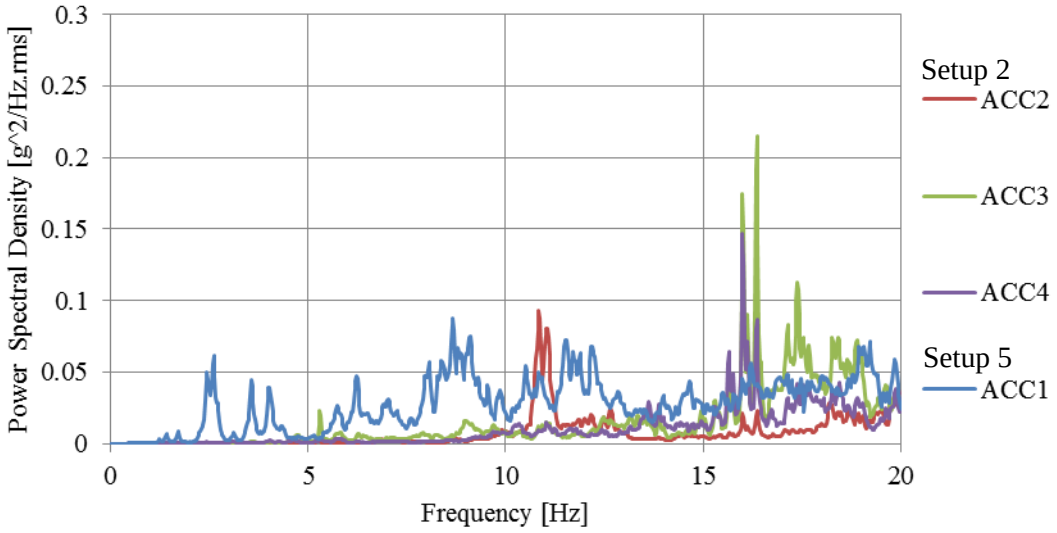

Figure 5-6. Averaged Normalized Power Spectral Density for the vertical accelerometers of the Setup 2 and 5.

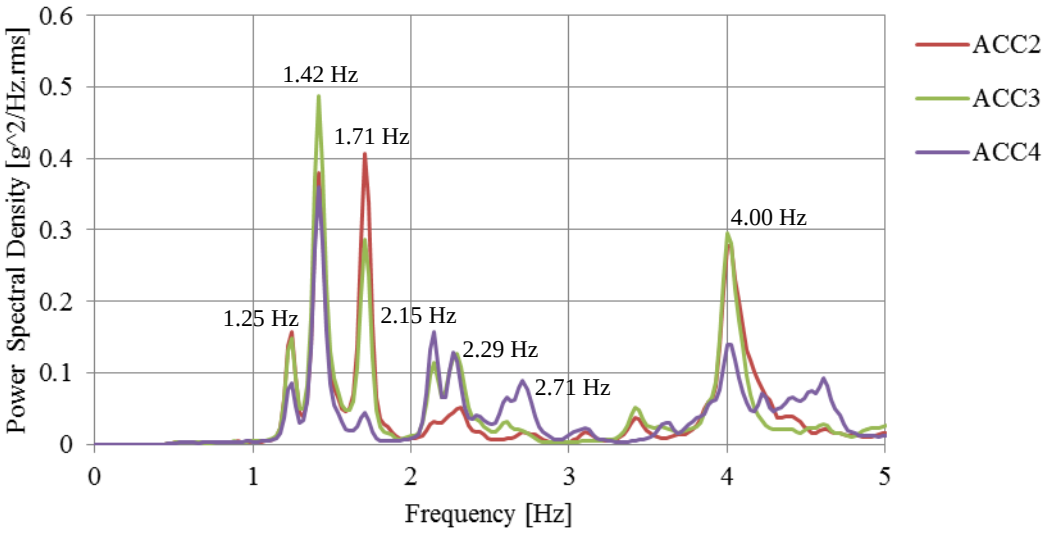

Figure 5-7. Averaged Normalized Power Spectral Density for the horizontal accelerometers of the Setup 5.

6. GRAPHIC STATICS – LINE OF THRUST

6.1 Stability of Gothic arches

An arch is considered stable if any possible thrust line is contained between its boundaries, defined by a maximum and a minimum thrust line. For a Gothic pointed arch, the failure mechanism for the minimum thrust, under uniform loading, consists of six hinges, considering the keystone block or boss, as shown in Figure 6-1 (Block et al. 2006). In case of spreading of the vertical abutments the collapse mechanism consists of five hinges, three of which form in the central portion of the arch (Romano et al. 2010). The other two can be formed either at the springings or at the base of the vertical abutments (Figure 6-2).

During the in situ inspection in the nave of Canterbury Cathedral, no cracks were identified in the arcade arches, the clerestory arches of the nave and the arches in the windows of the aisles that could indicate the formation of a certain number of hinges. Given the fact that the load in the arches is considered mostly uniform and symmetric, the line of thrust, which corresponds to the maximum horizontal load, will be used next in the graphic statics analysis.

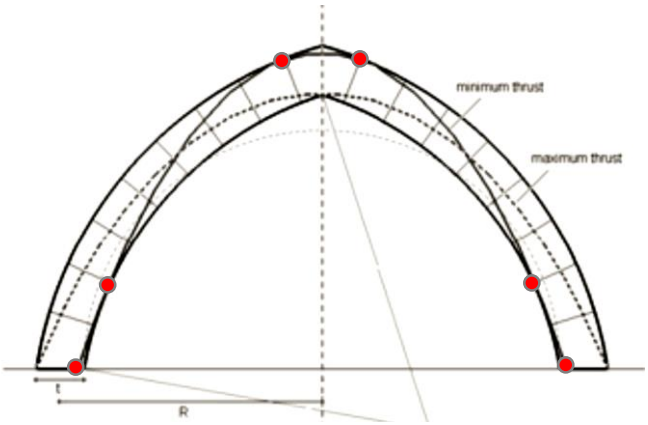

Figure 6-1. The minimum and maximum thrust line that defines the boundaries of the stability of a pointed Gothic arch. The five hinges for the maximum thrust are depicting (Block et al. 2006).

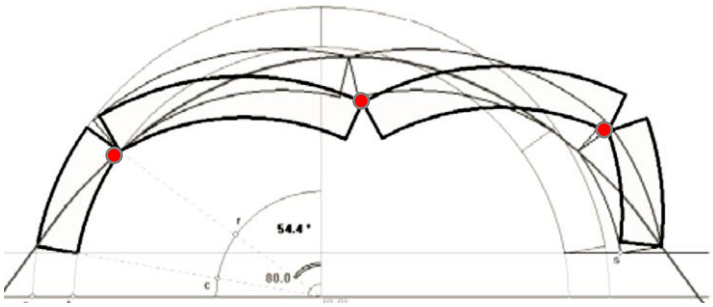

Figure 6-2. Failure mechanism in a circular arch under spreading of the abutments. The three hinges of central part of the arch are depicting (Block et al. 2006).

6.2 Stability of flying buttresses

Regarding the stability of flying buttresses, all valid thrust lines are bounded in between a maximum and a minimum value. According to the damage survey, the flying buttresses in sections 2 and 3 of the south aisle (Figure 3-1) experience significant joint failure in the intrados of the free span, initiated by the spreading of the abutments. Thus, a corresponding thrust line is closer to the state of minimum thrust, which is tangent to the hinge formed at the extrados (Figure 6-3) (Block 2005). For the purpose of conducting the thrust analysis the minimum thrust line will be assumed with a hinge at the extrados, between two voussoirs (Figure 6-4).

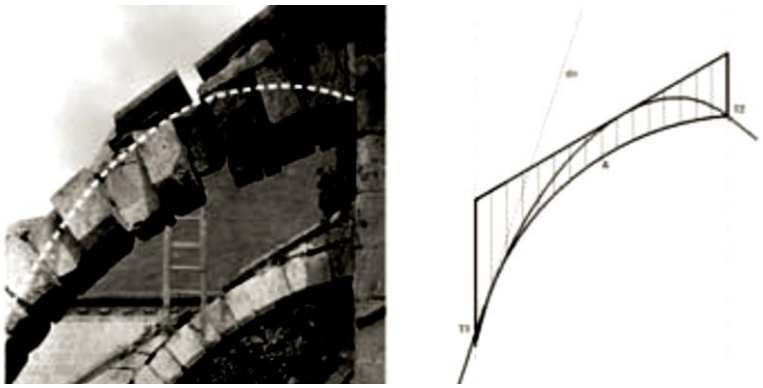

Figure 6-3. The flying arch in Agnicourt church in France is considered to be in state of minimum thrust (Block 2005).

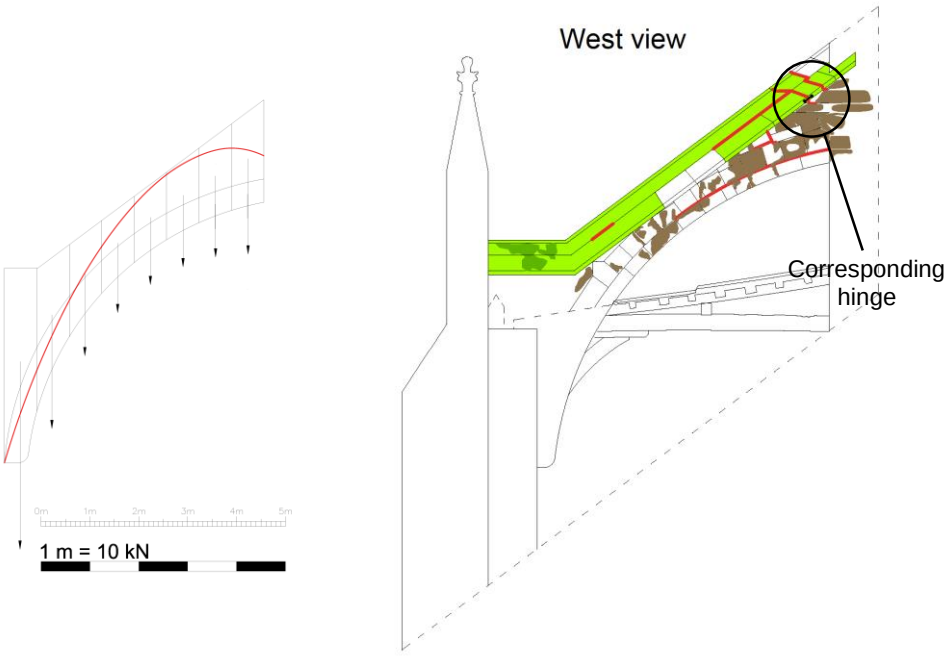

Figure 6-4. (Left) Line of thrust in flying buttress of the south aisle of Canterbury Cathedral in corresponding bay 3. (Right) Damage map of the flying buttress of section 3 with the documented hinge, which was used as reference to conduct the thrust analysis.

6.3 Stability of Gothic quadripartite cross vaults

The force trajectories in a Gothic quadripartite lierne cross vault under dead load follow the steepest descent towards the supports. Depending on the curvature of the vaults shell, these trajectories can either be targeted directly to the supports, coinciding with the principal ribs configuration or through the shortest path to the diagonal ribs or even a superposition of both. The most appropriate force path is dependent on the loading conditions and the geometry of the Gothic vault (Figure 6-5) (Block et al. 2014).

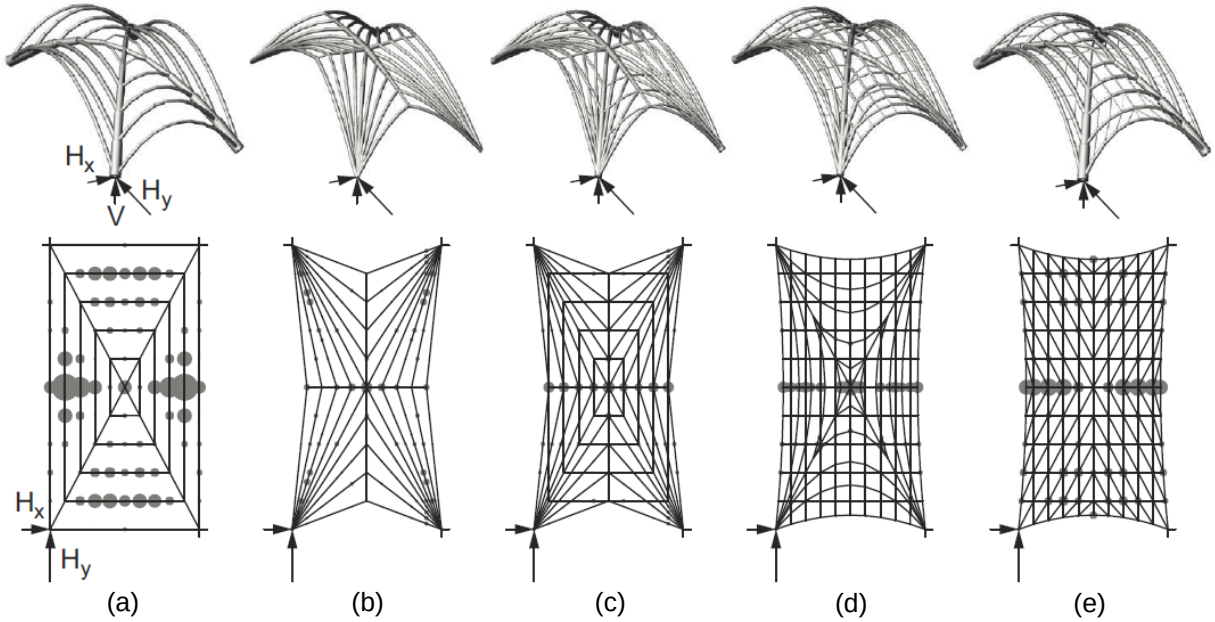

Figure 6-5. Thrust trajectories in cross vaults in three dimensional (Top row) and plan view (Bottom row), targeting the springings with different configurations, which are comprised of (a) parallel and diagonal arches, (b) arches directly from the springings, (c) superposition of first two patterns, (d) quadrilateral arches in plan, directly from the springings, (e) triangulated patterns in each quarter of the vault, parallel to the diagonals (Block et al. 2014).

6.4 Pseudo 3D thrust analysis with the sliding technique

The sliding technique, first discussed by Ungewitter (1890) and established schematically by Wittmann (1879), suggests that any three-dimensional vault can be analyzed using the 2D thrust line analysis technique, by decomposing the vault into two-dimensional strips. Thus, the vault behaves structurally as a combination of many small arches in both directions, redirecting the thrust to the diagonal rib arches in the form of increments, which is later transferred as diagonal thrust to the abutments (Figure 6-6) (Block 2009).

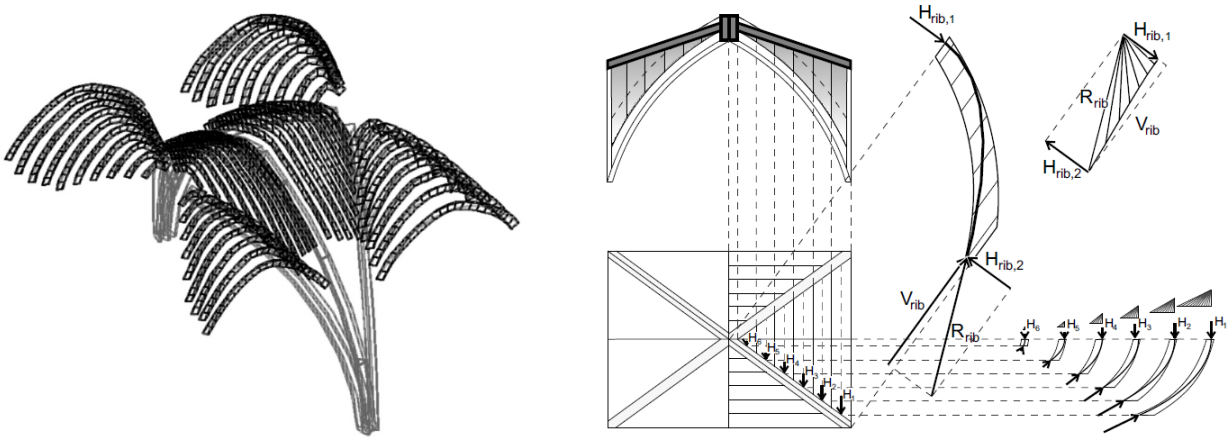

Figure 6-6. A 3D pseudo thrust analysis applied in a Gothic ribbed cross vault, using the sliding technique, in order to obtain the line of thrust (Block 2009).

Taking into account the thrust components in each springing, from each quarter of the Gothic vault, the thrust is in a diagonal cross plane, parallel to the corresponding diagonal rib. In the current case study, due to the symmetry, an identical thrust component will be applied from the adjoining quarter of the next cross vault. Thus, the two opposite thrust components in a plane vertical to the transversal rib are exempted and the resultant thrust of the Gothic cross vault system in each abutment will be in the plane of the transverse rib. Lastly, in the resultant thrust of the vaults the part from the transversal rib is added (Figure 6-7).

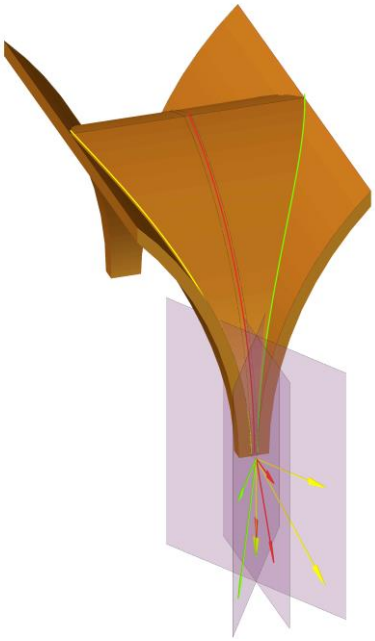

Figure 6-7. Schematic representation of the resultant thrust in the springing of a Gothic cross vault.

6.5 Line of thrust in a typical bay section

A graphic statics analysis was performed in the transverse cross section 3 from the nave of Canterbury Cathedral, in order to investigate graphically the global stability of the nave and the level of stresses at the base of the vertical elements. The analysis was conducted under self-weight forces, applied at the center of mass of each voussoir / discretized block. In order to obtain the resultant thrust at each quarter of the Gothic cross vaults, with the corresponding infill volume, the resultant force is applied at the center of mass, which graphically corresponds with sufficient approximation to the plane of the diagonal ribs. Lastly, regarding the thrust line in the cross section of the vaults, it corresponds to that of the diagonal ribs.

The nave's cross section is discretized in macroelements, in order to facilitate the calculation of body forces. The additional forces and points of application from the arches in the longitudinal and transversal direction, the cross vaults and the nave's roof are depicted in force vectors, as shown in Figure 6-8. The designed truss line and the values of the horizontal and vertical components at base are depicted in Figure 6-9.

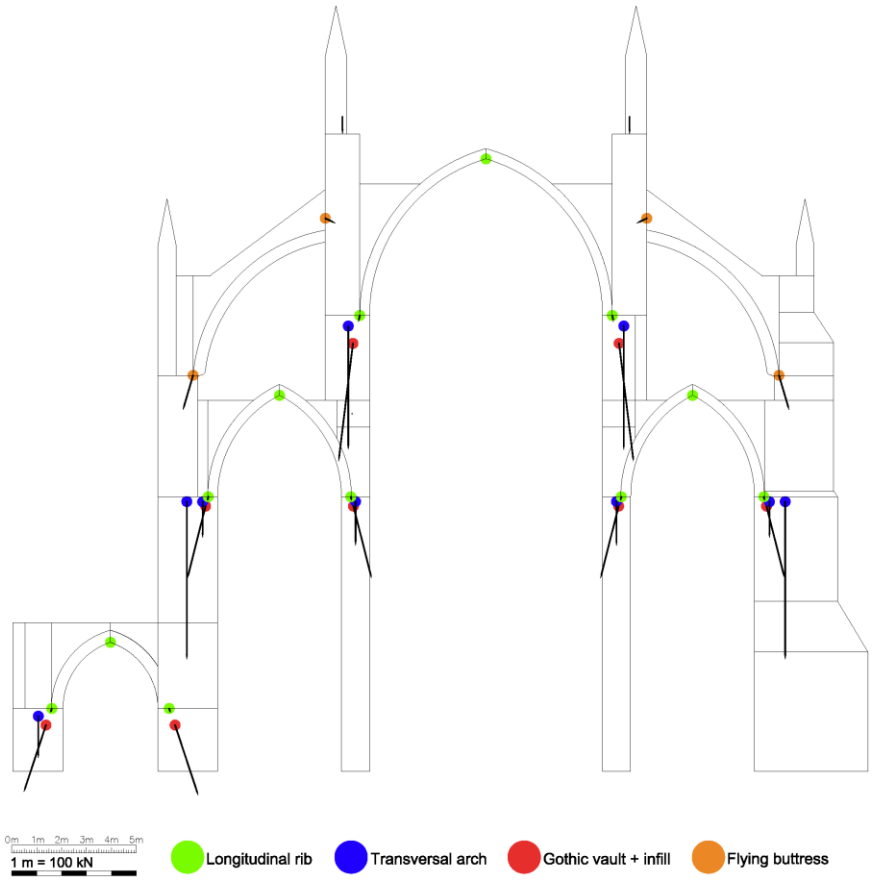

Figure 6-8. Cross section of the typical bay in the nave of Canterbury Cathedral depicting the macroblocks and the points of application with the force vectors of the transversal structural elements.

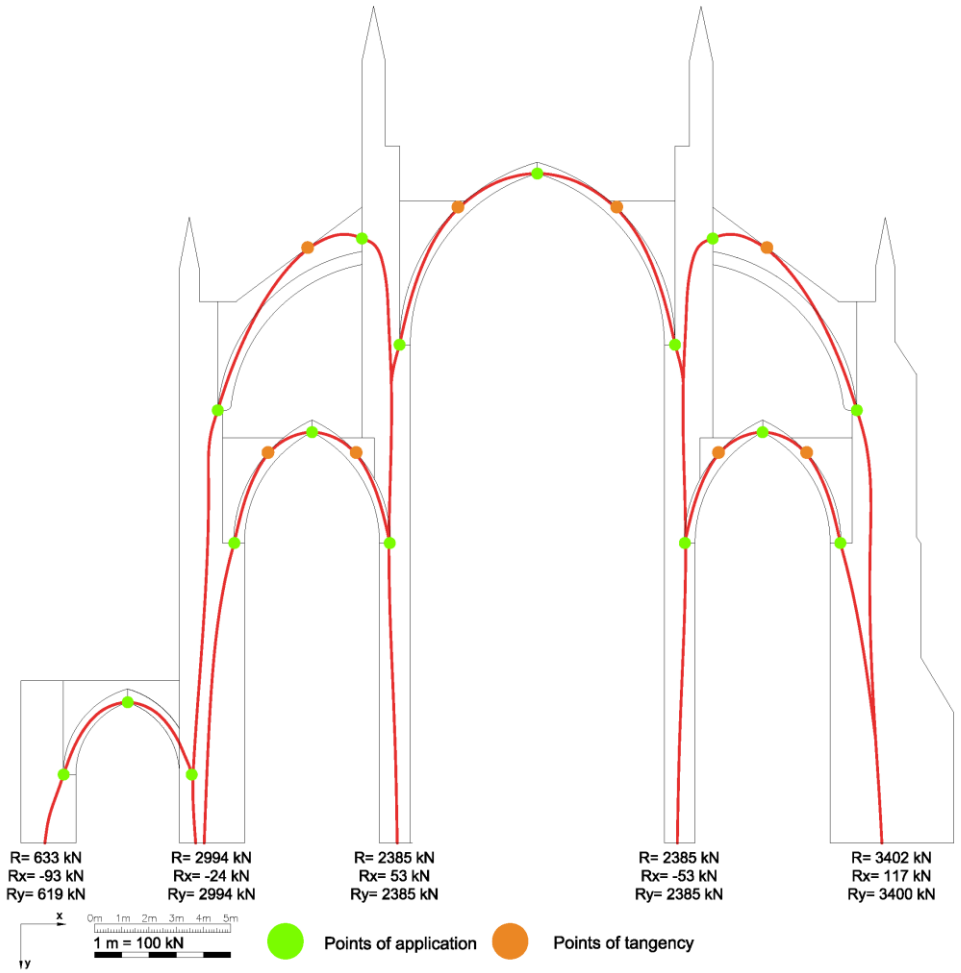

Figure 6-9. Cross section of the typical bay in the nave of Canterbury Cathedral depicting the line of thrust and the potential hinges, where the thrust line is tangent to the boundaries of the structural elements.

It can be concluded that the structural section of the nave of Canterbury Cathedral under self-weight, is stable, since a possible line of thrust is contained within its boundaries (Pela et al. 2014a). Regarding the current truss line, the points of tangency with the perimeter of the structural elements, correspond to potential hinges. In specific, the points of tangency in the extrados of the lateral vaults can be matched with the identified cracks arranged around the piers at the level of the infill (Figure 4-3).

The flying buttresses, due to their position and geometry do not counteract the thrust of the nave vaults, instead the resultant force from the nave vaults is taken from the piers and clerestory walls. It can also be concluded that the actual structural role of the flying buttresses is undertaken by the lateral aisles. It is noted that the roof and its possible thrust are not considered in this analysis.

6.6 Level of stresses

If the resultant force on a section stays within its middle third (Figure 6-10), the entire section is in compression and the maximum compressive stress is given by Eq. 6-1, where *N* is the vertical component of the resultant, *A* is the cross section area and *e* is the eccentricity (Pela et al. 2014b). For the pier section at base, which approximates a rectangular cross section, the eccentricity of the resultant force is inside the middle third and is located at 0.09 m from the centroid. Therefore, the maximum compressive stress in the base of the pier, with an equivalent rectangular cross section of dimensions 1.13*1.60 m, is 1.9 MPa, which seems acceptable according to the estimated material properties (see section 4.3.2).

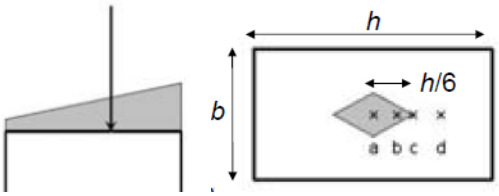

Figure 6-10. Stress distribution of a cross section when the resultant force is applied within its middle third (Pela et al. 2014b).

$$e < \frac{h}{6} \rightarrow \sigma_{max} = \frac{N}{A} + \frac{M}{W} = \frac{N}{A} + \frac{M\, y_{max}}{I_{xx}} = \frac{N}{A} + \frac{\frac{h}{2} Ne}{\frac{bh^3}{12}} = \frac{N}{A} + \frac{6Ne}{bh^2} \qquad \text{Eq. 6-1}$$

7. FE ANALYSIS

The main objective of the numerical analysis was to assess the building's capacity to sustain self-loads, but also lateral effects, from foundation settlements, excessive loading or geometrical inefficiencies, such as lateral thrusts from the roof trusses and excessive infill volumes. The main criterion of the study was the correlation with the existing damage patterns, aiming at providing a discussion on its possible causes. In specific, the structure was subject to dead loading, which was applied gradually in ten steps and then continuing to increase until the collapse is reached, in order to obtain also the ultimate load and the current safety level.

7.1 FE model generation

A finite element model was built in Midas FX+ Version 3.3.0 Customized Pre/Post-processor for DIANA software, according to the generated 3D CAD model. The model includes a typical transversal section of the nave, with the vertical abutments (piers, buttresses), the corresponding vaults of the nave and the lateral aisles, the flying buttresses, the resulting part of the adjoining cloister and the wrought iron tie over the vaults, anchored on pattress wrought iron plates (Figure 7-1, 2). In all stone masonry structural elements, the estimated properties of Caen stone masonry were assigned, except the infill volumes, for which reference values of irregular stone masonry were adopted (Table 6-5).

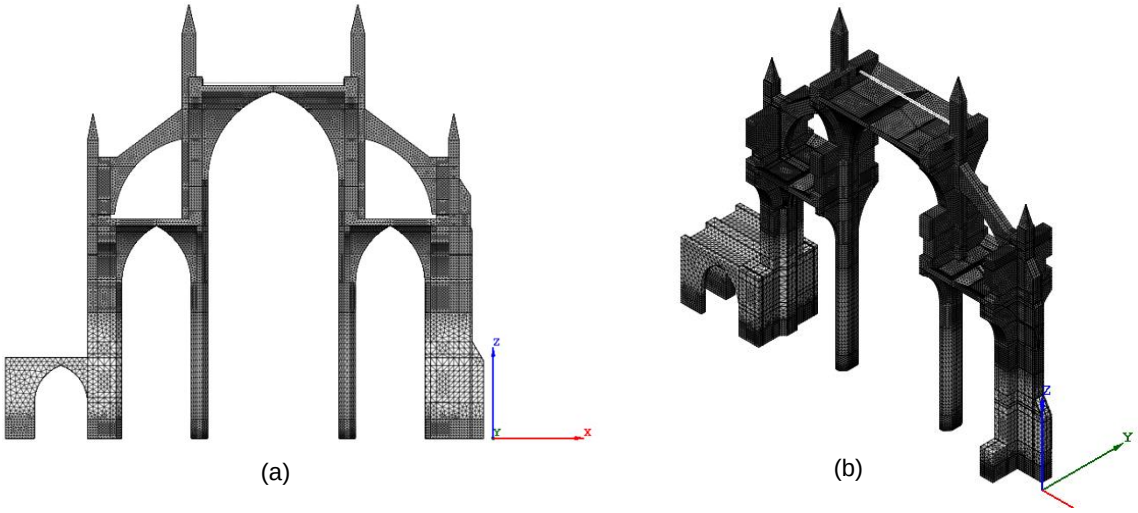

(a) (b)

Figure 7-1. East view (a) and 3D view (b) of the elaborated FE model of the typical bay in the nave of Canterbury Cathedral, depicting the FE mesh.

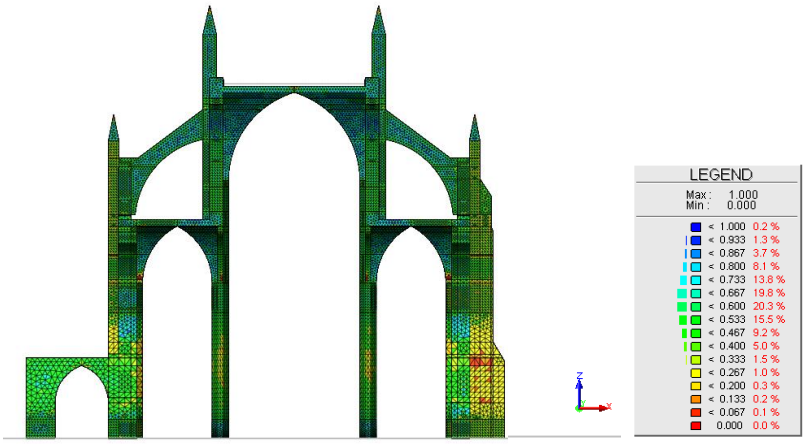

Figure 7-2. Quality mesh check in relation the aspect ratio of elements.

In the modelling process, various assumptions were incorporated. Regarding the boundary conditions, the base connection of the vertical elements was modelled as totally fixed. Reference horizontal and vertical stiffness coefficients for the foundation soil were assigned only in the soil settlements scenario. As far as the confinement and interaction with the adjacent bays, translations on the y-y (longitudinal) axis of vaults, arches and walls sections were restrained.

The discretized structural elements were composed of homogeneous masonry materials. The created FE mesh is composed of 501768 isoparametric pyramid elements TE12L, 20 two-node truss elements L2TRU and 106155 nodes in total (Figure 7-3) (DIANA 2014a).

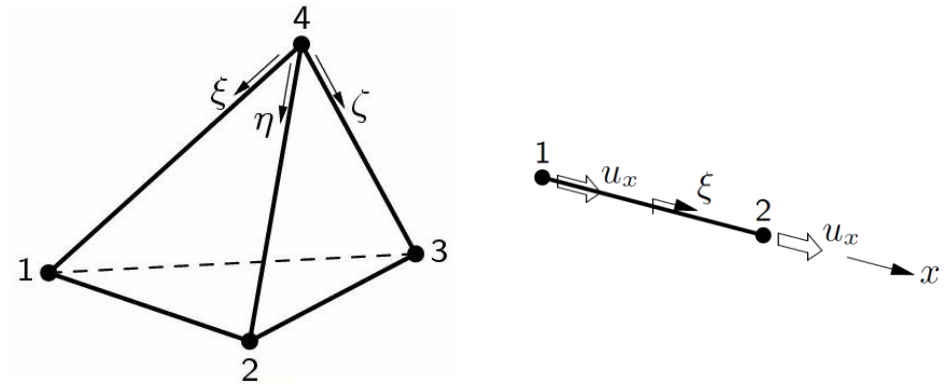

Figure 7-3. (Left) View of a TE12L isoparametric solid pyramid element, with three sides and four nodes. (Right) View of a L2TRU two-node directly integrated (1-point) truss element (DIANA 2014a).

7.2 Inelastic behavior

The cracking and crushing behavior of the material are described with a nonlinear relationship. The compressive and tensile behavior of stone masonry is described through a Total Strain Rotating crack model. For the tensile cracking, an exponential predefined softening curve, based on the fracture energy G_f^I, is assigned. In addition, the crushing under compression is described with a predefined parabolic function, based on the fracture energy G_C. A default value of the crack band width is assigned, equal to $\sqrt[3]{V}$, with V is the volume of the solid element (Figure 7-4) (DIANA 2014b).

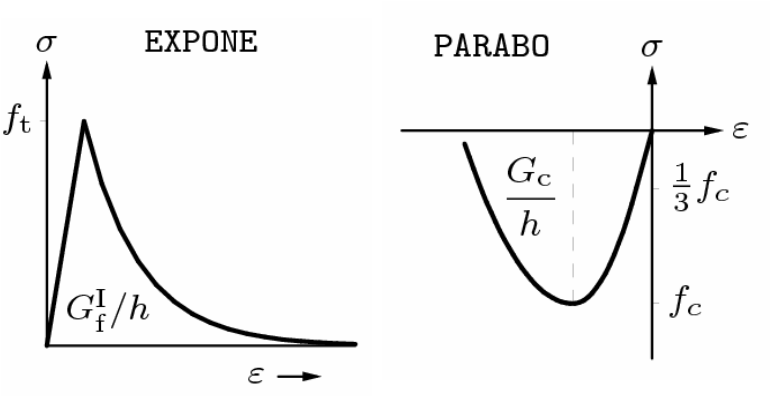

Figure 7-4. (Left) Crack stress and strain curve, specifying the tensile behavior of stone masonry with an exponential softening function, beyond the tensile strength. (Right) Crack stress and strain curve, specifying the compressive behavior of stone masonry with a parabolic curve (DIANA 2014b).

The explicitly specified load steps for the analysis execution were 10 with a 0.1 load step factor. The iterative method used was the Modified Newton-Raphson, where a tangential stiffness is set at the first iteration and is kept constant throughout each step. The convergence criterion for each equilibrium state is based on the energy norm, with an energy ratio between two iterations less than 0.001 (Figure 7-5) (DIANA 2014b).

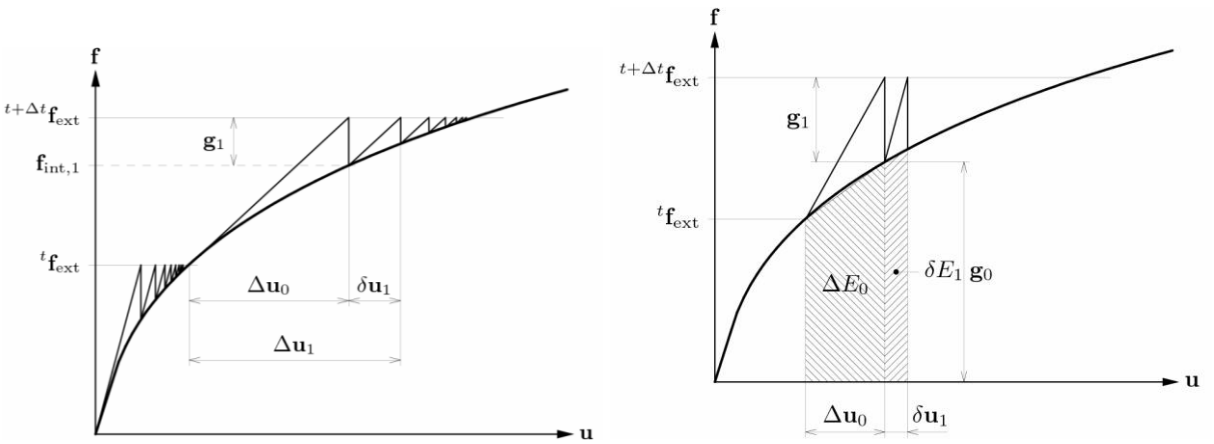

Figure 7-5. (Left) the Modified Newton-Raphson iteration method. (Right) Convergence under the energy norm (DIANA 2014b).

7.3 FE model update

The FE model was updated, by correlating the 1st mode shape of the experimental tests and the analytical model, with the modulus of elasticity as the updating parameter. There is some lack of agreement between the other mode shapes of the experimental tests and the analytical model, due to the in plane behavior of the FE model, which is different from the actual global modes of the structure. A modal analysis under linear elastic behavior was conducted and the natural frequency of the 1st mode is 1.31 Hz, which is a translational first order mode, as shown in Figure 7-6.

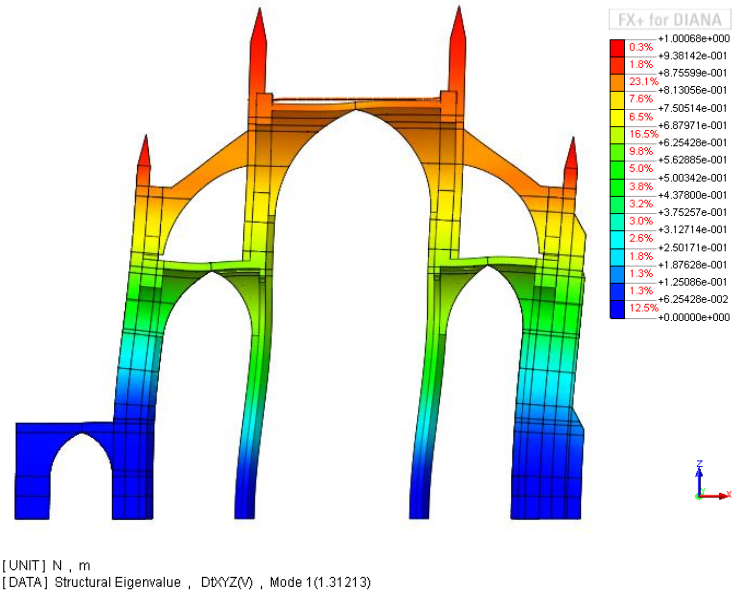

Figure 7-6. 1st mode shape configuration of the typical bay.

From the results of ambient vibration tests of Setup 5, the natural frequency of 1.42 Hz has the highest energy peak in all three accelerometers, which is likely to indicate a plane transverse mode. On the other hand, in the frequencies of 1.25 Hz, 1.71 Hz and 4.00 Hz the energy spectral densities of the measuring accelerometers are rather different, in alignment of a global 3D mode. Thus, from the experimental tests, the 1st plane (transversal) mode of the structure is considered the one of 1.42 Hz (Figure 6-6).

The stiffness of a single degree of freedom system is related to its natural frequency squared and mass as described in Eq. 7-1 (Chopra 2001).

$$f_n = \frac{1}{2\pi}\sqrt{\frac{k}{m}} \Rightarrow k = 4 \cdot \pi^2 \cdot f_n^2 \cdot m \qquad \text{(Eq. 7-1)}$$

As the modulus of elasticity is in direct relation with the stiffness, the updated value of the numerical model can be calculated by the following ratio (Eq. 7-2).

$$E_{updated} = E_{initial} \cdot \left(\frac{f_1^{exp.}}{f_1^{num.}}\right)^2 = 3000 \cdot \left(\frac{1.42}{1.31}\right)^2 = 3525 \text{ MPa} \quad \text{(Eq. 7-2)}$$

A modal analysis under linear elastic behavior was conducted, with the updated value of modulus of elasticity. The obtained mode shapes are depicted in Figure 7-7, 8.

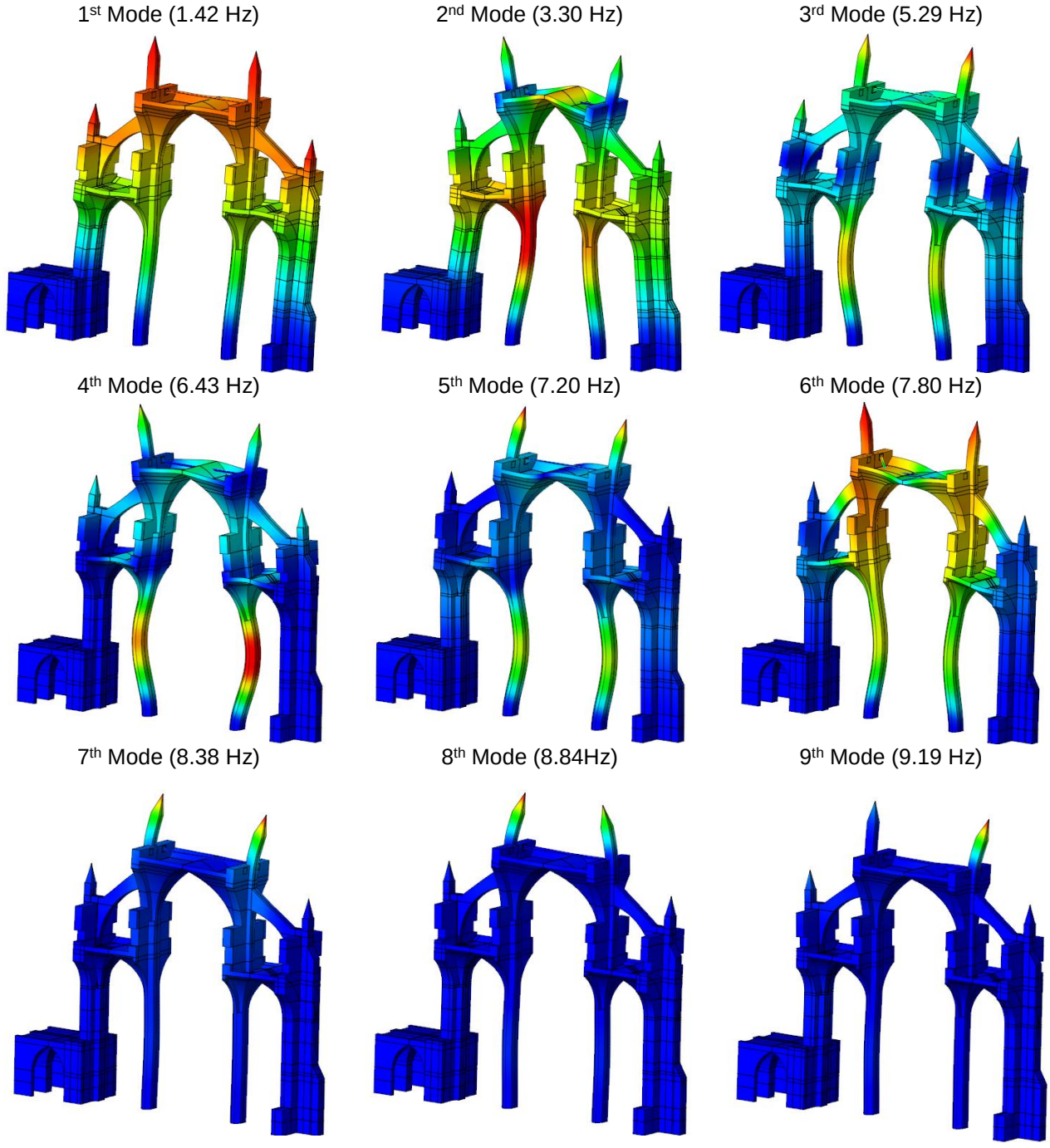

Figure 7-7. Mode shape configuration of modes 1 to 9, with the natural frequencies.

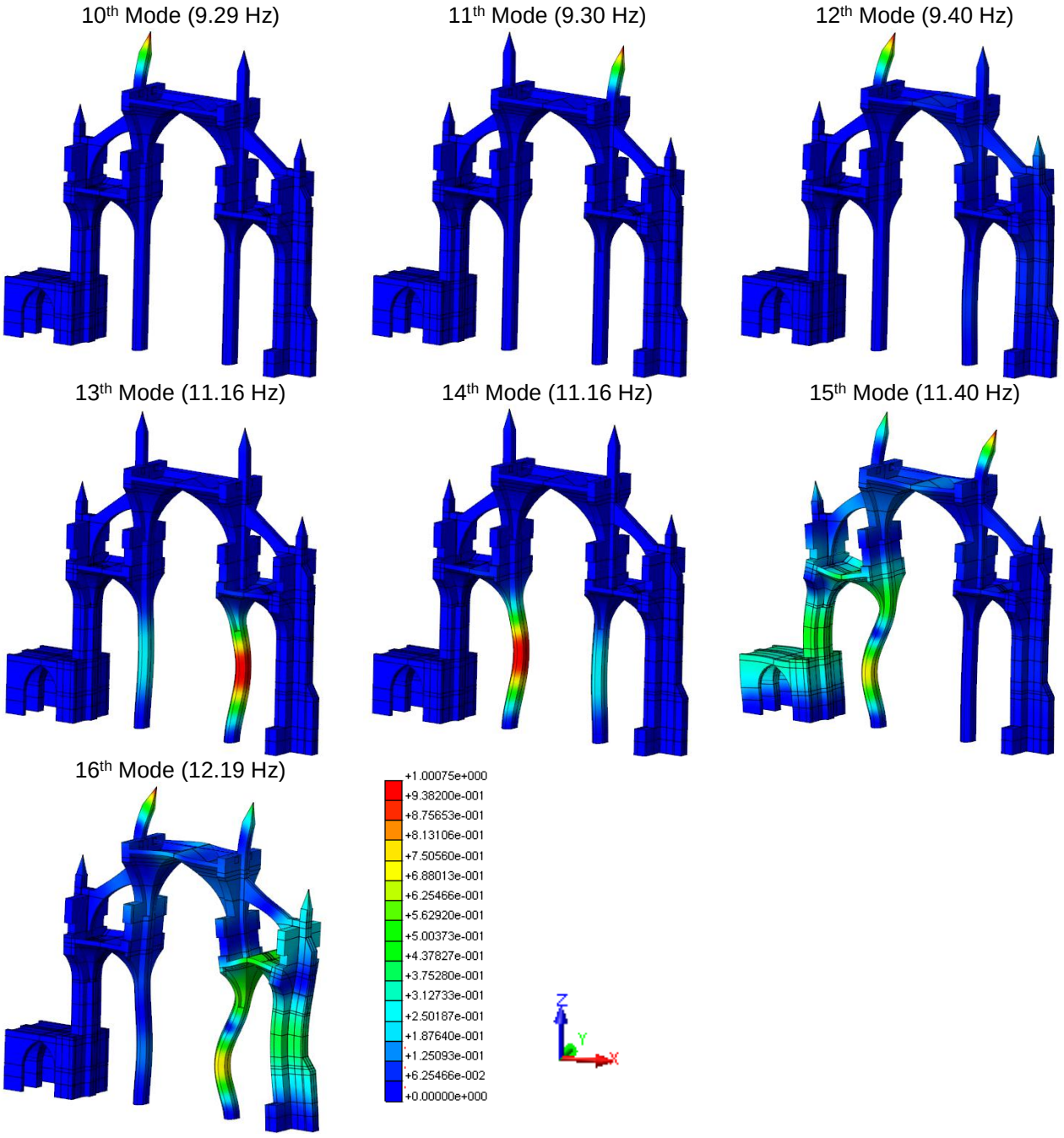

Figure 7-8. Mode shape configuration of modes 10 to 16, with the natural frequencies.

The 1st, 3rd and 5th modes are in phase, whereas the 2nd, 4th and 6th modes are configured in a symmetric (out of phase) pattern. The 7th to 12th modes are local modes of in plane and out of plane movement of pinnacles. The 13th and 14th modes are first order local modes of the columns, whereas the 15th and 16th are second order local modes of the columns, involving also partly the pinnacles and side naves.

7.4 Simulations

Various static nonlinear analyses were carried out, taking into account different hypotheses, in order to differentiate the existing damage and to investigate the level of safety of the cathedral's nave subjected to dead loading, lateral forces and foundation settlements.

7.4.1 Structural nonlinear analysis under dead loading

Regarding the fact that a concrete layer was added in the infill of the aisles and nave of Canterbury Cathedral during the 1990s, a nonlinear structural analysis under dead loading was performed, with the infill volume as a variable, in order to investigate the influence of infill in the existing damage (Figure 3-16) (Deeming 2014). Furthermore, the structural behavior of the roof framing was investigated, with different components of lateral thrust, applied as a distributed force on the wall plates surface. Lastly, a local soil settlement at the foundation level of the south part of the typical bay was set as a boundary condition in the analysis.

7.4.1.1 FE model at current state

The results of the FE model depicting the current state of the typical bay, with the current infill height, are presented in detail. Regarding the nave roof, an equivalent vertical distributed load was applied in the top surface of the clerestory walls of 12.7 kN/m^2, representing the self-weight of the corresponding roof part of the typical bay. The timber trusses work as a hinged joint system, which were considered fully functional, and no lateral thrust was accounted for.

The magnified deformed shape of the typical bay can provide qualitative information about the structural behavior under dead loads (Figure 7-9). The bay appears to deform in a symmetric way, with the upper part of the piers and the clerestory walls spreading and bending outwards, counteracting the thrust from the main vault, which appears not to be taken by the system of flying buttresses. At the springing of the aisle vaults, the lateral thrust pushes the piers inwards, whereas the vertical buttresses are deformed by rotating outwards. The cloister appears to restrain and stiffen the lower level of the north buttress. The depicted deformations are in the order of mm. Lastly, the tie, due to the deformation of the clerestory walls, is in compression and takes no residual thrust, with a compressive stress of 12 MPa. This conclusion can change if lateral thrusts from the roof are considered.

As expected, some cracking exists at 100% of the dead load. The tensile damage distribution is demonstrated in graphs of maximum principal strains in the 3D configuration and on a slice plane at the symmetry axis (Figure 7-10). The first major tensile damage appears at the 40% of dead load in both lateral vaults, in a symmetric distribution, along the longitudinal axis of the nave. The lateral vaults crack at the intrados, surrounding the columns and with the cracks located at the level of the infill, which corresponds to the cracks documented in the damage survey (Figure 4-5). In the extrados of the vault, close to the level of infill there is also cracking. Also cracks are formed at the interface between the

vaults and the aisle windows, which match the existing Sabouret's cracks (Figure 4-5, 7-10). The north flying buttress cracks on the extrados, close to the exterior pinnacle, when the dead load reaches 80%. At 100% of the dead load the same part of the south flying buttress, experiences tensile cracks. The nave vault remains with no tensile damage. It is also noted that the crack width is small (maximum crack strain of 0.1%)

The previously mentioned tensile damage can be correlated with the increased values of minimum principal stresses in the tip of the cracks (Figure 7-11). From the calculated crack widths diagram in Figure 7-11, the calculated crack width in the inner part of the south and north aisle vaults are around 1 mm, which correlates well with the existing cracks (Figure 4-3).

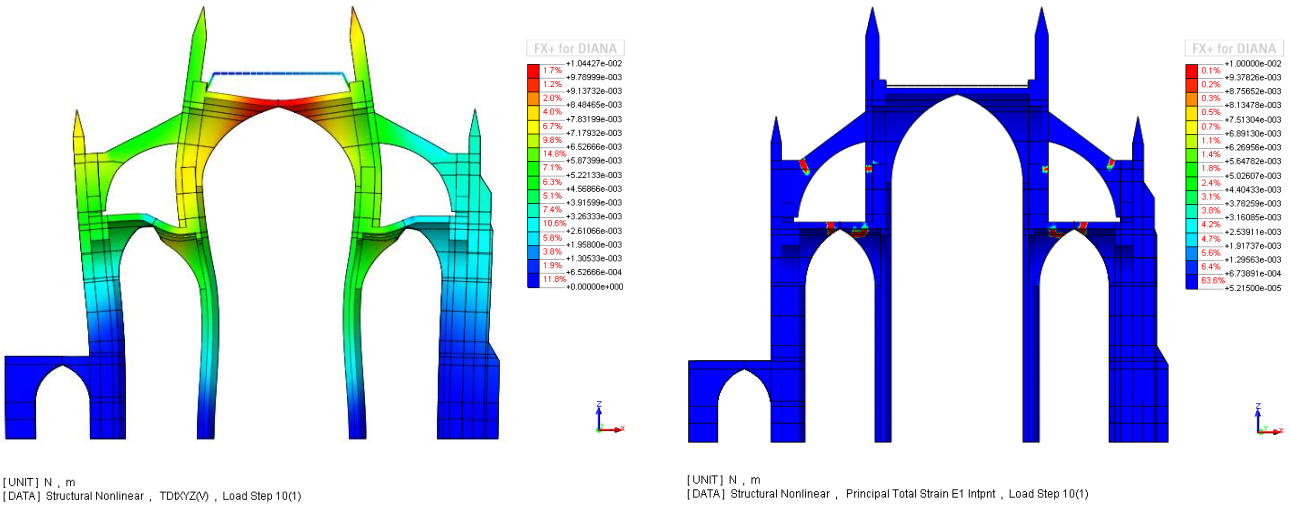

Figure 7-9. (Left) Deformed shape (x100) with displacement gradient at last load step. (Right) Distribution of maximum principal strains at last load step.

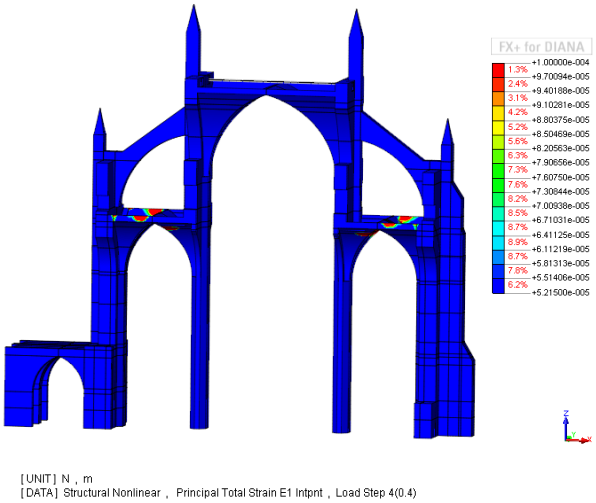

Figure 7-10. (Left) Distribution of maximum principal strains at the 40% of dead load.

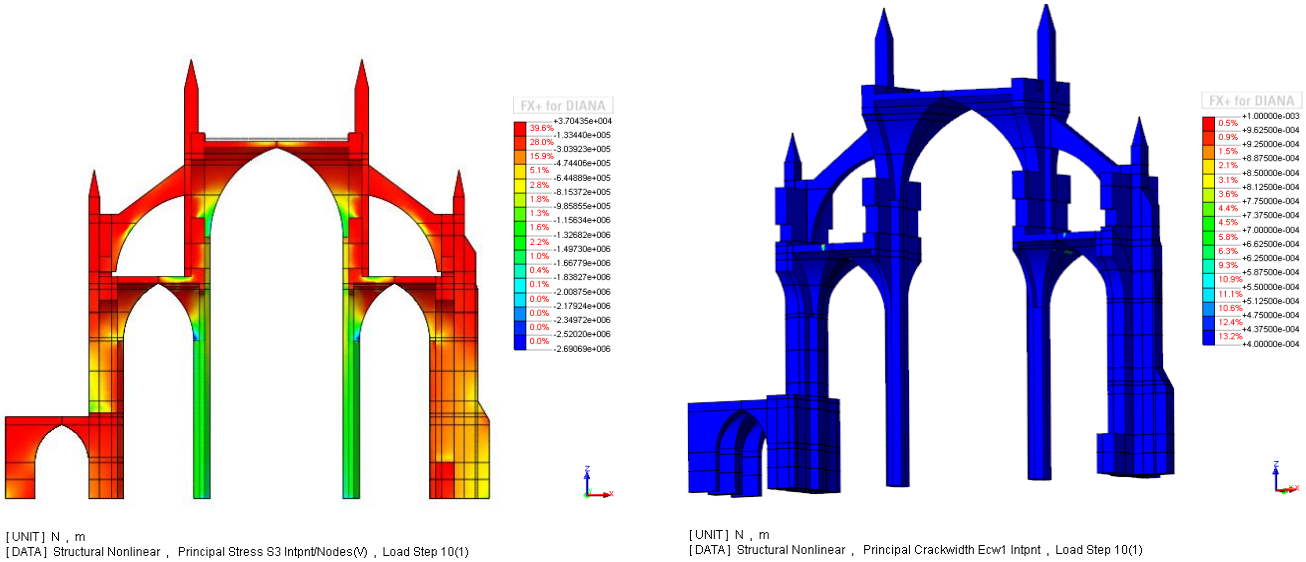

Figure 7-11. (Left) Distribution of minimum principal stresses at last load step. (Right) Distribution of crack width, depicting widths larger than 0.4 mm.

From the load displacement diagrams, depicting the vertical displacement of the crown and the span opening in the nave and lateral aisles, it is evident that around 40% of self-weight there is a significant loss of stiffness, which corresponds to structural damage and cracking (Figure 7-12, 13). Note that a load factor of 10 indicates the application of the full dead load. Considering the span opening, the trend line difference from the elastic response (dashed lines) is 38% for the nave vault, 63% for the lateral vaults. In the load – vertical displacement diagram the lateral vaults appear to be stiffer in the nonlinear response, but the measured total vertical displacement is a relative value. Because of the spreading of the columns from the lateral thrust of the nave vault, the half part of the lateral vaults deforms inwards and the other half deforms outwards, while the crown is moving upwards.

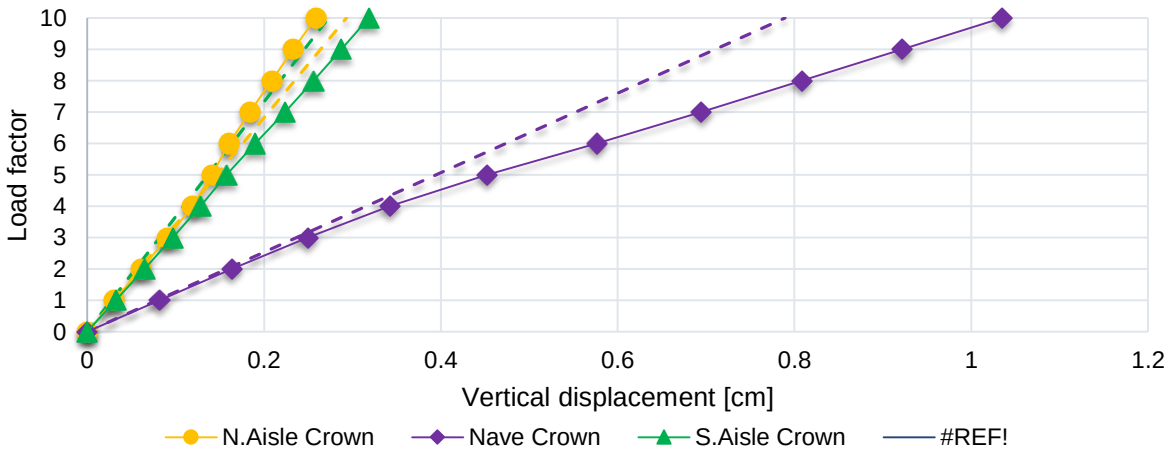

Figure 7-12. Load displacement diagram, depicting the vertical displacements of the crowns in the nave and lateral aisles versus the load steps in which the self-weight is applied.

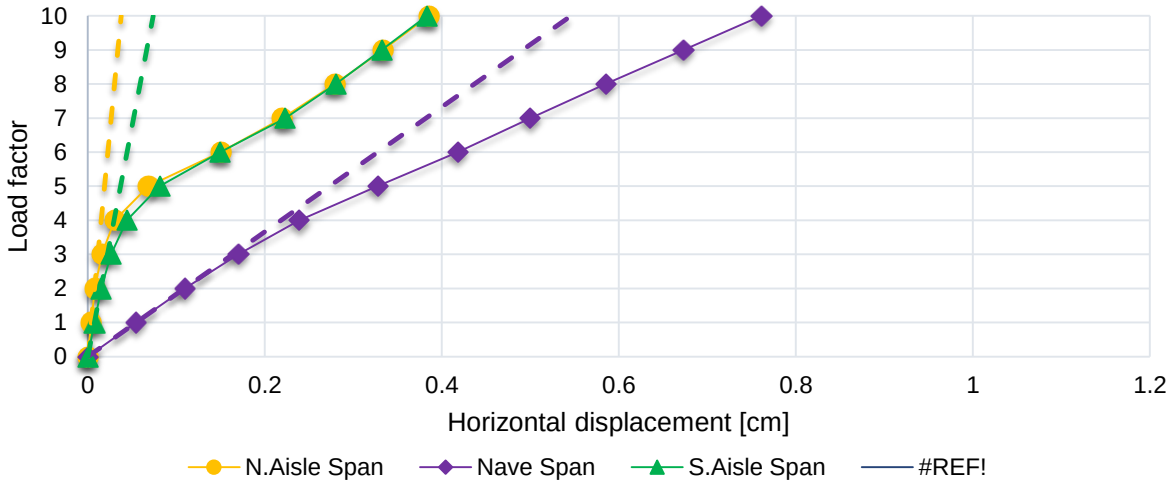

Figure 7-13. Load displacement diagram, depicting the horizontal displacements of the span in the nave and lateral aisles versus the 10 load steps in which the self-weight is applied.

7.4.1.2 Lateral thrust from nave's roof

Two nonlinear static analysis were performed, accounting the possibility of lateral thrust from the roof trusses in case of joint failure. For the analysis, an applied lateral distributed load on the pattress plates equal to 30% and 50% of the vertical component at the south side of the pattress plates was considered, equal to 3.8 and 6.4 kN/m^2 respectively. From the load displacement diagrams, depicting the span opening in the nave and south aisle, in comparison with the fully functional hinged trusses, there is a superposition in all three cases. Thus, there is no significant residual effect or damage is noticed, which justifies that the self-weight of the roof system is relatively small and doesn't affect the structural behavior of the Cathedral's bay (Figure 7-14).

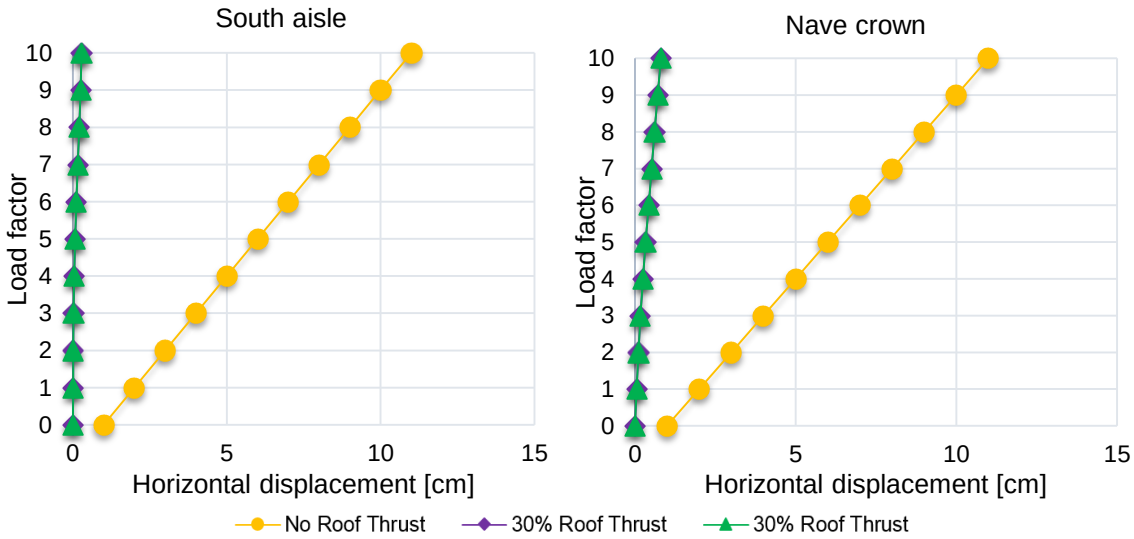

Figure 7-14. Load displacement diagrams depicting the South aisle and nave span opening, under dead loading.

7.4.1.3 Infill volume variables

Next, three different infill heights were considered (Figure 7-15). The current one, as configured in the geometrical survey is 5.8 m in height at the nave and 3.8 m at the lateral aisles. Through the correlation with the damage maps, the concrete layer was estimated around 0.40 m and placed above the past infill level, which can be estimated to 5.4 m for the nave and 3.4 m for the lateral aisles (Figure 3-16). A third infill height, corresponds to a rule of practice for the design of Gothic Cathedrals, is equal to the $^1/_3$ of the free rise of the vault and is 2.9 m and 1.8 m for the nave and the vaults respectively (Huerta 2004).

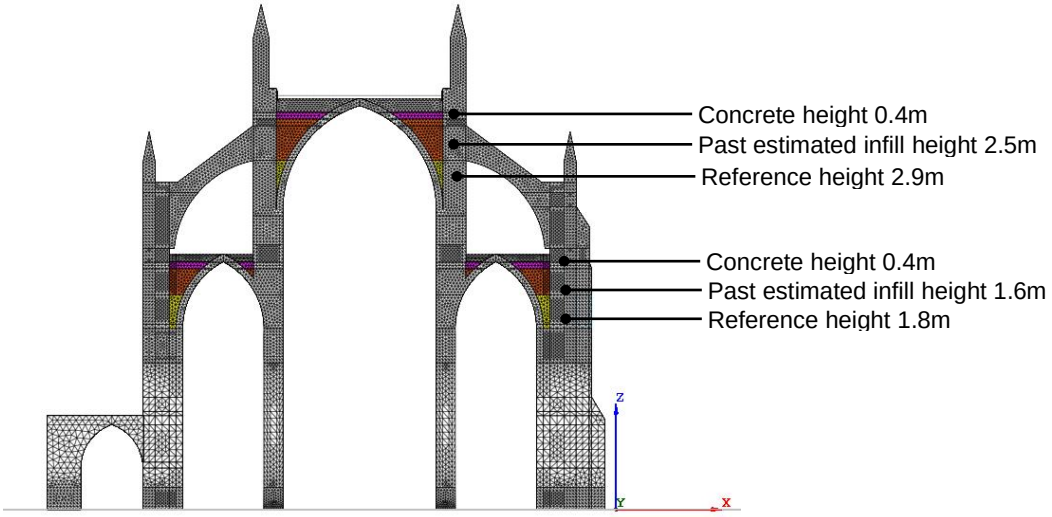

Figure 7-15. Cross section of the FE model of the typical bay, with the infill heights are depicted.

In the current state of the Cathedral's bay, the maximum vertical displacement of the crown at the nave vault is 9% and 22% larger than the one corresponding to the "past estimated infill" and the "reference height" respectively, which is logical, considering the grater counteracting thrust (Figure 7-16). For all three types of infill, a significant loss of stiffness is obtained with the 40% of self-weight application, as can be clearly seen in the horizontal displacement diagram of the south aisle and can be interpreted as tensile failure in the webs (Figure 7-17). From then on, the deformations in nave and aisle vaults engage in a linear estimated function.

The crack pattern is related to the spreading and deformation of the aisle vaults, depicting in the deformed shapes and disregarding the level of infill, as shown in Figure 7-17. The total displacements in all three cases are in the order of millimeters. The cracks produced from the inward pushing, in all the lateral vaults of the three cases, appear in the same height, along the longitudinal vertex. In the part of the lateral vaults that is pushed outwards the tensile damage of the current infill state is magnified, with a wider distribution along the thickness of the vault, compared with the other two cases. This difference is related to the additional stiffness from the infill, which suppresses the vault from deforming outwards and thus it cracks at the less stiff part, near the outer side of the longitudinal vertex. The infill volume can also be correlated with cracks in the nave and flying buttresses. In specific, in the model with the

current infill, the tensile damage in the springings of the nave vault and the extrados of both the flying buttresses is widely distributed along the thickness, which is larger compared with the other two cases (Figure 7-17).

Nevertheless, all three models are not able to reproduce the tensile crack pattern in the intrados of the south flying buttress, near the springing line with the clerestory walls. This indicates that the typical bay, besides the dead loading, is subject to additional effects that compromise its structural stability. Thus in the next section, the hypothesis of soil settlements, at the south part of the typical bay, will be investigated.

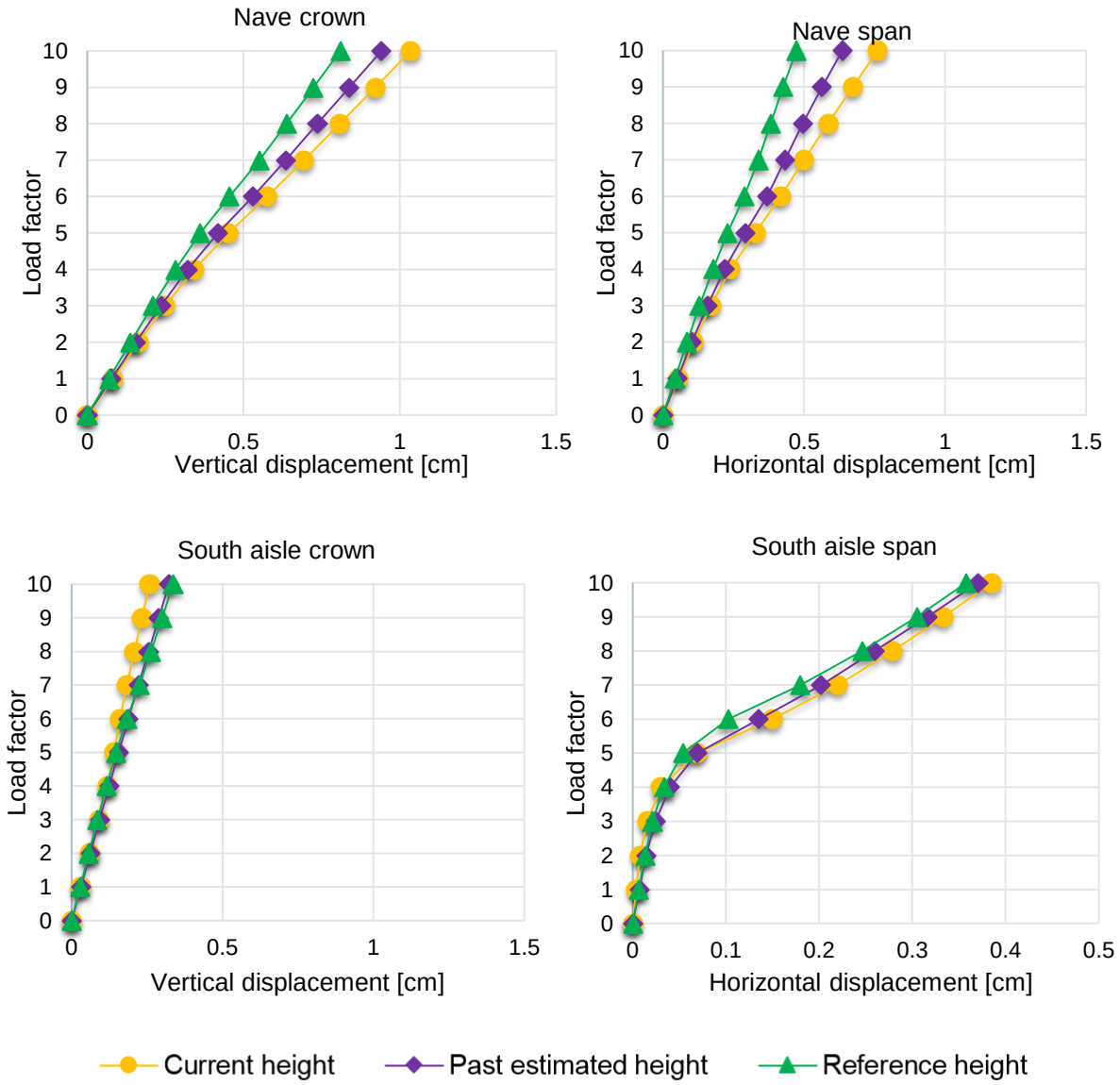

Figure 7-16. For the three different infill heights: (a) Load versus vertical displacement diagram of the nave's crown. (b) Load versus vertical displacement diagram of the south aisle's crown. (c) Load versus horizontal displacement diagram of the nave's crown. (d) Load versus horizontal displacement diagram of the south aisle's crown.

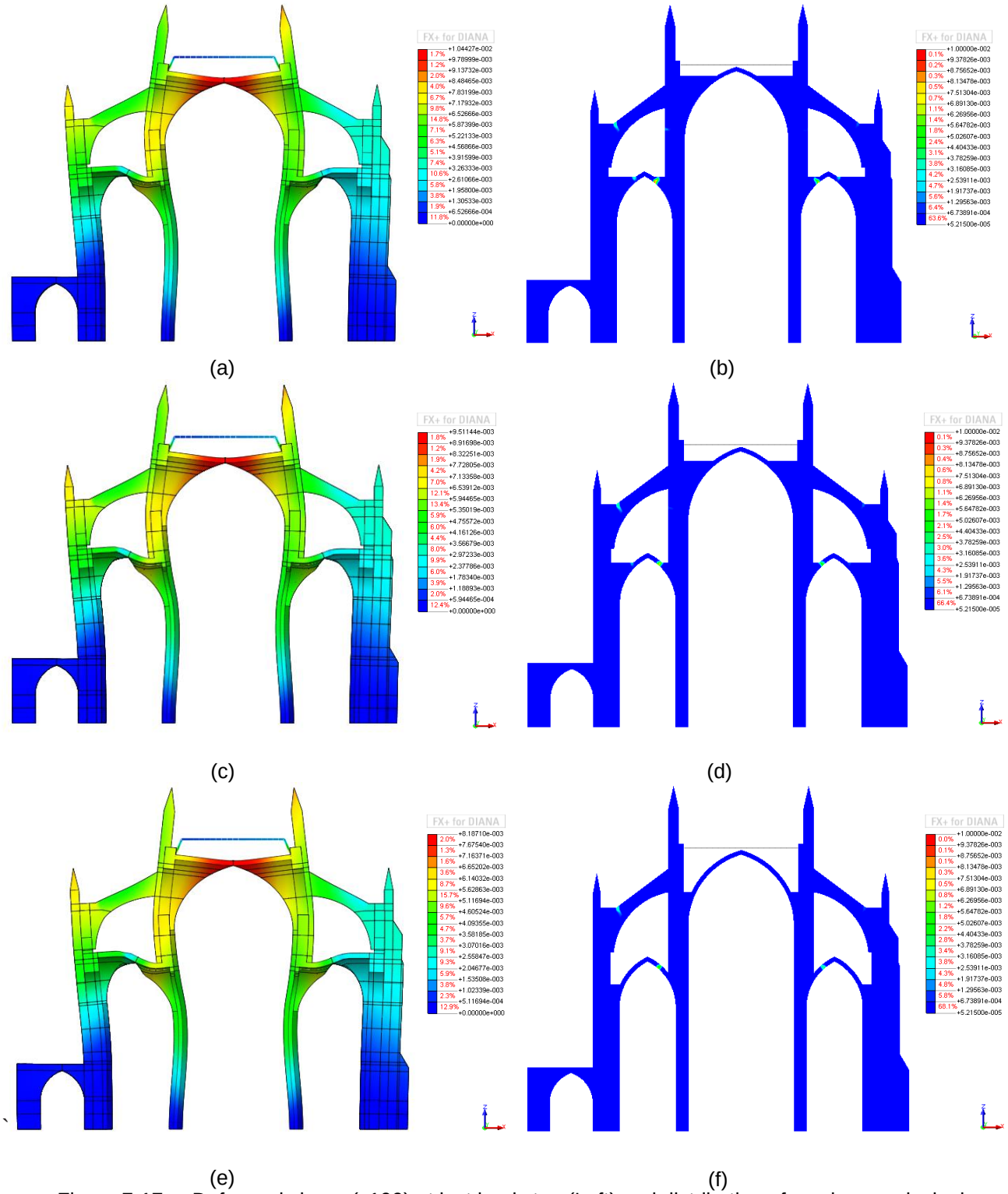

Figure 7-17. : Deformed shape (x100) at last load step (Left) and distribution of maximum principal strains at last load step in a slicing plane at the symmetry axis (Right), for the reference infill height (Top row), the past estimated infill height (Middle row) and the current infill (Bottom row).

7.4.1.4 Soil settlements as springs at base

An investigation was performed regarding the possibility that the structural damage on the cathedral's nave, and in particular in sections 2 and 3 (Figure 3-1), is induced by differential soil settlements on the south part of the foundation soil. This settlement can be the result of vibrations from civil works, dead load increase, water leakage from underground pipes and changes in underground water level. In specific, a large old drain pipe runs near the foundations of the south buttresses, which increases the risk that a potential leakage could wash away parts of the foundation soil and cause settlements (Corallo 2014).

The scenario of a non-uniform displacement field at the foundation base of the typical bay was implemented by the means of strings at the base (Figure 7-18). The soil stiffness coefficients in the vertical and horizontal direction, were computed based on the numerical and experimental work of (Gazetas et al. 1986).

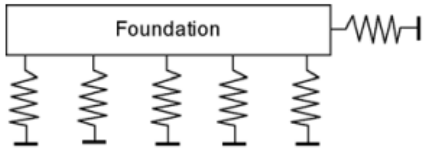

Figure 7-18. Modeling of the foundation soil with springs of vertical and horizontal stiffness coefficients.

The vertical stiffness coefficient of a foundation, with dimensions shown in Figure 7-19, is given by the Eq. 7-3, where A_b is the area of the foundation base (m^2), v_s is the Poisson ratio of the foundation soil, E_s is the modulus of elasticity of the soil and L is the longest dimension of the foundation. The μ coefficients take in to account the shape of the foundation, the trench and the wall respectively and are described in the Equations 7-4, 5 and 6. A_w is the contact area between the foundation footing and the lateral walls of the trench (Gazetas et al. 1986).

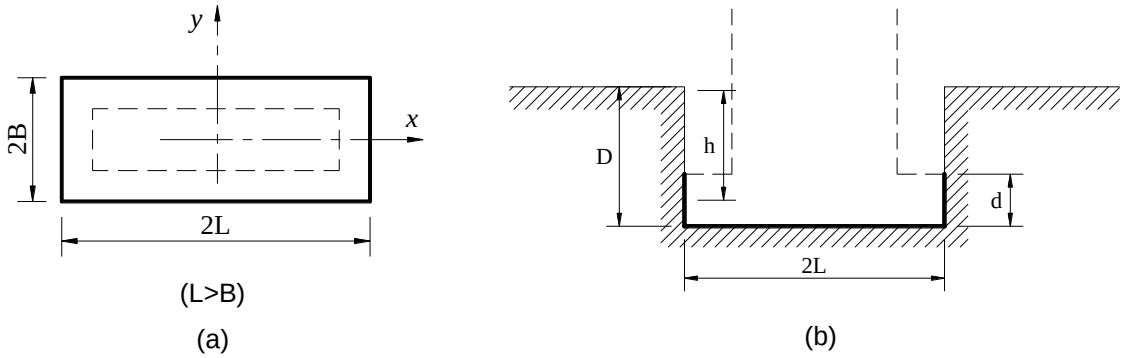

Figure 7-19. Geometric configuration of a foundation in plan (a) and cross section (b) view.

$$k_s^z = \frac{E_s \cdot L}{A_b \cdot (1 - v_s^2) \cdot \mu_{shape} \cdot \mu_{trench} \cdot \mu_{wall}} \quad \text{(Eq. 7-3)}$$

$$\mu_{shape} = 0.45 \cdot \left(\frac{A_b}{4 \cdot L^2}\right)^{-0.38} \quad \text{(Eq. 7-4)}$$

$$\mu_{trench} = 1 - 0.04 \cdot \frac{D}{B} \cdot \left(1 + \frac{4}{3} \cdot \frac{A_b}{4 \cdot L^2}\right) \quad \text{(Eq. 7-5)}$$

$$\mu_{wall} = 1 - 0.16 \cdot \left(\frac{A_w}{A_b}\right)^{0.54} \quad \text{(Eq. 7-6)}$$

The stiffness coefficient of the foundation at the horizontal direction is determined by the Eq. 7.7.

$$k_s^x = \frac{E_s \cdot L}{A_b \cdot (2 - \nu_s) \cdot (1 + \nu_s) \cdot \mu_0^x \cdot \mu_{trench} \cdot \mu_{wall}} \quad \text{(Eq. 7-7)}$$

The μ coefficients are described in the Eq. 7-8, 9 and 10.

$$\mu_0^x = \left[0.5 - 0.28 \cdot \left(\frac{A_b}{4 \cdot L^2}\right)^{0.45}\right] \cdot \left[1 + 1.12 \cdot \left(\frac{1 - B/L}{1 - \nu}\right)^{1.6}\right] \quad \text{(Eq. 4-8)}$$

$$\mu_{trench} \approx 1 - 0.14 \cdot \left(\frac{D}{B}\right)^{0.35} \quad \text{(Eq. 4-9)}$$

$$\mu_{wall} = 1 - 0.35 \cdot \left[\frac{h}{B} \cdot \frac{A_w}{L^2}\right]^{0.2} \quad \text{(Eq. 4-10)}$$

The foundation system in Gothic Cathedrals consists of spread foundations for the internal piers and stone walls in the perimeter (Coronelli et al. 2014). Because no evidence was found for the nave foundations of Canterbury Cathedral, a geometric configuration was assumed. Regarding the south buttress, from the complex cross section shape, a rectangular section was chosen with dimensions 4.6 m length, actual length of the south buttress at base and 2.0 m in width, which is the equivalent width, of an equal cross section area. The foundation is considered of the same cross section area and the foundation base is assumed to lie 6 m below the ground level, taken as reference from other studies (Coronelli et al. 2014). The foundation of the columns is considered of the same square cross section area, as that of the columns, i.e. 1.35x1.35 m and the foundation base was chosen at the same depth as that of the buttress, i.e. 6 m. Due to the lack of quantitative data regarding the mechanical properties of the foundation soil, values from other studies have been retrieved. The geological landscape of the region of Canterbury consists of Chalk and London clay, with a lower layer of Thanet Beds ("Kent Geology" 2014). The soil at the north part of the typical bay is assumed to be hard clay, with a Poisson ratio of 0.3, of dense consistency and a Young Modulus value of 100 MPa. In order to induce a medium

end displacement field, the foundation soil of the south buttress is considered clay of medium consistency, with a Poisson ratio of 0.3 and a Young Modulus value of 20 MPa (Bowles 1977). By assuming that the largest displacement field is in the foundation of the south buttress, the vertical stiffness coefficients at the base of the south column is calculated so as the resulting vertical displacement, under the imposed stresses, is half in relation to the south buttress, whereas for the north column to be equal with the vertical displacement of the north buttress. The horizontal stiffness coefficients were taken equal to those of the buttresses at each influential part respectively. The mass density of the foundations were chosen 19 kN/m^3. Lastly, the columns of the cloister were assigned with the same soil stiffness as the north buttress.

Table 7-1 includes the specified values, regarding the geometry and properties of the foundation soil at the base of the north and south buttress, as well the variables and coefficients regarding the vertical stiffness of the foundation soil. Table 7-2 presents the stiffness coefficients and the variables in the horizontal direction, at the base of the north and south buttress. Table 7-3 presents the vertical and horizontal stiffness coefficients chosen for the foundation soil at the piers.

Table 7-1. Coefficient and variables of vertical stiffness of the foundation soil at the north and south buttress.

	A_b [m^2]	A_w [m^2]	h [m]	d [m]	μ_{shape}	μ_{trench}	μ_{wall}	k_s^z [kN/m^3]
South buttress	9.3	79.1	6	6	0.611	0.624	0.491	26950
North buttress	9.3	79.1	6	6	0.611	0.624	0.491	134800

Table 7-2. Coefficient and variables of horizontal stiffness of the foundation soil at the north and south buttress.

	μ_o^x	μ_{trench}	μ_{wall}	k_s^x [kN/m^3]
South buttress	0.540	0.740	0.140	39900
North buttress	0.540	0.740	0.140	199500

Table 7-3. Coefficient and variables of horizontal and vertical stiffness of the foundation soil at the north and south pier.

	k_s^z [kN/m^3]	k_s^x [kN/m^3]
South pier	62250	39900
North pier	155650	199500

The corresponding distributed stiffness values for the continuous system of springs, used to simulate the foundation soil, are determined by dividing the stiffness coefficients by the number of nodes at the base.

From the static nonlinear analysis results the vertical and horizontal displacements at the base of the vertical abutments are presented in Figure 7-20. The maximum vertical displacement imposed by the soil foundation of the south buttress reaches 11 cm and the structure approaches failure. Note the high ductility level of the structure and the equilibrium state under such large imposed deformations.

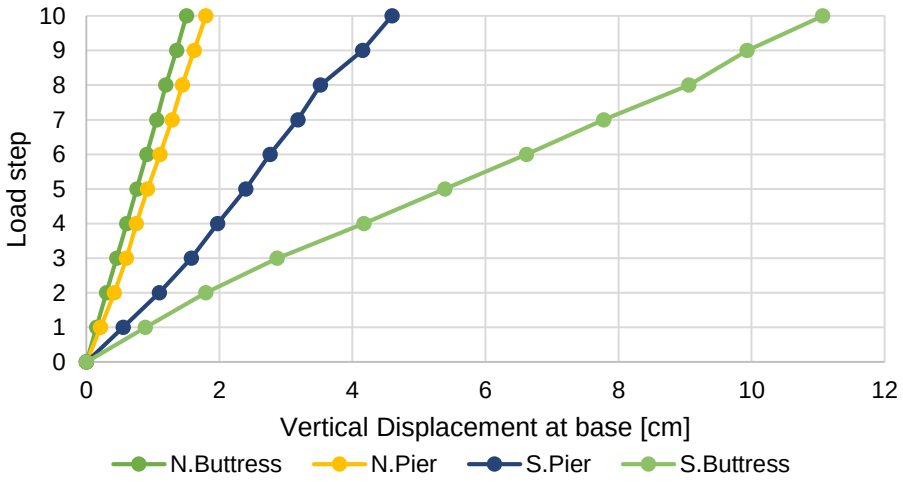

Figure 7-20. Load displacement diagram, depicting the vertical displacements at the base of vertical abutments, under dead loading.

The typical bay experiences large deformations in the south part, due to the imposed horizontal and vertical displacement field at the base. The load displacement diagram of the span opening in the south aisle justifies the outward rotating of the south buttress (Figure 7-21). The maximum opening of the south aisle span is 1.7 cm, associated with high tensile stresses in both the south aisle vault and south buttress, with major fragmentation cracks (Figure 7-22, 23). In specific, at a relative vertical displacement at the south buttress base of 2.2 cm, tensile failure cracks near the upper spring line and in the intrados at the middle span of the south flying buttress appear, covering a large part of the section. At the same step the aisle vault is subjected to a main fragmentation pattern, consisting of two tensile cracks near the longitudinal vertex, which propagate in the vault structure. The north buttress cracks as well at the extrados, near the upper spring line. With settlement increase, a serious loss of stiffness is evident which can result in the formation of a plastic hinge (Figure 7-21). The second plastic hinge is formed in step 8, as can be concluded from the second large loss of stiffness (Figure 7-21). In between steps 5-8 the south aisle has a relatively constant span opening, which can be linked to a rigid body in plane motion. The main fragmentation pattern, consists of two hinges at the near end of the longitudinal vertex of the south aisle vault and one hinge near the springing line of the south flying buttress (Figure 7-22, 23). The

nave vault is cracked at the longitudinal vertex in step 10, combined with high compressed zones at the hinges, as can be seen from the distribution of the minimum principal stresses (Figure 7-23).

The resulting damage from the imposed displacements of the foundation soil at the onset of flying arch cracking can be correlated with the observations in situ. The two tensile cracks of the south flying buttress correspond to the documented damage, which confirms the possibility that differential settlements of the south foundation in sections 2 and 3 in the nave of Canterbury Cathedral might actually be the generating mechanism. The large fragmentation crack at the extrados of the south aisle vault is formed at the same place, but in the inverse direction with the existing one. The existing crack pattern at the intrados of the lateral vaults correlates well with the dead load case of section 7.4.1.1 and the possibility of this preexisting crack was not incorporated in the current analysis. Nevertheless, due to the lack of information on the material properties of the foundation soil, for the validation of the FE model of section 7.4.1.1, an approach of simulating the soil failure with imposed displacements at the base will be followed, and the matching criterion will be the resulting crack width at the south flying buttress, as presented in the next section.

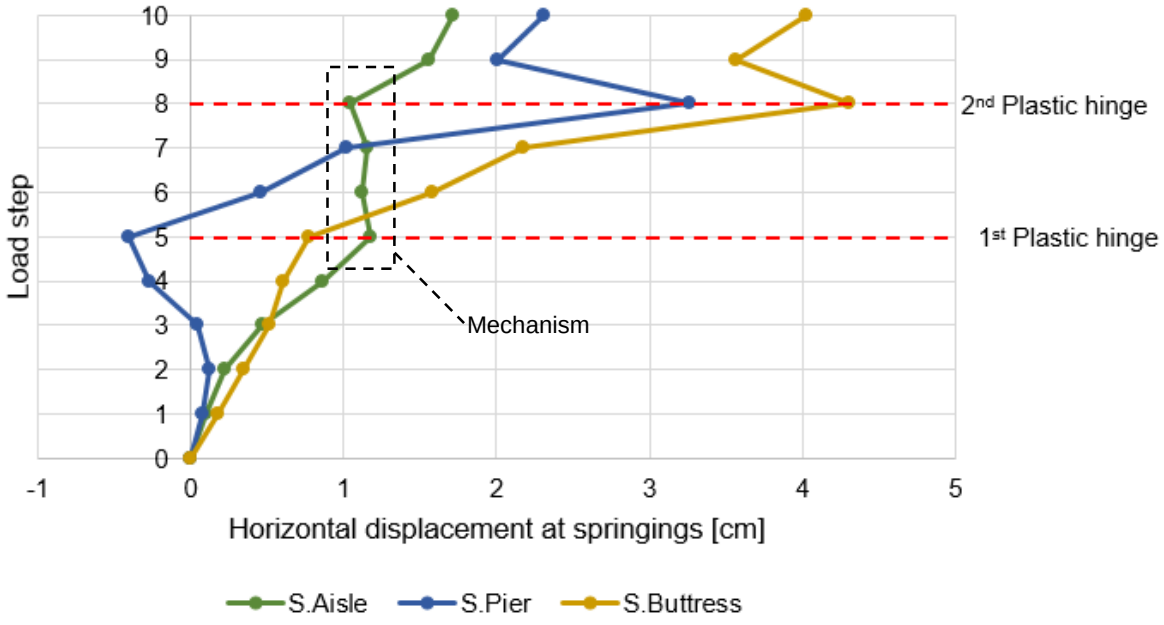

Figure 7-21. Load displacement diagram, depicting the span opening and absolute horizontal displacements of the south aisle vault, under dead loading.

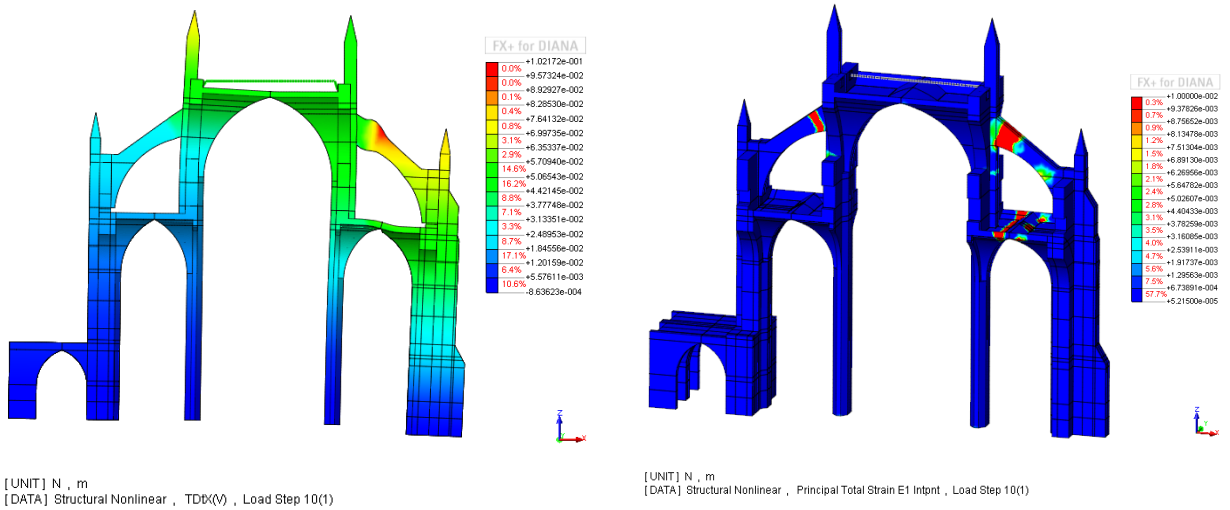

Figure 7-22. (Left) Deformed shape (x100) with displacement gradient at last load step. (Right) Distribution of maximum principal strains at last load step, in 3D view from above.

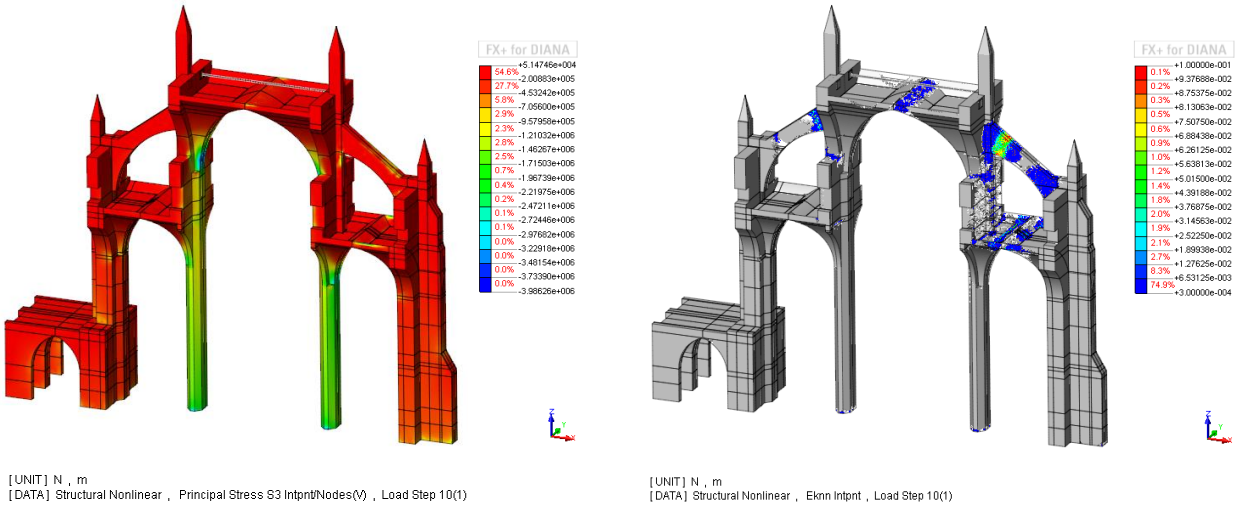

Figure 7-23. (Left) Distribution of minimum principal stresses at last load step. (Right) Distribution of normal strain cracks.

7.4.1.5 Soil settlements as displacements at base

In order to incorporate the hypothesis of soil settlements in the final configuration of the typical bay, with the existing crack pattern, vertical and horizontal displacements were applied as a load case at the base of the south buttress, after the self-weight. Two cases were examined, where the horizontal displacement at base is 10% (Model 1) and 50% (Model 2) of the vertical respective displacement, so that the one with the better correlation with the existing damage can be chosen. The vertical displacement increases until 10 cm and the size step which correlates best to the existing damage, will correspond to a crack width in the middle span of the south flying buttress of 0.003 m. The magnified

deformed shapes of the typical bay and the tensile damage distribution in graphs of maximum principal strains, minimum principal stresses and crack width at the principal direction, with the reference damage pattern for both models are shown in Figure 7-24, 25, 26 and 27.

According to results of the nonlinear analysis of Model 1 and 2 and after the application of the self-weight, with the resulting crack pattern, as described in section 7.4.1.1, the vertical and horizontal translation of the south buttress imposes tensile strains in the area of the existing crack at the inner part of the south aisle vault, but in an inversed way, with the hinge at the intrados (Figure 7-25). The first tensile cracks near the springings of the south flying buttress, located at the extrados near the left spring line, at the intrados near the right spring line and at the extrados of the clerestory walls underneath the flying buttress, correspond at 2 cm and 0.2 cm of vertical and horizontal displacement at base respectively in Model 1, whereas in Model 2 they correspond to 1 cm and 0.5 cm of vertical and horizontal displacement respectively. As the translations at the base of the south buttress progress, the tensile damage at the left springing of the south flying buttress propagates, while more tensile cracks appear at the intrados of the span, moving towards the middle. The nave vault suffers a longitudinal crack at the intrados, near the vertex, at 3.0 cm and 0.3 cm of vertical and horizontal displacement for Model 1 and at 2.5 cm and 1.25 cm of vertical and horizontal displacement for Model 2.

The crack width at the middle span of the south flying buttress, used as a reference for the imposed displacements, reaches 0.003 m at 5.0 cm and 0.5 cm of vertical and horizontal displacement for Model 1, whereas the reference width is obtained at 6.0 cm and 3.0 cm of vertical and horizontal displacements for Model 2 respectively (Figure 7-27). Due to the lower values of vertical displacements at the base of the south flying buttress that correspond to the same level of damage at a reference point, Model 1 is chosen as the validated FE model that correlates better with the existing damage.

Regarding the iron tie, it can be noted that it is under compressive stresses in all the analyses steps, thus remaining nonfunctional, due to the high values of lateral thrust of the nave vault, which pushes the clerestory walls outwards, while their upper part moves inwards.

From the current analysis the soil settlements, imposed at some point during the lifetime of the structure in the proximity of the south part of the foundations in sections 2 and 3 (Figure 3-1) are more likely to be the triggering mechanism for the existing damage.

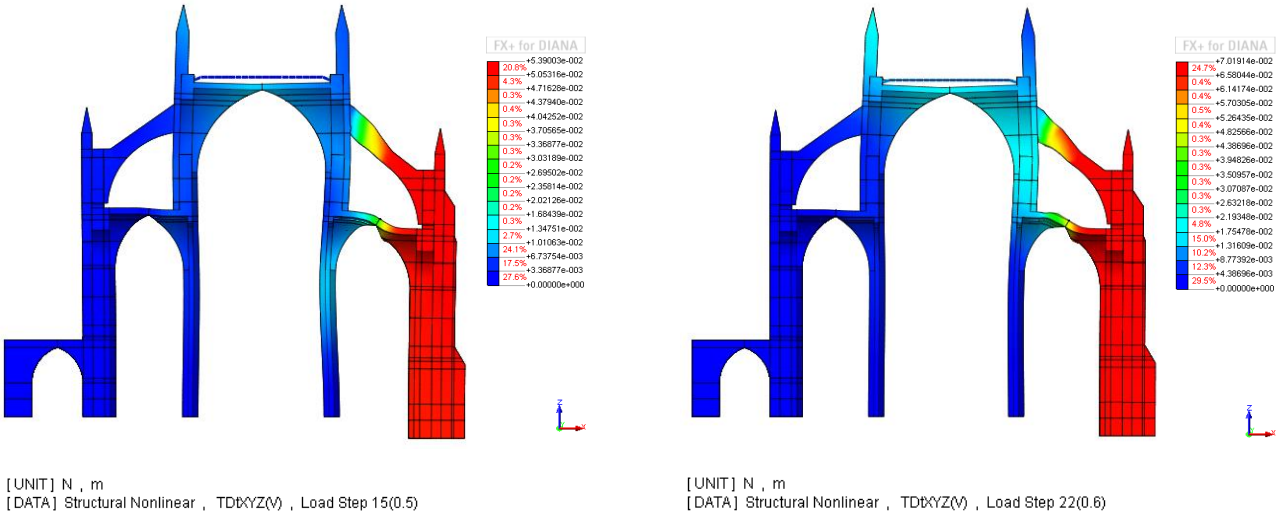

Figure 7-24. Deformed shape (x100) with displacement gradient of Model 1 (Left) and Model 2 (Right), at a corresponding load step of a 3 mm crack width at the middle span of the south flying buttress.

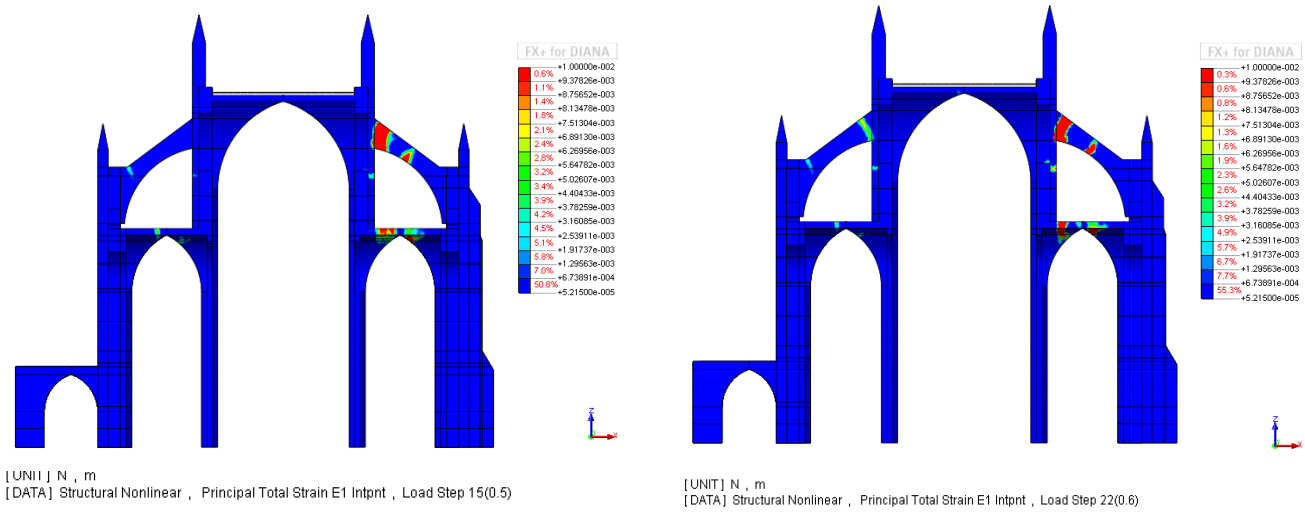

Figure 7-25. (Left) Distribution of minimum principal stresses of Model 1 (Left) and Model 2 (Right), at a corresponding load step of a 3 mm crack width at the middle span of the south flying buttress.

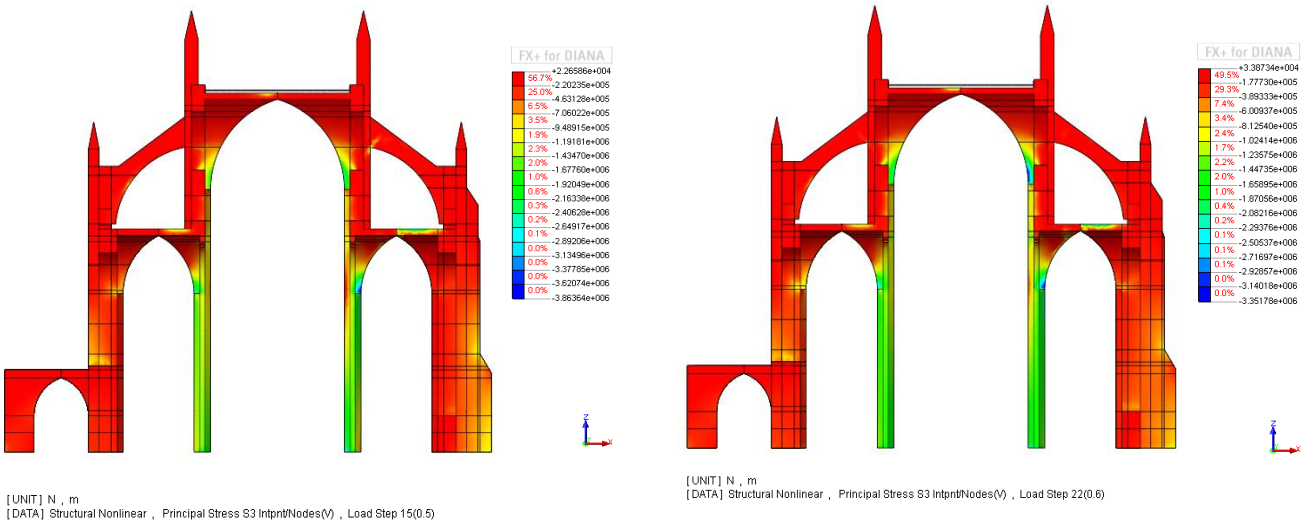

Figure 7-26. Distribution of minimum principal stresses of Model 1 (Left) and Model 2 (Right), at a corresponding load step of a 3 mm crack width at the middle span of the south flying buttress.

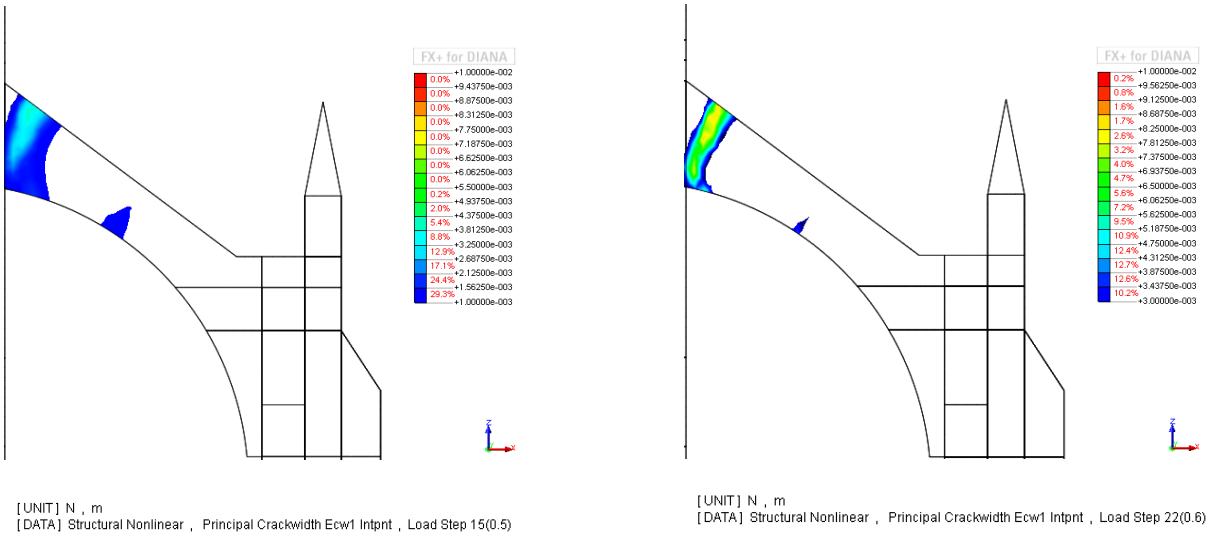

Figure 7-27. Distribution of crack width distribution at the south flying buttress, at load step 15 in Model 1 (Left) and at load step 22 in Model 2 (Right), with a gradient larger than 3mm.

7.4.2 Safety analysis

7.4.2.1 Vulnerability assessment under dead loads

In order to monitor the progression of tensile cracking and crushing zones until the global failure of the typical bay, and to discuss the present safety and vulnerability of the cathedral, the dead load in the model with the current level of infill (see section 7.4.1.1) was increased to obtain the vertical capacity using nonlinear static analysis. The obtained vertical capacity curve for the typical bay under dead load (7.4.1.1) is plotted in Figure 7-28.

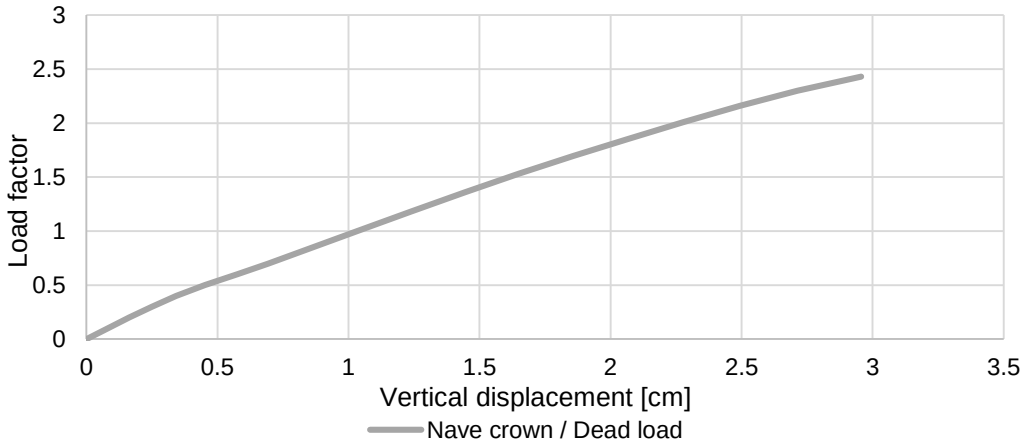

Figure 7-28. Load displacement diagram, depicting the vertical capacity in terms of vertical displacements of the nave crown.

For the FE model in section 7.4.1.1, the total applied vertical load, for which no convergence was reached, was 2.4 times larger than the self-weight (Figure 7-28). At that point, areas in the springings of the nave and lateral vaults are close to crushing, as shown in Figure 7-32. A large loss of stiffness in the typical bay section occurs around 40% of the dead load, when tensile damage in the lateral vaults appears, near the longitudinal vertex and the interface with aisle window arches (Sabouret's cracks) (Figure 7-28). The failure mechanism consists of large outward rotations for the clerestory walls. The piers follow a second order deformation, as they are partially constrained by the system of lateral vaults and counteract with the large thrust from the nave vault. The lateral aisles are pressed inwards. At all points of high curvature, tensile damage zones form, reaching deep in the structural parts. The nave vault, cracks along the vertex and crushing zones, close to failure at the springing of the nave vault and in the spring line of the lateral vaults with the piers are evident at the last step of convergence (Figure 7-30, 31).

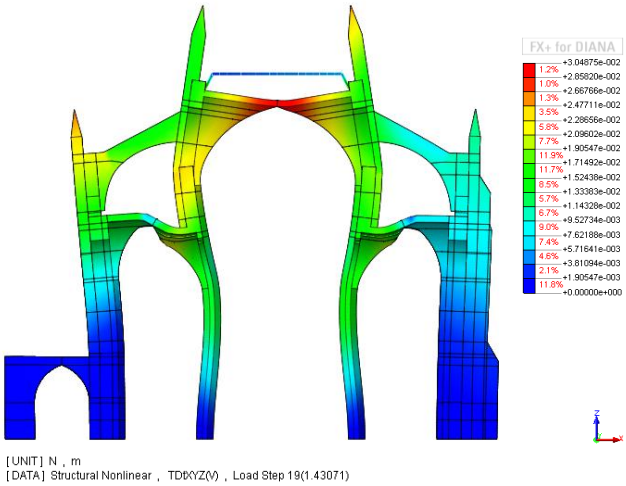

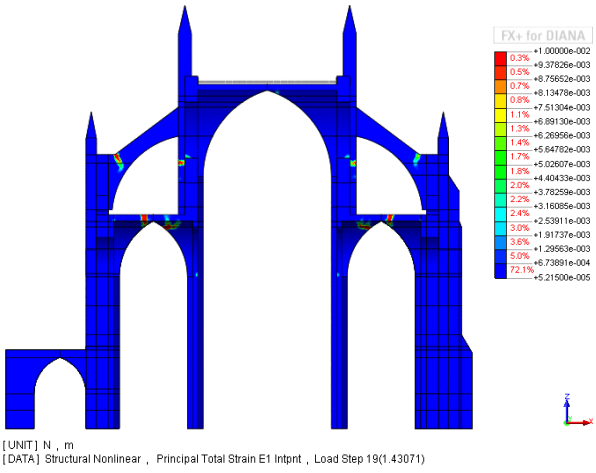

Figure 7-29. (Left) Deformed shape (x100) with displacement gradient at last load step of vertical capacity loading. (Right) Distribution of maximum principal strains at last load step of vertical capacity loading.

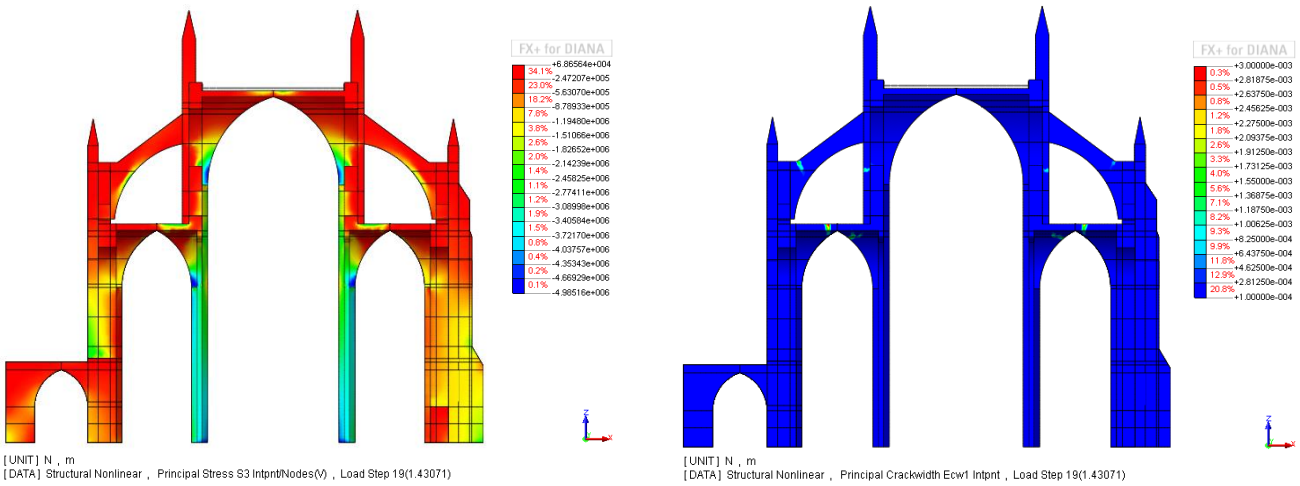

Figure 7-30. (Left) Distribution of minimum principal stresses at last load step at last load step of vertical capacity loading. (Right) Distribution normal strain cracks, depicting cracks larger than 0.3 mm at last load step of vertical capacity loading.

7.4.2.2 Vulnerability assessment under lateral loads

The lateral capacity was also evaluated, by applying a mass proportional lateral load. Because of the applied boundary conditions, which simulate the confinement of the typical bay in the y-y axis the lateral loads were applied in the x-x direction, from north to south, following the outward rotation of the south buttress. The obtained capacity curves for the typical bay under dead load (7.4.1.1) are plotted in Figure 7-29. The structure's capacity under horizontal loads is 0.09g. The pick of the base shear is reached at 0.088g and then until 0.09g, entering the post pick, the horizontal displacement at the south aisle crown increases, reaching over 0.1 m.

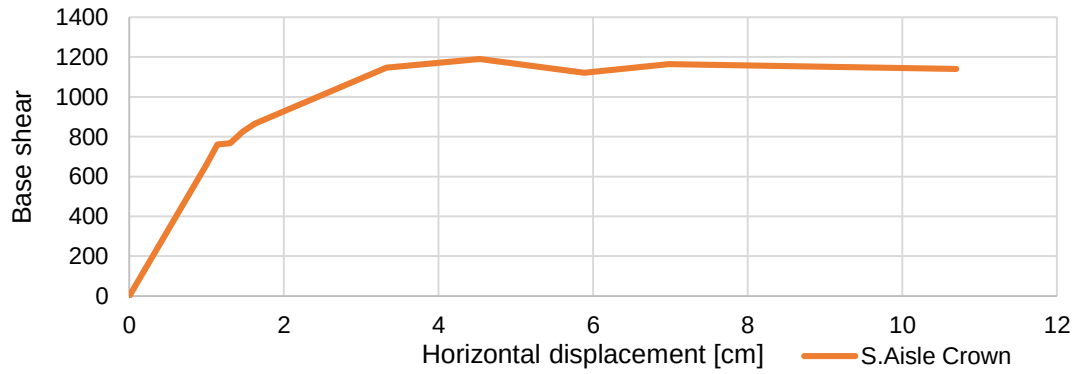

Figure 7-31 Load displacement diagram, depicting the lateral capacity in terms of horizontal displacements of the crown of the south aisle vault.

For the lateral loading, the failure mechanism consists of large deformations of high curvature for the lateral aisles, clerestory walls and the nave vault, while many fully formed plastic hinges appear in many structural elements, where the tensile failure zones have reached deep in the structural parts. In the nave vault, tensile failure is evident along the vertex, with crushing zones, close to failure at the corner of the south buttress and the right springing of the nave vault. A large tensile vertical crack fragments the south buttress near the base (Figure 7-32, 33).

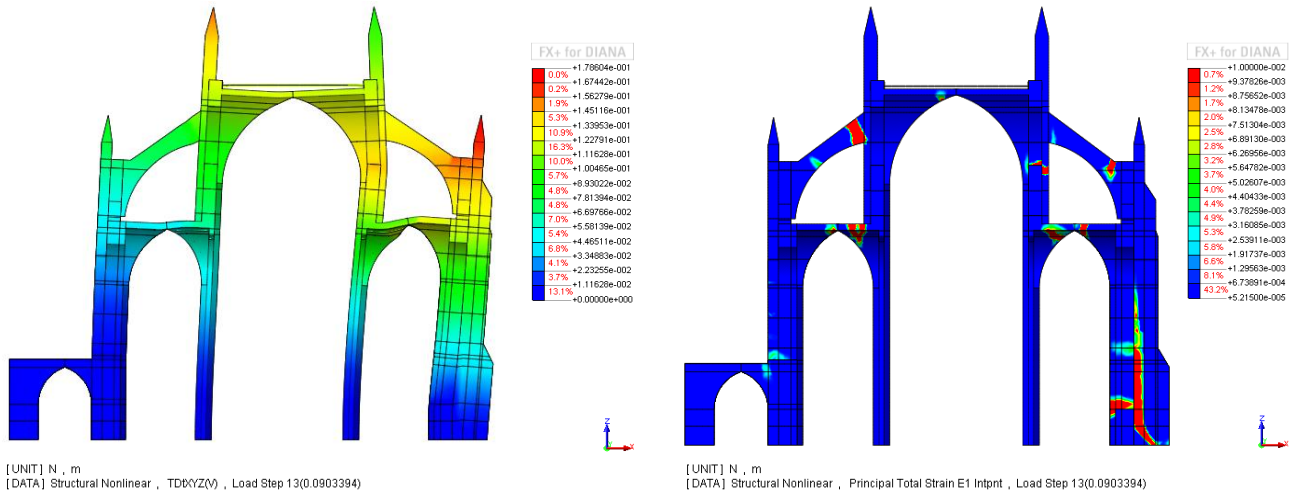

Figure 7-32. (Left) Deformed shape (x100) with displacement gradient at last load step of lateral capacity loading. (Right) Distribution of maximum principal strains at last load step of lateral capacity loading.

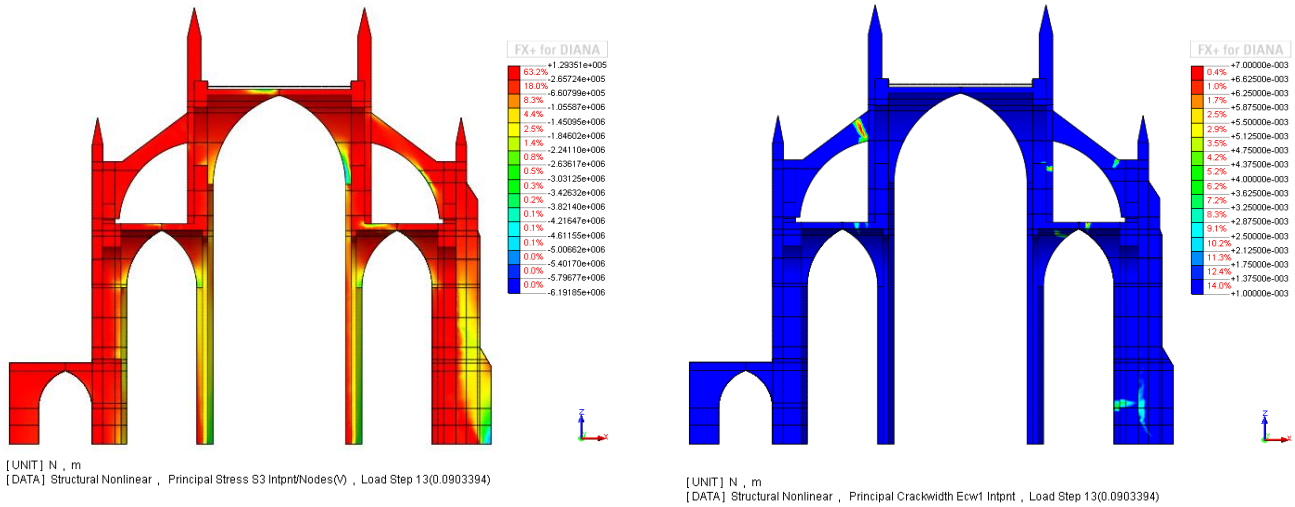

Figure 7-33. (Left) Distribution of minimum principal stresses at last load step of lateral capacity loading. (Right) Distribution normal strain cracks, depicting cracks larger than 0.3 mm at last load step of lateral capacity loading.

7.4.2.3 Vulnerability assessment under soil settlements

In order to evaluate the performance of the structure, under the presence of soil settlements in the south buttress and to assess the decrease of the safety levels, static nonlinear capacity analysis under mass proportional vertical loading was performed in the FE model of section 7.4.1.5. The obtained capacity curve is plotted in Figure 7-34. The total vertical applied load until no convergence was reached is 2.0 times larger than the dead load, decreased by 17% from the vertical capacity without settlements. The propagating failure mechanism is the fragmentation cracks along the longitudinal vertex of the south lateral vault and the south flying buttress, as well as the crushing areas at the springings of the nave and lateral vaults at the piers (Figure 7-35, 36).

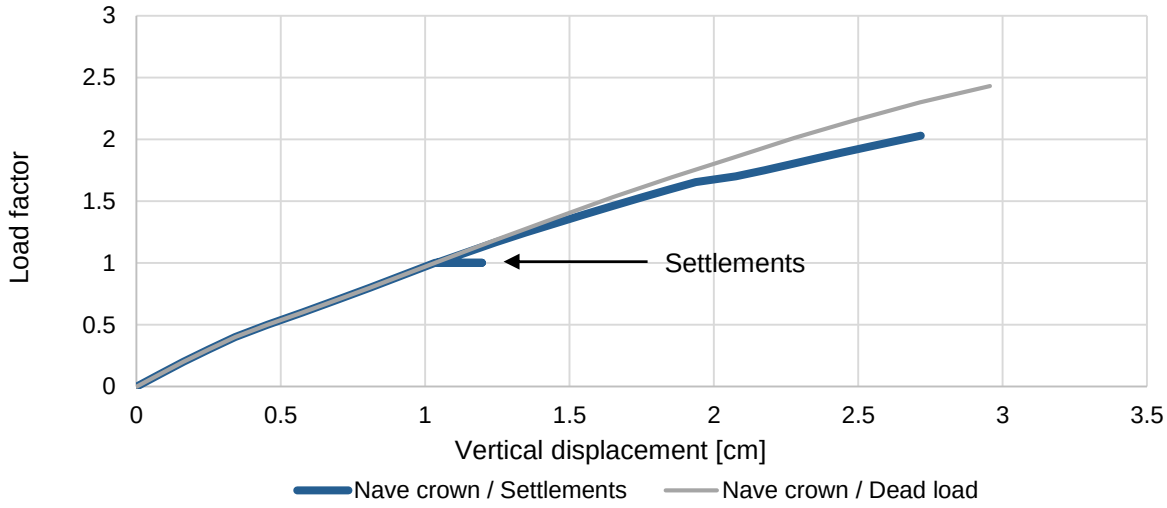

Figure 7-34. Load displacement diagram, depicting the vertical capacity in terms of vertical displacements of the nave crown.

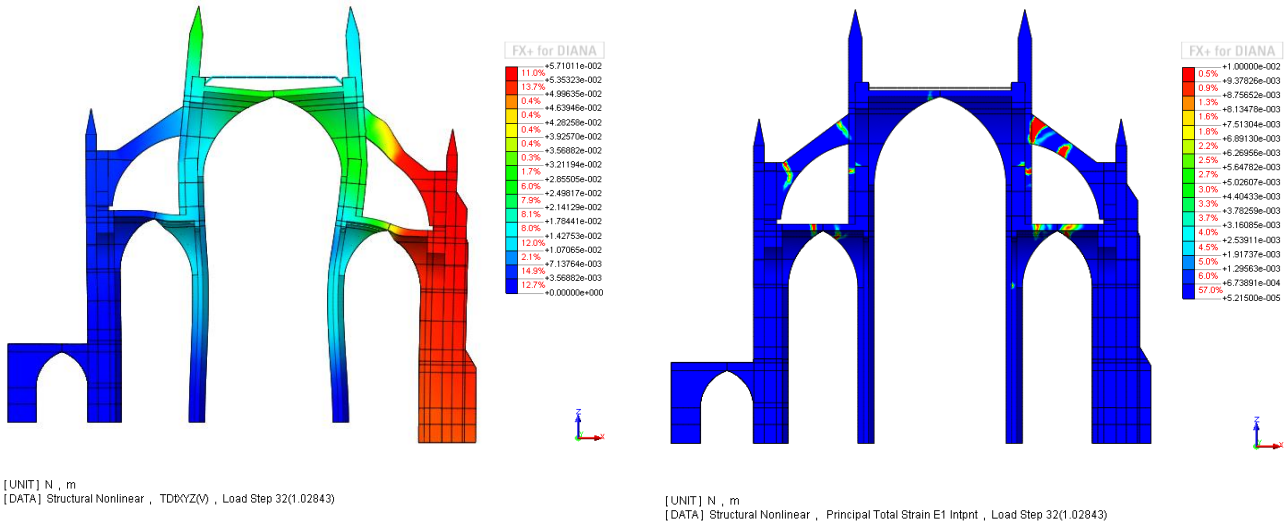

Figure 7-35. (Left) Deformed shape (x100) with displacement gradient at last load step of vertical capacity loading. (Right) Distribution of maximum principal strains at last load step of vertical capacity loading.

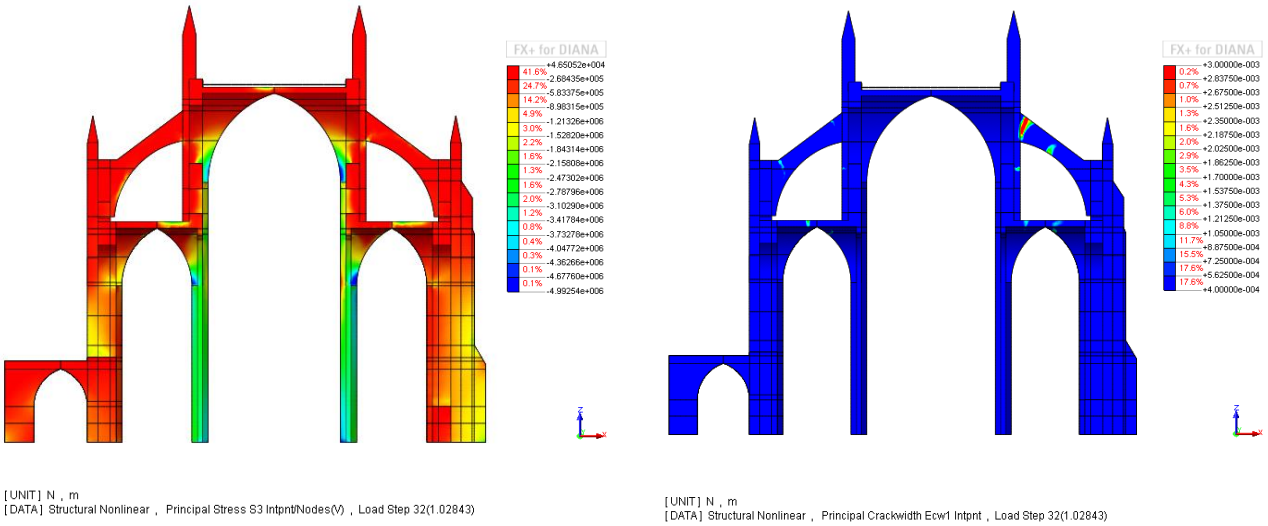

Figure 7-36. (Left) Distribution of minimum principal stresses at last load step at last load step of vertical capacity loading. (Right) Distribution normal strain cracks, depicting cracks at last load step of vertical capacity.

7.5 Conclusions

From the existing configuration of the typical bay of Canterbury Cathedral in present time, it is evident that the structure can sustain the dead loading, with some tensile damage, concentrated in the upper part of the left springing line in the flying buttresses, in the longitudinal vertex of the lateral aisles and the clerestory walls, at the level of the nave vault's springing. The location of the cracks is located over tension zones created from the inward pressure of the lateral vaults and the outward bending of the clerestory walls, which counteract the lateral thrusts. The damage pattern at the lateral vaults, consists of a longitudinal crack in the interior section of the vaults and Sabouret's cracks at the interface with the

window aisles, which can be accurately correlated with the FE model of under dead load (Figure 7-34, 35). From the deformed configuration it can also be concluded that the flying buttresses, due to their position, do not counteract the thrust from the nave vault and they are more likely to work under lateral loads from the roof system. The infill volume appears to correlate with the intensity of the damage and the propagation of tensile failure zones in the body of structural elements. The safety level of 2.43 for the dead loading provides a good safety margin.

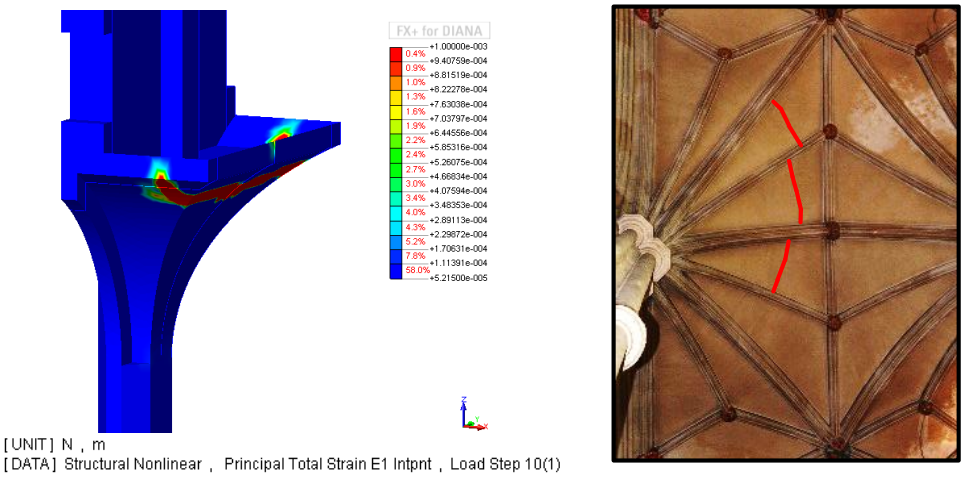

Figure 7-37. (Left) Distribution of maximum principal strains at last load step under dead loads and the present level of infill, in the interior section of the south aisle vault, under dead loading in the current state. (Right) Corresponding crack surrounding the pier of the south aisle at section 3.

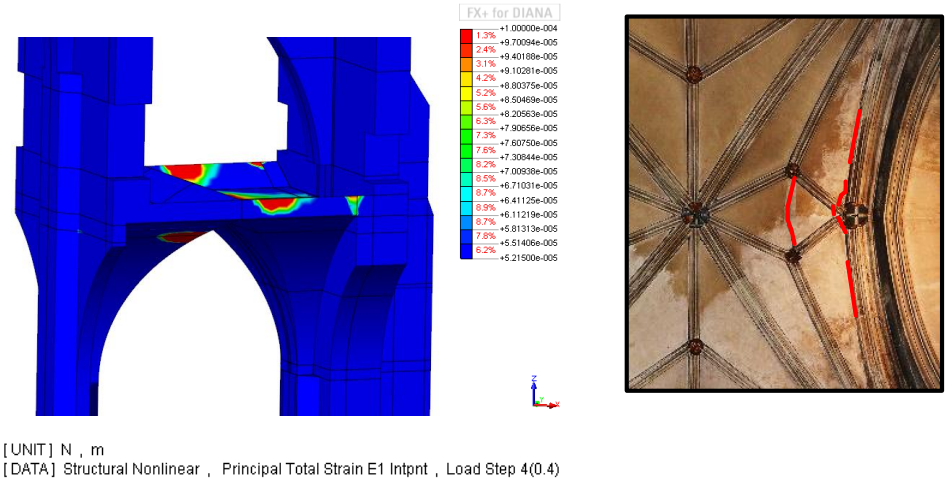

Figure 7-38. (Left) Distribution of maximum principal strains at 40% of dead loads and the present level of infill, in the interior section of the south aisle vault. (Right) Corresponding crack in the intersection between the web and the aisle window, at section 3.

The nonlinear static analysis under dead loading and stiff foundations cannot efficiently reproduce the existing damage pattern, in particular the cracks of the south flying buttresses at sections 2 and 3 (Figure

7-32). The presence of soil settlements / rotations at the south part of the typical bay, at some point during the lifetime of the structure, provides better correlation with the existing crack pattern in the south flying buttress, as shown in Figure 7-40. The tensile damage in the south flying buttress can be reproduced with an initiated vertical and horizontal displacement at the base of the south buttress of 5.0 cm and 1 cm respectively (see section 7.4.1.5). It seems therefore that foundation settlements are an important cause of the actual damage in the structure.

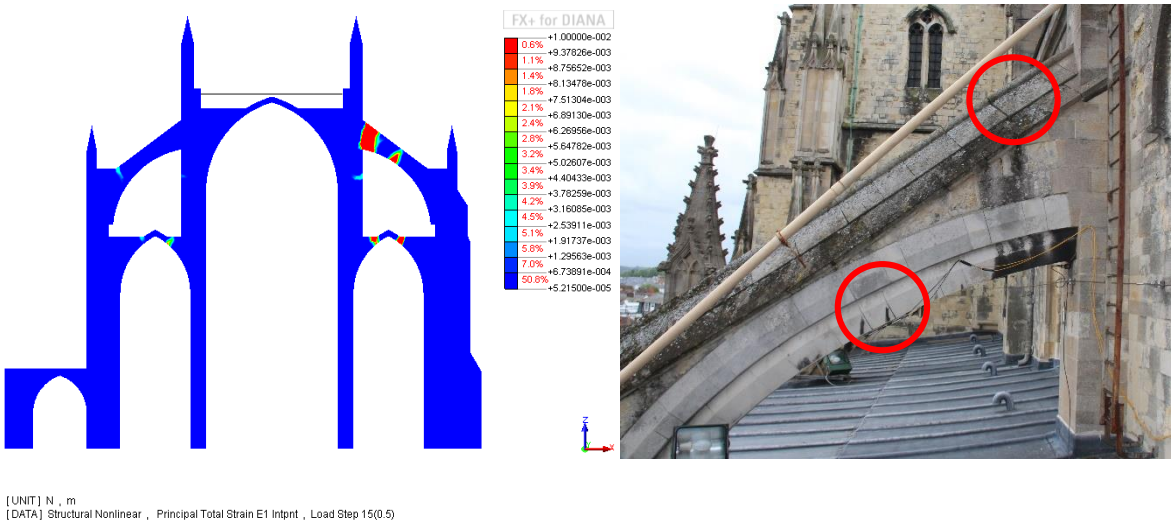

Figure 7-39. (Left) Distribution of maximum principal strains at last load step, in a slicing plane at the symmetry axis, under differential settlements. (Right) Cracks at the top part and the middle span of the south flying buttress, in section 3.

Regarding the vulnerability assessment under dead loading, the structure can sustain 143% more than the total dead load, which is considered a sufficient margin. This has been reduced by the settlements but the safety still seems acceptable for current conditions. On the other hand, the lateral capacity of 0.09 g for seismic loading is considerably low, which accounts for the fact that Gothic structural members, such as thin aisle vaults and flying buttresses have limited capacity to withstand lateral actions, because of tensile damage, under inversions of curvature (Roca 2001). But the hazard in Canterbury seems to be low, so no action seems needed.

8. CONCLUSIONS OF THE THESIS

In the current study, a multidisciplinary approach was followed, in order to assess the structural performance of the nave and lateral aisles of Canterbury Cathedral, with a main focus on the numerical nonlinear static analyses performed. Through different hypotheses on causes that could trigger structural damage, defined from the historic research and the in situ damage identification, FE models were built and analyzed under the scope of reproducing existing damage patterns and mainly providing a basis for a further discussion and survey on the Cathedral's nave structural behavior and pathology.

In specific, the Cathedral's nave and lateral aisles are in general in good condition, except from specific tensile damaged zones in the vaults system and the south buttresses. A repetitive diffused crack pattern in the intrados at the level of infill of the aisle vaults, surrounding the capitals and cracks forming at the interface between the vaults and the side walls, known as Sabouret's cracks, are caused due to self-weight, at an early stage of application. They are mainly caused, under the deflections and curvatures that suffer the structural members in the counteraction with the lateral loads from the vaults, which is common to many Gothic Cathedrals.

Regarding the geometric configuration of the typical bay, it appears that the position of the flying buttresses does not allow them to counteract the thrust from the nave vault, but instead they are more likely to sustain lateral loads from the roof system. Because of this, the large lateral thrust from the nave vault creates an outward bending deflection at the clerestory walls, just underneath the flying buttresses. The piers, due to their lateral constrain from the lateral aisles deform in a double curvature shape and are pushed inwards at a lower level. This deformed shape is the one responsible for the damage zones on the aisle vaults. The infill volume appears to correlate with the intensity and propagation of tensile damage, but not on the superposed and the roof's possible lateral load is too small compared to the large lateral thrust of the nave vault.

Furthermore, tensile damage and spreading of the south flying buttress in the central sections of the nave can be accurately reproduced with a rotating settlement at the south buttress foundation, enforcing the fact that the foundations are the main cause of the actual damage in the structure.

Regarding the vulnerability assessment under dead loading, in lateral and vertical direction, it appears that the structure performs sufficiently under vertical loads, with a safety margin of 2.4 times its self-weight, which is reduced to 1.8 under the influence of additional damage, taking account the settlements. The typical bay's lateral capacity under dead loads of 0.09g and is considered low, which states that the structure cannot withstand large lateral actions. Given the local hazard, this capacity can be considered adequate, both for vertical and horizontal loading under current condition.

Through the conducted ambient vibration tests and the identification of the modal shapes, the updating of the FE model was possible, through the correlation with the 1st mode shape. Nevertheless, the

calibration of a FE model is a time consuming procedure and requires a high level of expertise, since many modes are not plane and are associated with modes of the entire structure.

Given the complexity of the structure many aspects would require further investigation and future suggested work is the following:

- The process of the large collection of monitoring data from 2010, regarding the crack and tilt meters placed at the south flying buttresses, will reveal the level of regression of the outward rotating movement and its propagation over the course of time.
- The application of strain gauges could actually determine the changes in level of stresses of the iron ties and whether or not they are functional.
- The installation of a monitoring system of settlement would determine the existence and propagation of the displacement field at the foundation level. Also, in situ inspection can be applicable, in order to confirm the possibility that the soil failure is caused from a suspected leakage of an old drain pipe, running near the south buttresses (Corallo 2014).
- Further ambient vibration tests can determine the actual 3D modes of the nave and lateral aisles, offering better insight for future modal analyses and FE model updating.
- A phased nonlinear static analysis would take into account the construction process of Canterbury Cathedral and the imposition of deformations in a more accurate time frame, which would lead to results of higher accuracy.
- Non- and minor-destructive tests (NDTs, MDTs) such as sonic pulse velocity tests and double flat jack testing could serve to obtain values that can better approximate the actual material properties of the structure.

9. REFERENCES

"ACNS - Anglican News Service" (2007) Save Canterbury Cathedral Appeal Reaches 7 Million (http://www.anglicannews.org/news/2007/11/save-canterbury-cathedral-appeal-reaches-7-million.aspx).

"AD 1000 - Canterbury Cathedral" (2007) Current Archaeology. (http://www.archaeology.co.uk/specials/the-timeline-of-britain/canterbury-cathedral.htm)

"An Introduction to the History of York." (2014) York 360° - The History of York. (http://www.york360.co.uk/history-of-york.htm)

"Anglo-European Stone" (2014) Anglo-European Stone. (http://www.anglo-european-stone.com/index.htm)

"Caen Stone" (2014) Wikipedia. Wikimedia Foundation. (http://en.wikipedia.org/wiki/Caen_stone)

"Canterbury Cathedral Aerial" (2013) Flickr. Yahoo!. (https://www.flickr.com/photos/john_fielding/8636098050/)

"Canterbury Cathedral" (2014a) Gotik-Romanik.de (http://www.gotik-romanik.de/Canterbury%20Thumbnails/Thumbnails.html)

"Canterbury Cathedral" (2014b) Wikipedia. Wikimedia Foundation. (http://en.wikipedia.org/wiki/Canterbury_Cathedral)

"Canterbury Cathedral" (1992) UNESCO/CLT/WHC. (http://whc.unesco.org/en/list/496)

"Canterbury Cathedral" (2005) Attraction in Canterbury. (http://www.discoverkent.com/attractions/canterbury-cathedral)

"Canterbury Cathedral: Great South Window." (2013) The Natural Stone Specialist. (http://www.naturalstonespecialist.com/currentissue/unlockednewsarticle.php?id=631)

"Cathedral of Notre-Dame" (2014) A&A Nave, Section, Cathedral of Notre-Dame. (http://www.artandarchitecture.org.uk/images/conway/d93834f4.html)

"Completed Corona Is Finally Revealed" (2012) Completed Corona Is Finally Revealed. (http://www.canterbury-cathedral.org/2012/08/22/completed-corona-is-finally-revealed/)

"Durham Cathedral" (2014) (http://en.wikipedia.org/wiki/Durham_Cathedral)

"Ely Cathedral" (2014) (http://en.wikipedia.org/wiki/Ely_Cathedral)

"English Gothic Architecture" (2014) Wikipedia. Wikimedia Foundation. (http://en.wikipedia.org/wiki/English_Gothic_architecture)

"Exeter Cathedral" (2014) (http://en.wikipedia.org/wiki/Exeter_Cathedral)

"Gloucester Cathedral" (2014) Wikipedia. Wikimedia Foundation. (http://en.wikipedia.org/wiki/Gloucester_Cathedral)

"Gothic Arches" (2014) A Summary of Western Architecture. (http://lookuparchitecture.com/historygothic.htm)

"Gothic Architecture" (2014a) Wikipedia. Wikimedia Foundation. (http://en.wikipedia.org/wiki/Gothic_architecture)

"Gothic Architecture" (2014b) Simple English Wikipedia, the Free Encyclopedia. (http://simple.wikipedia.org/wiki/Gothic_architecture)

"Gothic Cathedral and Church Construction" (2014) Abelard Public Education Website. (http://www.abelard.org/france/cathedral-construction.php)

"Gothic Revival Architecture" (2014) Wikipedia. Wikimedia Foundation. (http://en.wikipedia.org/wiki/Gothic_revival_architecture)

"Index of /URBS110/Gothic." (2014). (http://aytch.mnsu.edu/URBS110/Gothic/)

"Medieval Construction" (2014) Index of /lectures/04-history-of-building. (http://www.mileslewis.net/lectures/04-history-of-building/)

"Milan cathedral" (2014) (http://en.wikipedia.org/wiki/Milan_Cathedral)

"Nevertopia" Nevertopia. (2014) (http://nevertopia.blogspot.pt/)

"Notre Dame de Paris" (2014) http://en.wikipedia.org/wiki/Notre_Dame_de_Paris

"Reims Cathedral" (2014) (http://en.wikipedia.org/wiki/Reims_Cathedral)

"Sainte-Chappelle" (2014) (http://en.wikipedia.org/wiki/Sainte-Chappelle)

"Salisbury Cathedral" (2014) (http://en.wikipedia.org/wiki/Salisbury_Cathedral)

"St. Albans Cathedral" (2014) (http://en.wikipedia.org/wiki/St_Albans_Cathedral)

"Stained Glass Studio" (2013) Stained Glass Studio. (http://www.canterbury-cathedral.org/conservation/stainedglass/)

"The Great South Window" (2014) The Great South Window. (http://www.canterbury-cathedral.org/2014/04/07/the-great-south-window/)

"The World's Oldest Space Frame" (2011) The World's Oldest Space Frame. (http://www.canterbury-cathedral.org/2011/09/16/the-worlds-oldest-space-frame/)

"Timber Roof Truss" (2014) Wikipedia. Wikimedia Foundation. (http://en.wikipedia.org/wiki/Timber_roof_truss)

"York Minster" (2014) Wikipedia. Wikimedia Foundation. (http://en.wikipedia.org/wiki/York_Minster)

Adams, D. (2012) "Britain's Greatest Cathedrals." Britain Magazine. (http://www.britain-magazine.com/features/region/england/south-east/kent/britains-greatest- cathedrals/)

Binda L., Cantini L., Cardani G., Saisi A., Tiraboschi C. (2007) "Use of Flat-jack and Sonic Tests for the Qualification of Historic Masonry". Conference Proceedings: 10th North American Masonry Conference, St. Louis, Missouri, USA, 791-803.

Binda L., Roca P., Martínez G., Casarin F., Modena C., Rossi P. P., Rodríguez I., Garay A. (2008) "Chapter 6: Monitoring of Long-term Damage in Long-span Masonry Constructions." Learning from Failure: Long-term Behaviour of Heavy Masonry Structures. Southampton: WIT. 125-52.

Block, Philippe (2005) "Equilibrium Systems: Studies in Masonry Structure". Master Thesis. Massachusetts Institute of Technology, US.

Block, Philippe (2005) "Equilibrium Systems: Studies in Masonry Structure". Master Thesis. Massachusetts Institute of Technology, US.

Block, Philippe (2009) "Thrust Network Analysis Exploring Three-dimensional Equilibrium". PhD Thesis. Massachusetts Institute of Technology, US.

Blockley K., and Bennett P. "Canterbury Cathedral" (2008) Canterbury Cathedral. Canterbury Archaeological Trust Ltd. (http://www.hillside.co.uk/arch/cathedral/nave.html)

Blows J.F., Carey P.J., and Poole A.B. (2003) "Preliminary Investigations into Caen Stone in the UK; Its Use, Weathering and Comparison with Repair Stone." Building and Environment 38.9-10: 1143-149.

Bowles J. (1977). "Foundation analysis and design". New York: McGraw-Hill.

Cardani G., Binda L. (2013) "Guidelines for the masonry quality evaluation in built heritage". Online Proceedings of Conference: Built Heritage 2013 - Monitoring Conservation and Management, Milan, Italy.

Casarin F., Modena C. (2007) "Dynamic Identification of S. Maria Assunta Cathedral, Reggio Emilia, Italy".2nd, International operational modal analysis conference. Copenhagen Denmark, 2, 637-644.

Chopra A. (2001) "Dynamics of Structures: Theory and applications to earthquake engineering". 3rd Edition, Prentice Hall.

Climent M. (2014) “Presentation SA1_04: Vaults and Domes Overall Structural arrangement Part 2”. SAHC Masters. Universitat Politècnica de Catalunya.

Collinson P, Ramsay N, and Sparks M. (1995) “A History of Canterbury Cathedral”. Oxford: Oxford UP.

Corallo C. (2014), Private Communication.

Coronelli D., di Prisco C., Pisanò F., Imposimato S., Ghezzi S., Pesconi M. (2014), The Tiburio of the cathedral of Milan: structural analysis of the construction & 20th century foundation settlements, Proceedings of the 15th International Conference on Structural Faults & Repair, London (UK), July 9-10, Forde M.C. (Ed.).

Daniel Oliveira (2014) “Presentation SA3_03: Seismic behavior and structural dynamics – Part 1”. SAHC Masters. University of Minho, Portugal.

D'ayala D., Smars P. (2003) "Architectural and Structural Modelling for the Conservation of Cathedrals." Journal of Architectural Conservation 9:3. 51-72.

Deeming, J. (2014), Private Communication.

DIANA (2014a) “DIANA – Finite Element Analysis. User’s Manual. Element Library”. TNO DIANA BV, Release 9.5, Netherlands.

DIANA (2014b) "Manuals TNO DIANA" (http://tnodiana.com/DIANA-manuals)

Dudley C. (2010) “Canterbury Cathedral: Aspects of Its Sacramental Geometry”. United States of America: Xlibris.

Erdogmus E., Hanagan L.M., Boothby T.E. (2004). “Modal Experiments for the Validation of Masonry Vault Models”, 22nd Conference & Exposition on Structural Dynamics. Michigan, United States.

Filippoupolitis M. (2011) “The south oculus at Canterbury cathedral”. Master Thesis. University of Minho, Portugal. (http://hdl.handle.net/1822/18896)

Fitchen J. (1981) "The Construction of Gothic Cathedrals: A Study of Medieval Vault Erection." Chicago: The University of Chicago Press.

Foti D., Debernardis M. and Paparella V. (2012) “Structural Safety Control of Masonry Buildings: Non-Linear Static Seismic Analysis with a Non-Linear Shear Strength Criterion”. Proceedings of the Eleventh International Conference on Computational Structures Technology. Civil-Comp Press, Stirlingshire, Scotland.

Foyle J., Newton H. and Greshoff R. (2013) "Chapter 6: Stone Repair and Conservation after 1945." Architecture of Canterbury Cathedral. London: Scala.

Franchetti P. (2014) “Presentation SA3_10: Structural Dynamics in Building Codes”. SAHC Masters. University of Padova, Italy.

Gazetas G. et al., (1986). “Elastic Settlement of Arbitrarily Shaped Foundations Embedded in Half-Space”, Rensselaer Polytechnic Institute, Troy, New York."

Holický M., Marková J. (2005), “Characteristics of materials”, Kloknerův Institute. Czech Technical University in Prague, Czech Republic (In Czech).

Huerta S.F. (2004) “Arcos, Bóvedas Y Cúpulas: Geometría Y Equilibrio En El Cálculo Tradicional De Estructuras De Fábrica”. Instituto Juan De Herrera, Madrid (In Spanish)

Kent Geology (2014) “Kent Geology” (http://www.kgg.org.uk/kentgeo.html)

Lourenço P.B., Filippoupoliti M., Corallo C., Mendes N. (2012). “Safety Assessment of the South Oculus, Canterbury Cathedral (UK)”, 8th International Conference on Structural Analysis of Historical Constructions. Wroclaw, Poland, 302-310. (http://hdl.handle.net/1822/21485)

Lourenço P.B. (1996) "Chapter 2: Modelling Masonry: A Material Description” Computational Strategies for Masonry Structures. Delft, Netherlands: Delft UP, 11-26.

Lourenço P.B. (1998). "Experimental and numerical issues in the modelling of the mechanical behavior of masonry." Structural Analysis of Historical Constructions II: Possibilities of Numerical and Experimental Techniques. Barcelona: International Center for Numerical Methods in Engineering.

Lourenço P.B. (2008). “Structural masonry analysis: recent developments and prospects". Book part. University of Newcastle, Australia. (http://hdl.handle.net/1822/17176)

Lourenço P.B. (2014) “Presentation SA2_12: Modeling of masonry and homogenization”. SAHC Masters. University of Minho, Guimarães, Portugal.

Lourenço P.B., Ramos L. F., Vasconcelos G., Peña F. (2008), “Monastery of Salzedas (Portugal) intervention in the cloister and information management”. ISISE – Livros. (http://hdl.handle.net/1822/14552)

Luca P., Roca P. (2014) “Presentation SA1_07: Ancient Rules and Classical Approaches Part 1”. SAHC Masters. Universitat Politècnica de Catalunya.

Luca P., Roca P. (2014b) “Presentation SA1_08: Ancient Rules and Classical Approaches Part 2”. SAHC Masters. Universitat Politècnica de Catalunya.

Magenes G., Penna A. (2009) “Existing masonry buildings: General code issues and methods of analysis and assessment” Eurocode 8 Perspectives from the Italian Standpoint Workshop notes. Napoli, Italy, 185-198.

Mendes N. (2012) “Seismic assessment of ancient masonry buildings: shaking table tests and numerical analysis”. PhD Thesis. University of Minho, Portugal. (http://hdl.handle.net/1822/23110)

Philippe B., Dejong M., Ochsendorf J. (2006) "As Hangs the Flexible Line: Equilibrium of Masonry Arches." Nexus Network Journal, 8.2: 13-24.

Philippe B., Lachauer L. (2014) "Three-Dimensional (3D) Equilibrium Analysis of Gothic Masonry Vaults." International Journal of Architectural Heritage. 8.3: 312-35.

Ramírez-Cisneros J., Lozano J., Ferrer-Toledo H., Rojas-Palacios J., Vázquez-Rosas R., Mijares-Arellano H. (2012) “Dynamic Behavior of Puebla City Cathedral”. 15th World Conference on Earthquake Engineering. Lisbon, Portugal.

Ramos L. (2007) “Damage identification on masonry structures based on vibration signatures”. PhD Thesis. University of Minho, Portugal. (http://hdl.handle.net/1822/7380)

Ramos L., Alaboz M., Aguilar R. (2010). “Dynamic Identification and Monitoring of St. Torcato Church”. 7th International Conference of Structural Analysis of Historical Constructions. Shanghai, China, 275-280. (http://hdl.handle.net/1822/18796)

Ramos L., Binda L. (2014b) “Presentation SA4_01-6: Damage in heritage structures”. SAHC Masters. University of Minho, Polytechnic University of Milan.

Ramos L., Lourenço P. B. (2014) “Presentation SA1_07: Inspection and diagnosis applied to historical structures”. SAHC Masters. University of Minho, Portugal.

Ramos L., Pipinato A. (2014c) “Presentation SA4_06-1: In situ tests for concrete structures”. SAHC Masters. University of Minho, Polytechnic University of Padua.

Roca P. (2001) “Studies on the structure of Gothic Cathedrals”. Historical Constructions, Guimarães, 71-90.

Roca P. (2014) “Presentation SA1_09: Damage and Collapse Mechanisms Part 1”. SAHC Masters. Universitat Politècnica de Catalunya.

Roca P., Cervera M., Gariup G. and Pela P. (2010) "Structural Analysis of Masonry Historical Constructions. Classical and Advanced Approaches." Archives of Computational Methods in Engineering 17:3, 299-325.

Roca P., Cervera M., Pelà L., Clemente R., Chiumenti M. (2013) "Continuum FE Models for the Analysis of Mallorca Cathedral." Engineering Structures 46: 653-70.

Roca P., Clemente R. (2005) “Studies on the origin of deformation and damage in long-span historical structures”. 11th International Conference on Fracture. Torino, Italy.

Romano A., Ochsendorf J. A. (2009) "The Mechanics of Gothic Masonry Arches." International Journal of Architectural Heritage, 4.1: 59-82.

Simson V. O. (1988) "The Gothic Cathedral: Origins of Gothic Architecture and the Medieval Concept of Order." Princeton: Princeton UP.

Theodossopoulos D. (2006) "Technology and Geometry in the Design of "Gothic" Vaults in Britain". Proceedings of the Second International Congress on Construction History. Vol. 3. 3079-3095

Theodossopoulos D. (2008) "Structural Design of High Gothic Vaulting Systems in England." International Journal of Architectural Heritage. 2:1. 1-24.

Theodossopoulos D., Sinha B. (2008) “Structural safety and failure modes in Gothic vaulting systems”. 8th International seminar on structural masonry. Istanbul, Turkey.

Theodossopoulos D., Sinha B. P., Usmani A. S., Macdonald A. J. (2002) "Assessment of the Structural Response of Masonry Cross Vaults." Strain 38.3: 119-27.

Theuerkauf H. "Canterbury Cathedral" (2007) (http://www.gotik-romanik.de/Canterbury%20Thumbnails/Thumbnails.html)

Willis R. (1845) “The Architectural History of Canterbury Cathedral”. London: Longman.